

TARGET DETECTION BY THE AMBIGUITY FUNCTION
TECHNIQUE AND THE CONVENTIONAL FOURIER
TRANSFORM TECHNIQUE IN FREQUENCY CODED
CONTINUOUS WAVE RADARS

A THESIS SUBMITTED TO
THE GRADUATE SCHOOL OF NATURAL AND APPLIED SCIENCES
OF
MIDDLE EAST TECHNICAL UNIVERSITY

BY

MEHMET AKANGÖL

IN PARTIAL FULFILLMENT OF THE REQUIREMENTS
FOR
THE DEGREE OF MASTER OF SCIENCE
IN
ELECTRICAL AND ELECTRONICS ENGINEERING

DECEMBER 2005

Approval of the Graduate School of Natural And Applied Sciences

Prof. Dr. Canan Özgen
Director

I certify that this thesis satisfies all the requirements as a thesis for the degree of Master of Science.

Prof. Dr. İsmet Erkmen
Head of Department

This is to certify that we have read this thesis and that in our opinion it is fully adequate, in scope and quality, as a thesis for the degree of Master of Science.

Prof. Dr. Gönül Turhan Sayan
Supervisor

Examining Committee Members

Prof. Dr. Mustafa Kuzuoğlu	(METU, EE)	_____
Prof. Dr. Gönül Turhan Sayan	(METU, EE)	_____
Prof. Dr. Kemal Leblebicioğlu	(METU, EE)	_____
Prof. Dr. Gülbin Dural	(METU, EE)	_____
Kürşad Yıldırım, M. Sc.	(Hacettepe Univ., EE)	_____

I hereby declare that all information in this document has been obtained and presented in accordance with academic rules and ethical conduct. I also declare that, as required by these rules and conduct, I have fully cited and referenced all material and results that are not original to this work.

Name, Last name: Mehmet , Akangöl

Signature :

ABSTRACT

TARGET DETECTION BY THE AMBIGUITY FUNCTION TECHNIQUE AND THE CONVENTIONAL FOURIER TRANSFORM TECHNIQUE IN FREQUENCY CODED CONTINUOUS WAVE RADARS

Akangöl, Mehmet

M.Sc., Department of Electrical and Electronics Engineering

Supervisor: Prof. Dr. Gönül Turhan Sayan

December 2005, 191 pages

Continuous Wave (CW) radars are preferred for their low probability of intercept by the other receivers. Frequency modulation techniques, the linear frequency modulation (LFM) technique in particular, are commonly used in CW radars to resolve the range and the radial velocity of the detected targets. The conventional method for target detection in a linear FMCW radar makes use of a mixer followed by a low-pass filter whose output is Fourier transformed to get the range and velocity information. In this thesis, an alternative target detection technique based on the use of the Ambiguity Function (AF) will be investigated in frequency modulated CW

radars. Results of the AF-based technique and the conventional Fourier-based technique will be compared for different target detection scenarios.

Keywords: Radar Target Detection, FMCW Radar, Ambiguity Function, Frequency Modulation

ÖZ

FREKANS KODLAMALI SÜREKLİ DALGALI RADARLARDA HEDEF TESBİTİ İÇİN BELİRSİZLİK FONKSİYONU TEKNİĞİNİN VE BİLİNER FOURIER DÖNÜŞÜM TEKNİĞİNİN KULLANILMASI

Akangöl, Mehmet

Yüksek Lisans, Elektrik-Elektronik Mühendisliği Bölümü

Tez Yöneticisi: Prof. Dr. Gönül Turhan Sayan

Aralık 2005, 191 sayfa

Sürekli dalgali radarlar, diğler alıcılar tarafından yakalanma olasılıklarının düşüklüğü nedeniyle tercih edilirler. Tespit edilen hedeflerin uzaklık ve hızlarının çözümlenebilmesi için bu radarlarda frekans kipleme, özellikle de doğrusal frekans kipleme, yöntemlerinin kullanılması yaygındır. Doğrusal frekans kiplemeli sürekli dalgali radarlarda hedef tespiti için kullanılan alışlagelmiş yöntemde, gönderilen ve alınan sinyaller önce karıştırılıp alçak geçirgen bir süzgeçten geçirilir ve çıkış sinyaline Fourier dönüşümü uygulanır. Bu tezde ise, Belirsizlik Fonksiyonunun kullanımına dayanan alternatif bir hedef tespit yöntemi incelenecektir. Çeşitli hedef

tespit senaryoları için her iki yöntemin sonuçları karşılaştırılacaktır.

Anahtar Kelimeler: Radarla hedef tespiti, frekans kodlamalı sürekli dalgalı radar, belirsizlik fonksiyonları, frekans modülasyonu

To My Parents

ACKNOWLEDGEMENTS

The author wishes to express his deepest gratitude to his supervisor, Prof. Dr. Gönül Turhan Sayan for her guidance, advice, criticism, encouragement and insight throughout the research.

I also thank to Kürşad Yıldırım for his support to provide a comfortable office space through all my thesis work.

I also thank to Emre Çakır, Emre Ağırnas, Özkan Ünver, Timuçin Bük and Kurtuluş Erinç Akdoğan for the emotional support.

Last but not the least, I also thank to my parents for everything.

TABLE OF CONTENTS

PLAGIARISM.....	III
ABSTRACT.....	IV
ÖZ	VI
ACKNOWLEDGEMENTS	IX
TABLE OF CONTENTS.....	X
LIST OF FIGURES	XIV
CHAPTER	
1. INTRODUCTION.....	1
2. CONTINUOUS WAVE CODING TECHNIQUES.....	7
2.1 Advantages of FMCW.....	7
2.2 FMCW Radar Basics	8
2.3 Advantages of the FSK Radar	16
2.4 FSK Radar Basics	17

2.5	Costas Codes	20
2.5.1	Characteristics of a Costas Array or Sequence.....	21
2.5.2	Computing the Difference Triangle	22
2.5.3	Deriving the Costas Sequence AF	23
3.	AMBIGUITY FUNCTION	25
3.1	Introduction.....	25
3.2	Main Properties of the Ambiguity Function	27
3.3	Cuts Through the Ambiguity Function	33
4.	TARGET DETECTION WITH AMBIGUITY FUNCTION AND CONVENTIONAL FFT METHOD.....	35
4.1	Construction of Complex Envelopes of Radar Signals for Ambiguity Function Process.....	35
4.2	Construction of Modified Costas Signal	40
4.3	Simulations	50
4.3.1	Radar Resolution with Auto-Ambiguity Function	51
4.3.1.1	Radar Resolution with FMCW Coding Technique	52
4.3.1.2	Radar Resolution with Costas Coding Technique	55
4.3.2	Target Detection Scenarios	60
4.3.2.1	Stationary Target Scenarios	60

4.3.2.2	Moving Target Scenarios	74
4.3.2.3	Multiple Target Scenarios.....	88
4.3.3	Noise Analysis in Detection Methods	157
4.3.3.1	Noise Analysis in Conventional FFT Method.....	158
4.3.3.2	Noise Analysis in Cross-Ambiguity Method with FMCW Coding	160
4.3.3.3	Noise Analysis in Cross-Ambiguity Method with Costas Coding	162
5.	CONCLUSIONS.....	165
	REFERENCES	168
APPENDICES		
A.	PRIMITIVE ROOTS AND COSTAS SEQUENCES.....	171
A.1	Primes	171
A.2	Complete and Reduced Residue Systems	171
A.3	Primitive Roots	174
A.4	Welch Construction of Costas Arrays	178
B.	MATCHED FILTER.....	180
B.1	Complex Representation of Bandpass Signals.....	180

B.2	Matched Filter	182
B.3	Matched Filter for a Bandpass Signal	187
B.4	Matched-Filter Response to its Doppler-Shifted Signal	189

LIST OF FIGURES

Figure 2. 1: Transmitted triangular waveform and delayed and Doppler shifted received waveform.....	8
Figure 2. 2: Costas sequence $f_j = \{2, 4, 8, 5, 10, 9, 7, 3, 6, 1\}$ kHz, showing (a) the binary time-frequency matrix, and (b) the power spectrum magnitude for several code periods.....	22
Figure 2. 3: Difference triangle for a $N_F = 10$ Costas sequence	23
Figure 2. 4: The AF derive from the difference triangle for a $N_F = 10$ Costas sequence	24
Figure 4. 1: (a) amplitude (b) phase (c) frequency parameters of $N=10$ $t_b = 1$ ms, and $\Delta f = 10$ kHz Costas signal	42
Figure 4. 2: 3-D Ambiguity Function plot of the $N=10$ $t_b = 1$ ms, and $\Delta f = 10$ kHz Costas signal.....	43
Figure 4. 3: 2-D Ambiguity Function plot of the $N=10$ $t_b = 1$ ms, and $\Delta f = 10$ kHz Costas signal.....	44
Figure 4. 4: (a) amplitude (b) phase (c) frequency parameters of $N=10$ $t_b = 1$ ms, and	

$\Delta f = 50$ kHz Costas signal	45
Figure 4. 5: 3-D Ambiguity Function plot of the $N=10$ $t_b = 1$ ms, and $\Delta f = 50$ kHz Costas signal.....	46
Figure 4. 6: 2-D Ambiguity Function plot of the $N=10$ $t_b = 1$ ms, and $\Delta f = 50$ kHz Costas signal.....	47
Figure 4. 7: (a) amplitude (b) phase (c) frequency parameters of $N=10$ $t_b = 1$ ms, and $\Delta f = 50$ kHz modified Costas signal	48
Figure 4. 8: 3-D Ambiguity Function plot of the $N=10$ $t_b = 1$ ms, and $\Delta f = 50$ kHz modified Costas signal.....	49
Figure 4. 9: 2-D Ambiguity Function plot of the $N=10$ $t_b = 1$ ms, and $\Delta f = 50$ kHz modified Costas signal.....	50
Figure 4. 10: (a) amplitude, (b) phase, and (c) frequency parameters of the transmitted signal with FMCW coding with triangular waveform used in the Auto-Ambiguity function calculation.....	53
Figure 4. 11: 3-D Auto-Ambiguity function plot of FMCW coding technique.....	54
Figure 4. 12: 2-D Auto-Ambiguity function plot of FMCW coding technique.....	55
Figure 4. 13: (a) amplitude, (b) phase, and (c) frequency parameters of the transmitted signal with Costas coding used in the Auto-Ambiguity function	

calculation.	57
Figure 4. 14: 3-D Auto-Ambiguity function plot of Costas coding technique	58
Figure 4. 15: 2-D Auto-Ambiguity function plot of Costas coding technique	59
Figure 4. 16: Beat frequency of a stationary target (a) beat frequency extracted from RF signal (b) beat frequency extracted from baseband signal	62
Figure 4. 17: FFT display of a stationary target (a) range extracted from RF signal (b) range extracted from baseband signal.....	63
Figure 4. 18: (a) amplitude, (b) phase, and (c) frequency parameters for the FMCW coded transmitted signal used in stationary target simulation.....	65
Figure 4. 19: (a) amplitude, (b) phase, and (c) frequency parameters for the FMCW coded received signal used in stationary target simulation.....	66
Figure 4. 20: 3-D Cross-Ambiguity function plot of FMCW coding technique ($\Delta R = 70$ m and $\Delta V = 7$ m/s) used in stationary target simulation.....	67
Figure 4. 21: Cross-Ambiguity function contour plot of FMCW coding technique ($\Delta R = 70$ m and $\Delta V = 7$ m/s) used in stationary target simulation	68
Figure 4. 22: (a) amplitude, (b) phase, and (c) frequency parameters for the Costas coded transmitted signal used in stationary target simulation.....	70
Figure 4. 23: (a) amplitude, (b) phase, and (c) frequency parameters for the Costas coded received signal used in stationary target simulation.....	71

Figure 4. 24: 3-D Cross-Ambiguity function plot of Costas coding technique ($\Delta R = 120$ m and $\Delta V = 12$ m/s) used in stationary target simulation.....	72
Figure 4. 25: Cross-Ambiguity function contour plot of Costas coding technique ($\Delta R = 120$ m and $\Delta V = 12$ m/s) used in stationary target simulation	73
Figure 4. 26: (a)Beat frequency of a moving target obtained from the differences between the received and transmitted waveform frequency expressions directly. (b) Zoom in into Figure 4.26 (a) about beat frequencies.....	75
Figure 4. 27: Contour plot of the spectrogram of the filtered mixer output for moving target simulation	76
Figure 4. 28: FFT results of (a) upswing and (b) downswing segments separately. .	77
Figure 4. 29: (a) amplitude, (b) phase, and (c) frequency parameters for the FMCW coded transmitted signal used in moving target simulation.	79
Figure 4. 30: (a) amplitude, (b) phase, and (c) frequency parameters for the FMCW coded received signal used in moving target simulation.	80
Figure 4. 31: 3-D Cross-Ambiguity function plot of FMCW coding technique ($\Delta R = 70$ m and $\Delta V = 7$ m/s) used in moving target simulation	81
Figure 4. 32: Cross-Ambiguity function contour plot of FMCW coding technique ($\Delta R = 70$ m and $\Delta V = 7$ m/s) used in moving target simulation.....	82
Figure 4. 33: (a) amplitude, (b) phase, and (c) frequency parameters for the Costas coded transmitted signal used in moving target simulation.	84

Figure 4. 34: (a) amplitude, (b) phase, and (c) frequency parameters for the Costas coded received signal used in moving target simulation.	85
Figure 4. 35: 3-D Cross-Ambiguity function plot of Costas coding technique ($\Delta R = 120$ m and $\Delta V = 12$ m/s) used in moving target simulation	86
Figure 4. 36: Cross-Ambiguity function contour plot of Costas coding technique ($\Delta R = 120$ m and $\Delta V = 12$ m/s) used in moving target simulation.....	87
Figure 4. 37: Beat frequency of multiple targets in different range and in different velocity, obtained from the differences between the received and transmitted waveform frequency expressions directly.....	90
Figure 4. 38: Contour plot of the spectrogram of the filtered mixer output for multiple targets in different range and in different velocity simulation	91
Figure 4. 39: (a) amplitude, (b) phase, and (c) frequency parameters for the FMCW coded transmitted signal used in multiple targets in different range and in different velocity simulation.....	93
Figure 4. 40: (a) amplitude, (b) phase, and (c) frequency parameters for the FMCW coded 1.st target received signal used in multiple targets in different range and in different velocity simulation.	94
Figure 4. 41: (a) amplitude, (b) phase, and (c) frequency parameters for the FMCW coded 2.nd target received signal used in multiple targets in different range and in different velocity simulation.	95
Figure 4. 42: 3-D Cross-Ambiguity function plot of FMCW coding technique ($\Delta R =$	

70 m and $\Delta V = 7$ m/s) used in multiple targets in different range and in different velocity simulation.....96

Figure 4. 43: Cross-Ambiguity function contour plot of FMCW coding technique ($\Delta R = 70$ m and $\Delta V = 7$ m/s) used in multiple targets in different range and in different velocity simulation.97

Figure 4. 44: (a) amplitude, (b) phase, and (c) frequency parameters for the Costas coded transmitted signal used in multiple targets in different range and in different velocity simulation.....98

Figure 4. 45: (a) amplitude, (b) phase, and (c) frequency parameters for the Costas coded 1.st target received signal used in multiple targets in different range and in different velocity simulation.99

Figure 4. 46: (a) amplitude, (b) phase, and (c) frequency parameters for the Costas coded 2.nd target received signal used in multiple targets in different range and in different velocity simulation.100

Figure 4. 47: 3-D Cross-Ambiguity function plot of Costas coding technique ($\Delta R = 120$ m and $\Delta V = 12$ m/s) used in multiple targets in different range and in different velocity simulation.....101

Figure 4. 48: Cross-Ambiguity function contour plot of Costas coding technique ($\Delta R = 120$ m and $\Delta V = 12$ m/s) used in multiple targets in different range and in different velocity simulation.102

Figure 4. 49: Beat frequency of multiple targets in same range and in different velocity, obtained from the differences between the received and transmitted

waveform frequency expressions directly.....	104
Figure 4. 50: Contour plot of the spectrogram of the filtered mixer output for multiple targets in different range and in different velocity simulation	105
Figure 4. 51: (a) amplitude, (b) phase, and (c) frequency parameters for the FMCW coded transmitted signal used in multiple targets in same range and in different velocity simulation.....	107
Figure 4. 52: (a) amplitude, (b) phase, and (c) frequency parameters for the FMCW coded 1.st target received signal used in multiple targets in same range and in different velocity simulation.	108
Figure 4. 53: (a) amplitude, (b) phase, and (c) frequency parameters for the FMCW coded 2.nd target received signal used in multiple targets in same range and in different velocity simulation.	109
Figure 4. 54: 3-D Cross-Ambiguity function plot of FMCW coding technique ($\Delta R = 70$ m and $\Delta V = 7$ m/s) used in multiple targets in same range and in different velocity simulation.....	110
Figure 4. 55: Cross-Ambiguity function contour plot of FMCW coding technique ($\Delta R = 70$ m and $\Delta V = 7$ m/s) used in multiple targets in same range and in different velocity simulation.....	111
Figure 4. 56: (a) amplitude, (b) phase, and (c) frequency parameters for the Costas coded transmitted signal used in multiple targets in same range and in different velocity simulation.....	112

Figure 4. 57: (a) amplitude, (b) phase, and (c) frequency parameters for the Costas coded 1.st target received signal used in multiple targets in same range and in different velocity simulation.	113
Figure 4. 58: (a) amplitude, (b) phase, and (c) frequency parameters for the Costas coded 2.nd target received signal used in multiple targets in same range and in different velocity simulation.	114
Figure 4. 59: 3-D Cross-Ambiguity function plot of Coatas coding technique ($\Delta R = 120$ m and $\Delta V = 12$ m/s) used in multiple targets in same range and in different velocity simulation.....	115
Figure 4. 60: Cross-Ambiguity function contour plot of Costas coding technique ($\Delta R = 120$ m and $\Delta V = 12$ m/s) used in multiple targets in same range and in different velocity simulation.	116
Figure 4. 61: Beat frequency of multiple targets in different range and in same velocity, obtained from the differences between the received and transmitted waveform frequency expressions directly.....	118
Figure 4. 62: Contour plot of the spectrogram of the filtered mixer output for multiple targets in different range and in same velocity simulation.....	119
Figure 4. 63: (a) amplitude, (b) phase, and (c) frequency parameters for the FMCW coded transmitted signal used in multiple targets in different range and in same velocity simulation.....	121
Figure 4. 64: (a) amplitude, (b) phase, and (c) frequency parameters for the FMCW coded 1.st target received signal used in multiple targets in different range and in	

same velocity simulation.....	122
Figure 4. 65: (a) amplitude, (b) phase, and (c) frequency parameters for the FMCW coded 2.nd target received signal used in multiple targets in different range and in same velocity simulation.....	123
Figure 4. 66: 3-D Cross-Ambiguity function plot of FMCW coding technique ($\Delta R = 70$ m and $\Delta V = 7$ m/s) used in multiple targets in different range and in same velocity simulation.....	124
Figure 4. 67: Cross-Ambiguity function contour plot of FMCW coding technique ($\Delta R = 70$ m and $\Delta V = 7$ m/s) used in multiple targets in different range and in same velocity simulation.....	125
Figure 4. 68: (a) amplitude, (b) phase, and (c) frequency parameters for the Costas coded transmitted signal used in multiple targets in different range and in same velocity simulation.....	127
Figure 4. 69: (a) amplitude, (b) phase, and (c) frequency parameters for the Costas coded 1.st target received signal used in multiple targets in different range and in same velocity simulation.....	128
Figure 4. 70: (a) amplitude, (b) phase, and (c) frequency parameters for the Costas coded 2.nd target received signal used in multiple targets in different range and in same velocity simulation.....	129
Figure 4. 71: 3-D Cross-Ambiguity function plot of Costas coding technique ($\Delta R = 120$ m and $\Delta V = 12$ m/s) used in multiple targets in different range and in same	

velocity simulation.....	130
Figure 4. 72: Cross-Ambiguity function contour plot of Costas coding technique ($\Delta R = 120$ m and $\Delta V = 12$ m/s) used in multiple targets in different range and in same velocity simulation.....	131
Figure 4. 73: 3-D Cross-Ambiguity function plot of FMCW coding technique ($\Delta R = 70$ m and $\Delta V = 7$ m/s) used in multiple targets in the range resolution value of the radar simulation.	133
Figure 4. 74: Cross-Ambiguity function contour plot of FMCW coding ($\Delta R = 70$ m and $\Delta V = 7$ m/s) technique used in multiple targets in the range resolution value of the radar simulation.	134
Figure 4. 75: 3-D Cross-Ambiguity function plot of FMCW coding technique ($\Delta R = 70$ m and $\Delta V = 7$ m/s) used in multiple targets near the range resolution value of the radar simulation.	135
Figure 4. 76: Cross-Ambiguity function contour plot of FMCW coding technique ($\Delta R = 70$ m and $\Delta V = 7$ m/s) used in multiple targets near the range resolution value of the radar simulation.	136
Figure 4. 77: 3-D Cross-Ambiguity function plot of Costas coding technique ($\Delta R = 120$ m and $\Delta V = 12$ m/s) used in multiple targets in the range resolution value of the radar simulation.	137
Figure 4. 78: Cross-Ambiguity function contour plot of Costas coding technique ($\Delta R = 120$ m and $\Delta V = 12$ m/s) used in multiple targets in the range resolution value	

of the radar simulation.	138
Figure 4. 79: 3-D Cross-Ambiguity function plot of Costas coding technique ($\Delta R = 120$ m and $\Delta V = 12$ m/s) used in multiple targets near the range resolution value of the radar simulation.	139
Figure 4. 80: Cross-Ambiguity function contour plot of Costas coding technique ($\Delta R = 120$ m and $\Delta V = 12$ m/s) used in multiple targets near the range resolution value of the radar simulation.	140
Figure 4. 81: 3-D Cross-Ambiguity function plot of FMCW coding technique ($\Delta R = 70$ m and $\Delta V = 7$ m/s) used in multiple targets in the Doppler resolution value of the radar simulation.	141
Figure 4. 82: Cross-Ambiguity function plot of FMCW coding technique ($\Delta R = 70$ m and $\Delta V = 7$ m/s) used in multiple targets in the Doppler resolution value of the radar simulation.	142
Figure 4. 83: 3-D Cross-Ambiguity function plot of FMCW coding technique ($\Delta R = 70$ m and $\Delta V = 7$ m/s) used in multiple targets near the Doppler resolution value of the radar simulation.	143
Figure 4. 84: Cross-Ambiguity function contour plot of FMCW coding ($\Delta R = 70$ m and $\Delta V = 7$ m/s) technique used in multiple targets near the Doppler resolution value of the radar simulation.	144
Figure 4. 85: 3-D Cross-Ambiguity function plot of Costas coding technique ($\Delta R = 120$ m and $\Delta V = 12$ m/s) used in multiple targets in the Doppler resolution value of	

the radar simulation.	145
Figure 4. 86: Cross-Ambiguity function contour plot of Costas coding technique ($\Delta R = 120$ m and $\Delta V = 12$ m/s) used in multiple targets in the Doppler resolution value of the radar simulation.	146
Figure 4. 87: 3-D Cross-Ambiguity function plot of Costas coding technique ($\Delta R = 120$ m and $\Delta V = 12$ m/s) used in multiple targets near the Doppler resolution value of the radar simulation.	147
Figure 4. 88: Cross-Ambiguity function contour plot of Costas coding technique ($\Delta R = 120$ m and $\Delta V = 12$ m/s) used in multiple targets near the Doppler resolution value of the radar simulation.	148
Figure 4. 89: Beat frequency of multiple targets (four target), obtained from the differences between the received and transmitted waveform frequency expressions directly.	150
Figure 4. 90: Contour plot of the spectrogram of the filtered mixer output for multiple targets (four targets) simulation.....	151
Figure 4. 91: FFT plot of the filtered mixer output for multiple targets (four targets) simulation.	152
Figure 4. 92: 3-D Cross-Ambiguity function plot of FMCW coding technique ($\Delta R = 70$ m and $\Delta V = 7$ m/s) used in multiple targets (four targets) simulation.	153
Figure 4. 93: Cross-Ambiguity function contour plot of FMCW coding ($\Delta R = 70$ m	

and $\Delta V = 7$ m/s) technique used in multiple targets (four targets) simulation.	154
Figure 4. 94: 3-D Cross-Ambiguity function plot of Costas coding technique ($\Delta R = 120$ m and $\Delta V = 12$ m/s) used in multiple targets (four targets) simulation.....	155
Figure 4. 95: Cross-Ambiguity function contour plot of Costas coding technique ($\Delta R = 120$ m and $\Delta V = 12$ m/s) used in multiple targets (four targets) simulation.	156
Figure 4. 96: (a) FFT plot of RF beat frequency (b) FFT plot of baseband beat frequency for stationary target simulation without noise	159
Figure 4. 97: (a) FFT plot of RF beat frequency (b) FFT plot of baseband beat frequency for stationary target simulation with noise	160
Figure 4. 98: 3-D Cross-Ambiguity function plot of FMCW coding technique used stationary target simulation without noise.	161
Figure 4. 99: 3-D Cross-Ambiguity function plot of FMCW coding technique used stationary target simulation with noise.	162
Figure 4. 100: 3-D Cross-Ambiguity function plot of Costas coding technique used stationary target simulation without noise.	163
Figure 4. 101: 3-D Cross-Ambiguity function plot of Costas coding technique used stationary target simulation with noise.	164
Figure B. 1: Matched filter definitions.....	183

CHAPTER 1

INTRODUCTION

RADAR (RAdio Detection And Ranging) is an electromagnetic system used for the detection of the targets. It operates by transmitting a particular type of waveform and, detects the existence, location and radial velocity of the target from the nature of the echo signal.

An elementary form of radar consists of a transmitting antenna emitting electromagnetic radiation generated by an oscillator of some sort, a receiving antenna, and an energy detecting device, or receiver. A portion of the transmitted signal is intercepted by a scattering object (target) and is reradiated in all directions. It is the energy reradiated in the back direction that is of prime interest to monostatic radar. The receiving antenna collects the returned energy and delivers it to a receiver, where it is processed to detect the presence of the target and to extract its position and radial velocity. The distance to the target is determined by measuring the time taken for the radar signal to travel to the target and back. The direction, or angular position, of the target may be determined from the direction of arrival of the reflected wavefront. If relative motion exists between target and radar, the shift in the carrier frequency of the reflected wave (Doppler Effect) is a measure of the targets radial velocity [1].

Radars can be considered in two main categories depending on the type of waveform

used in the radar. These are pulsed radar and CW (Continuous Wave) radar.

Pulsed radar transmits a relatively short burst of electromagnetic energy, after which the receiver is turned on to listen for the echo. The echo not only indicates that a target is present, but the time that elapses between the transmission of the pulse and the receipt of the echo is a measure of the distance to the target and relative frequency difference between the transmitted echo and received echo is a measure of the Doppler information of the target.

A CW radar transmits electromagnetic energy continuously. To extract the target's range and velocity, the transmitted wave is modulated in frequency and the frequency of the return signal from the target is measured. Comparison of the return signal with the transmitted signal can help for the extraction of both the range and the velocity information of the target [2].

In this thesis CW radars are investigated. The main drawback of a pulsed radar waveform is the high peak-to-average power ratio put out by the transmitter. The average power is what determines the detection characteristics of the radar but the high peak power transmission can also easily be detected by noncooperative intercept receivers. However, a CW radar emits considerably lower transmit power to maintain the same detection performance as the pulsed radar. Consequently, most LPI (Low Probability of Intercept) emitters use CW signals [3].

Historically, the earlier radar experimenters worked almost exclusively with continuous rather than pulsed transmission. Two of the more important early applications of the CW radar principle were the proximity (VT) fuze and the FMCW (Frequency Modulated Continuous Wave) altimeter. The CW proximity fuze was first employed in artillery projectiles during World War II and greatly enhanced the effectiveness of both field and antiaircraft artillery. The first practical model of the

FMCW altimeter was developed by the Western Electric Company in 1938, although the principle of altitude determination using radio-wave reflections was known ten years earlier, in 1928.

The CW radar is of interest not only because of its many applications, but its study also serves as a means for better understanding the nature and use of the Doppler information contained in the echo signal also the CW radar provides a measurement of relative velocity which may be used to distinguish moving targets from stationary objects or clutter.

Some sort of timing mark must be applied to a CW carrier if range is to be measured. The timing mark permits the time of transmission and the time of return to be recognized. The sharper or more distinct the mark, the more accurate the measurement of the transit time. But the more distinct the timing mark, the broader will be the transmitted spectrum as it follows the properties of the Fourier transform. Therefore a finite spectrum must of necessity be transmitted if transit time or range is to be measured.

The spectrum of a CW transmission can be broadened by the application of modulation, either amplitude, or phase. An example of an amplitude modulation is the pulse radar. The narrower the pulse, the more accurate the measurement of range and the broader the transmitted spectrum. A widely used technique to broaden the spectrum of CW radar is to frequency-modulate the carrier. The timing mark is the changing frequency. The transmit time is proportional to the difference in frequency between the echo signal and the transmitter signal. The greater the transmitter frequency deviation in a given time interval, the more accurate the measurement of the transit time and the wider will be the transmitted spectrum [1].

There are several techniques to modulate the frequency in CW radars. In this thesis

the FMCW coding techniques and the Costas coding techniques are used for modulate the frequency in CW radars.

In FMCW coding technique to extract the range information and the Doppler frequency, the modulation waveform must have equal up-sweep and down-sweep time intervals. So, the transmitter frequency is increases linearly with time during the up-sweep interval up to a certain frequency value and from this frequency value begins decreasing linearly with time during the down-sweep interval up to a certain frequency value.

In Costas coding technique, the transmitter frequency hops from one frequency to other in every time interval. The hopping orders of frequencies are determined by a frequency hopping sequence (Costas code). The number of frequencies used in a Costas code constitutes the code number and the time interval that transmitter emits one frequency is the sub-code period so sub-code period times code number gives the Costas code length and the period.

Ambiguity analysis is important to understand the properties of the CW waveform and its effect on measurement accuracy, target resolution, ambiguities in range, and radial velocity, and its response to clutter.

The CW radar designer chooses the necessary bandwidth in order to get the range resolution properties needed. He then chooses the modulation code necessary to get the ambiguity properties i.e., the resolution and cross term properties, needed. Ambiguity Function (AF) is a time-frequency representation type tool for investigating the ambiguity properties of the waveform modulation used in the radar. In this thesis ambiguity function is also used for target detection.

The ambiguity function represents the response of a filter matched to a given finite

energy signal when the signal is received with a delay τ and a Doppler shift ν relative to the nominal values (zeros) expected by the filter. The Ambiguity Function definition is

$$|\chi(\tau, \nu)| = \left| \int_{-\infty}^{\infty} u(t) u^*(t + \tau) \exp(j2\pi\nu t) dt \right| \quad (1.1)$$

where u is the complex envelope of the signal. A nonzero ν implies a target moving at a certain radial velocity with respect to radar. Positive τ refers to round trip delay time when the target is away from the radar by a certain distance [4].

In equation (1.1), if $u(t)$ and $u(t + \tau)$ are the complex envelopes of the transmitted signal then the result in equation (1.1) is called the Auto-Ambiguity Function. Auto-Ambiguity Function is used for determining the waveform effects on measurement accuracy, ambiguities in range and velocity, and target resolution [5].

In equation (1.1) if $u(t)$ is the complex envelope of transmitted signal and $u(t + \tau)$ is the complex envelope of the received signal then $\chi(\tau, \nu)$ is called Cross-Ambiguity Function. Cross-Ambiguity Function may be used for determining the waveform effects in response to clutter [6]. In this thesis the Cross-Ambiguity Function is mainly used for target detection.

The organization of thesis is as follows:

Chapter 2, presents the advantages and the basic principles of FMCW coding technique and the advantages and the basic principles of Costas coding technique in CW radars.

Chapter 3, includes the Ambiguity Function, its properties and its basic use in radar

target detection.

Chapter 4, presents various radar target detection applications for single and multi-target scenarios with and without additive noise. The detection simulations will be based on both the conventional Fourier Transform technique and on the Ambiguity Function technique.

Finally, in Chapter 5, the concluding remarks will be presented.

CHAPTER 2

CONTINUOUS WAVE CODING TECHNIQUES

This chapter describes the coding techniques of continuous wave (CW) radars. In this chapter frequency modulated continuous wave (FMCW) and frequency shift keying (FSK) (or frequency hopping (FH)) coding techniques are presented with a special emphasis on Costas codes.

2.1 Advantages of FMCW

CW radars that use unmodulated waveforms can not measure a target's range. To measure the target's range and/or speed, the transmit frequency must be varied in time, and the frequency of the return signal from the target measured. Correlation of the return signal with the transmit signal can give a measure of the both the range and the Doppler information of the target. Since the modulation can not be continually changed in one direction (e.g., up or down), a periodic modulation is normally used. Frequency modulation can create a wideband LPI waveform and take many forms, with sinusoidal and linear modulation being used most frequently. The most popular linear modulation utilized is the triangular FMCW emitter, since it can measure the targets range and range rate. In this thesis for FMCW coding triangular modulation is used.

FMCW is an effective LPI technique for many reasons. The frequency modulation

spreads the transmitted energy over a large modulation bandwidth ΔF , providing good range resolution that is critical for discriminating targets from clutter. The power spectrum of the FMCW signal is nearly rectangular over the modulation bandwidth, so non-cooperative interception is difficult. Since the transmit waveform is deterministic, the form of the return signals can be predicted. This gives the added advantage of being resistant to interference (such as jamming), since any signal not matching this form can be suppressed. Consequently, it is a difficult matter for a non-cooperative receiver to detect the FMCW waveform and measure the parameters accurately enough to match the jammer waveform to the radar waveform.

2.2 FMCW Radar Basics

Frequency Modulated Continuous Wave Radar transmits a frequency sweep, in the form of a triangular waveform. The signal is scattered from distant targets and detected by the receiver where the returned signal is mixed by the copy of the transmitted signal to determine the range and the radial speed of the target.

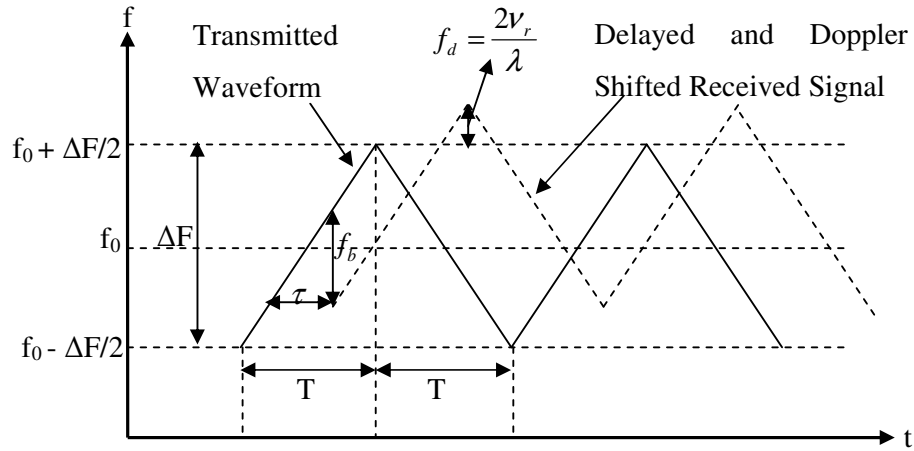


Figure 2. 1: Transmitted triangular waveform and delayed and Doppler shifted received waveform

The frequency of the transmitted waveform for the first (up-ramp) section is [7], [8]

$$f_1(t) = f_0 - \frac{\Delta F}{2} + \frac{\Delta F}{T}t \quad (2.1)$$

for $0 < t < T$. Here f_0 is the RF carrier frequency, ΔF is the transmit modulation bandwidth, and T is the modulation period. The modulation (sweep) bandwidth ΔF is chosen to provide the required range resolution

$$\Delta R = \frac{c}{2\Delta F} \quad (\text{m}) \quad (2.2)$$

In choosing the modulation period “T”, two factors must be considered

$$1) T < \frac{\Delta R}{V_t}$$

where ΔR is the range resolution and V_t is the maximum closing velocity of the target. This relationship requires that the target must remain in a range bin for at least an entire modulation period T . Otherwise; the target return will smear across several range bins.

2) T should be several times the maximum round-trip delay τ_{\max} , of the target’s return signal.

This is in order to minimize the loss in effective transmit bandwidth and power and to also provide a high velocity resolution. For the same detection characteristics of a radar a longer modulation time allows a lower average transmit power and

bandwidth. Also a longer modulation time allows a better resolution in frequency.

$$\tau_{\max} = \frac{2R_{\max}}{c} \quad (2.3)$$

$$T = K * \tau_{\max} \quad (2.4)$$

where K is a selectable number, and R_{\max} is the maximum range detectable by radar.

Satisfying the conditions cited above, the modulation period must be chosen as

$$T = K * \tau_{\max} < \frac{\Delta R}{V_t} \quad (2.5)$$

The rate of change of frequency or chirp rate α is

$$\alpha = \frac{\Delta F}{T} \quad (2.6)$$

The phase of the transmitted RF signal can be expressed as

$$\phi_1(t) = 2\pi \int_0^t f_1(x) dx \quad (2.7)$$

Assuming that $\phi_0 = 0$ at $t = 0$,

$$\phi_1(t) = 2\pi \left[(f_0 - \frac{\Delta F}{2})t + \frac{\Delta F}{2T}t^2 \right] \quad (2.8)$$

for $0 < t < T$. The transmit signal is given by

$$s_1(t) = a_0 \sin 2\pi \left[\left(f_0 - \frac{\Delta F}{2} \right) t + \frac{\Delta F}{2T} t^2 \right] \quad (2.9)$$

The frequency of the transmitted waveform for the second (down-ramp) section is similarly

$$f_2(t) = f_0 + \frac{\Delta F}{2} - \frac{\Delta F}{T} t \quad (2.10)$$

for $0 < t < T$. Accordingly, the transmitted signal for this section is given by

$$s_2(t) = a_0 \sin 2\pi \left[\left(f_0 + \frac{\Delta F}{2} \right) t - \frac{\Delta F}{2T} t^2 \right] \quad (2.11)$$

The received signal is the transmitted signal delayed in time by the round trip propagation time (τ)

$$s_r(t) = \frac{b_0}{a_0} s_t(t - \tau) \quad (2.12)$$

Where τ is the transit time and for $\tau < t < T$ the received signal becomes

$$s_r(t) = b_0 \sin 2\pi \left[\left(f_0 - \frac{\Delta F}{2} \right) (t - \tau) + \frac{\Delta F}{2T} (t - \tau)^2 \right] \quad (2.13)$$

For a homodyne FMCW radar, the received signal is mixed with the transmitted signal. The beat frequencies are derived as the difference between the transmitted and received frequencies. The beat frequency is sometimes referred to as an

intermediate frequency, although the information is not modulated onto a conventional carrier. The mixer signal for the first segment of the triangular waveform is

$$\begin{aligned}
s_{1b}(t) &= c_0 \cos 2\pi \left[\left(f_0 - \frac{\Delta F}{2} \right) \tau - \frac{\Delta F}{2T} \tau^2 + \frac{\Delta F}{T} \tau t \right] \\
&= c_0 \cos \left[2\pi \left(\frac{\Delta F}{T} \tau \right) t + 2\pi \left(f_0 - \frac{\Delta F}{2} \right) \tau - 2\pi \frac{\Delta F}{2T} \tau^2 \right] \\
&= c_0 \cos [2\pi f_b t + \phi_1]
\end{aligned} \tag{2.14}$$

For the second segment of the triangular waveform, the mixer output beat frequency signal is

$$\begin{aligned}
s_{2b}(t) &= c_0 \cos 2\pi \left[\left(f_0 + \frac{\Delta F}{2} \right) \tau + \frac{\Delta F}{2T} \tau^2 - \frac{\Delta F}{T} \tau t \right] \\
&= c_0 \cos \left[-2\pi \left(\frac{\Delta F}{T} \tau \right) t + 2\pi \left(f_0 + \frac{\Delta F}{2} \right) \tau + 2\pi \frac{\Delta F}{2T} \tau^2 \right] \\
&= c_0 \cos \left[2\pi \left(\frac{\Delta F}{T} \tau \right) t - 2\pi \left(f_0 + \frac{\Delta F}{2} \right) \tau - 2\pi \frac{\Delta F}{2T} \tau^2 \right] \\
&= c_0 \cos [2\pi f_b t + \phi_2]
\end{aligned} \tag{2.15}$$

Equations (2.14) and (2.15) contain term in the form of $ft + \frac{\phi}{2\pi}$ where ϕ_1 and ϕ_2 are phase terms while

$$f_b = \frac{\Delta F}{T} \tau \tag{2.16}$$

is the beat frequency.

Since $\tau = \frac{2R}{c}$ (round trip delay) for a stationary target at a range of R

$$f_b = \frac{2\Delta F}{cT} R. \quad (2.17)$$

If the target is moving with a radial velocity V , the beat frequency for the first segment (up-ramp) is

$$f_{1b} = \frac{2R\Delta F}{cT} - \frac{2V}{\lambda} \quad (2.18)$$

and the beat frequency for the second segment (down-ramp) is

$$f_{2b} = \frac{2R\Delta F}{cT} + \frac{2V}{\lambda} \quad (2.19)$$

where the second terms $\mp \frac{2V}{\lambda}$ are due to the target's Doppler frequency. For multiple targets, multiple beat frequencies would be present and would depend on each target's range and velocity.

Thus knowing the beat frequencies f_{1b} and f_{2b} together with the radar parameters ΔF , T , and the wavelength λ , we can retrieve the range and Doppler information from the return signal by solving equations (2.18) and (2.19) simultaneously for R and V . In this process, the frequency modulation waveform must have equal up-sweep and down-sweep time intervals. FMCW radars often store the beat frequency signal to allow for off-line processing using Fourier transform techniques.

In the case of stationary target, Fast Fourier Transform (FFT) is the mathematical tool used to interpret the spectrum of the beat frequency signal in terms of radar range. In case of moving target, on the other hand, the Spectrogram is the mathematical tool used to interpret the spectrum of the beat frequency signals in terms of radar range and radar Doppler frequency.

In order to use FFT or spectrogram for range and Doppler information the received signal must be sampled. In order to satisfy the Nyquist sampling criterion, the analog-to-digital sampling rate f_s must be at least two times the maximum beat frequency.

$$2f_{b\max} \leq f_s \quad (2.20)$$

$$2\left(\frac{2R_{\max}\Delta F}{cT} + \frac{2V}{\lambda}\right) \leq f_s \quad (2.21)$$

The receiver FFT processing is often matched to the frequency sweep period. This yields spectral samples spaced at the inverse of the sweep period ($\Delta f = 1/T$), corresponding to range spacing equal to the ideal range resolution. Computing the FFT over a modulation period and taking the number of samples as a power of two, we will get

$$T = \frac{N}{f_s} = \frac{2^n}{f_s} \Rightarrow f_s = \frac{2^n}{T} \quad (2.22)$$

In FMCW radar ΔF , and T , are chosen for the required radar operating parameters. After choosing T according to (2.5) FMCW radar operates with the resulting coherent processing interval

$$T_0 = T - \tau_{\max} . \quad (2. 23)$$

The increment along the frequency axis is the inverse of the coherent processing interval

$$\Delta f = \frac{1}{T_0} = \frac{1}{T - \tau_{\max}} \approx \frac{1}{T} \quad (2. 24)$$

For the first section of the triangular waveform, the partial overlap results in a reduced processed bandwidth. The effective bandwidth is

$$\Delta F' = \Delta F (1 - \frac{\tau_{\max}}{T}) \text{ Hz} \quad (2. 25)$$

with an effective time bandwidth product of $T_0 \Delta F'$. The range resolution is also slightly degraded as

$$\Delta R' = \frac{c}{2\Delta F'} = \frac{c}{2\Delta F (1 - \tau_{\max}/T)} \text{ m} \quad (2. 26)$$

The resulting beat frequencies are of the form

$$f'_{1b} = \frac{2R\Delta F'}{cT_0} - \frac{2V}{\lambda} \quad (2. 27)$$

$$f'_{2b} = \frac{2R\Delta F'}{cT_0} + \frac{2V}{\lambda} \quad (2. 28)$$

Then the resulting sampling frequency is of the form

$$2\left(\frac{2R_{\max}\Delta F'}{cT} + \frac{2V}{\lambda}\right) \leq f'_s \quad (2.29)$$

2.3 Advantages of the FSK Radar

Much of the LPI radar technology used today is based on the linear FMCW, with the simplicity of this technology being its main advantage. The FMCW approach spreads the transmitted energy out over the modulation bandwidth to effectively reduce the power spectral density. The main disadvantage is the high sidelobe values that occur in the order of 13 dB down from the peak response.

An LPI radar that uses FH techniques, hops or changes the transmitting frequency in time over a wide bandwidth in order to prevent an unintended receiver from intercepting the waveform. The frequency slots used are chosen from an FH sequence, and it is this unknown sequence that gives the radar the advantage in terms of processing gain. That is, the frequency sequence appears random to the intercept receiver, and so possibility of it following the changes in frequency is remote. This prevents a jammer from reactively jamming the transmitted frequency. In contrast to the FMCW, the FH technique of rapidly changing the transmitter frequency does not lower the power spectrum of the emission, but instead moves the power spectrum density about according to the FH hopping sequence. Consequently, the FH radar has a higher probability of detection than a FMCW waveform, but retains a significantly low probability of interception.

Another advantage of the FH radar is that the range resolution is independent of the hopping bandwidth (unlike that of the FMCW technique). Range resolution in an FH radar depends only on the hop rate. A significant benefit also resides in the secrecy of the FH sequence that is used. FH radar performance depends only slightly on the code used, given that certain properties are met. This allows for a larger variety of

codes, making it more difficult to intercept.

The order in which the frequencies are transmitted significantly affects the ambiguity performance of the signal. The ambiguity function (AF) for FH signals can easily be approximated, because the cross correlation signals at different frequencies approach zero when the frequency difference is large relative to the inverse of the signal duration (or multiples of that inverse) [9]. In a multiple LPI emitter environment, an important requirement is to keep the mutual interference between transmitters as low as possible. Mutual interference occurs when two or more emitters transmit the same frequency slot at the same time. The degree of mutual interference is related to the cross correlation properties of the FH sequences.

2.4 FSK Radar Basics

In an FSK radar, the transmitted frequency f_j is chosen from the FH sequence $\{f_1, f_2, \dots, f_{N_f}\}$ of available frequencies for transmission at a set of consecutive time intervals $\{t_1, t_2, \dots, t_{N_f}\}$. The frequencies are placed in the various time slots corresponding to a binary time-frequency matrix. Each frequency is used once within the code period, with one frequency per time slot and one time slot per frequency. The expression for the complex envelope of the transmitted CW FSK signal is given by

$$s(t) = Ae^{j2\pi f_j t} \quad (2.30)$$

The transmitted waveform has N_f contiguous frequencies within a band B , with each frequency lasting t_p second in duration.

CW FSK radars using multiple frequencies can compute very accurate range measurements. To illustrate, consider a CW radar that transmits the waveform

$$s(t) = A \sin(2\pi f_j t) \quad (2.31)$$

where the received signal from a target at a range R_T is

$$\begin{aligned} s_r(t) &= s(t - t_d) \\ &= A \sin(2\pi f_j (t - t_d)) \\ &= A \sin\left(2\pi f_j t - \frac{4\pi f_j R_T}{c}\right) \\ &= A \sin(2\pi f_j t - \phi_r) \end{aligned} \quad (2.32)$$

Solving for R_T

$$R_T = \frac{c}{4\pi f_j} \phi_r \quad (2.33)$$

The unambiguous range occurs when ϕ_r is maximum or $\phi_r = 2\pi$ and therefore with one frequency, R_T is limited to extremely small values that are not practical [10]. If two frequencies are used

$$s_1(t) = A_1 \sin(2\pi f_1 t) \quad (2.34)$$

and

$$s_2(t) = A_2 \sin(2\pi f_2 t) \quad (2.35)$$

the received signals are

$$s_{r1}(t) = A_1 \sin(2\pi f_1 t - \phi_{T1}) = A \sin\left(2\pi f_1 t - \frac{4\pi f_1 R_T}{c}\right) \quad (2.36)$$

and

$$s_{r2}(t) = A_2 \sin(2\pi f_2 t - \phi_{T2}) = A \sin\left(2\pi f_2 t - \frac{4\pi f_2 R_T}{c}\right) \quad (2.37)$$

After mixing the carrier frequency in the receiver, the phase difference between the two signals is

$$\Delta\phi_T = \frac{4\pi R_T}{c} (f_2 - f_1) = \frac{4\pi R_T}{c} \Delta f \quad (2.38)$$

Since R_T is maximum when $\Delta\phi = 2\pi$, the maximum unambiguous range is

$$R_u = \frac{c}{2\Delta f} \quad (2.39)$$

and is very large since $\Delta f \ll c$. From measurement of the phase difference, $\Delta\phi_T$, the range of the target is then

$$R_T = \frac{c\Delta\phi_T}{4\pi\Delta f} \quad (2.40)$$

This can also be written as a function of just phase difference as

$$R_r = R_u \frac{\Delta\phi_r}{2\pi} \quad (2.41)$$

Since the range to the target depends on the frequency difference, the range resolution then depends on the duration of each frequency as

$$\Delta R = \frac{ct_p}{2} \quad (2.42)$$

The transmitted power for each frequency must be such that the energy content within the target echo is sufficient for detection, and enough to ensure that accurate phase measurements can be made.

In summary, for the FSK CW radar, the frequency difference Δf determines the maximum unambiguous detection range. The target's range is computed by measuring the return signal phase difference from two consecutive transmitted frequencies. The range resolution, ΔR , depends only on the FH period.

2.5 Costas Codes

In a study by J. P. Costas, techniques were presented for generating a sequence of frequencies that produce unambiguous range and Doppler measurements while minimizing the cross talk between frequencies [11]. In general, the Costas sequence of frequencies provides an FH code that produces peak side lobes in the AF, that are down from the main lobe response by a factor of $1/N$, where N is the number of frequencies used in the code, for all regions in the delay-Doppler frequency plane. That is, the order of frequencies in a Costas sequence or array is chosen in a manner to preserve an ambiguity response with a thumbtack nature (the narrow main lobe and side lobes are as low as possible). The firing order of these frequencies based on

primitive roots (elements) of finite fields and explained in Appendix A.

2.5.1 Characteristics of a Costas Array or Sequence

A Costas array or (frequency) sequence f_1, \dots, f_{N_F} is a sequence that is a permutation of the integers $1, \dots, N_F$ satisfying the property

$$f_{k+i} \neq f_{j+i} - f_j \quad (2.43)$$

for every i, j , and k such that $1 \leq k < i < i + j \leq N_F$. An array that results from a Costas sequence in this way is called a Costas array [12]. The nonequivalence condition in (2.43) can be checked easily when the frequency sequence is expressed in an $N_F - 1 \times N_F$ difference triangle. As an added bonus, the difference triangle can also be used to derive the AF. I discuss how to derive Costas sequences in the next section and in Appendix A.

Consider a frequency sequence $f_j = \{2, 4, 8, 5, 10, 9, 7, 3, 6, 1\}$ kHz. Figure 2.2 (a) shows the binary time frequency matrix for this sequence. The frequencies are fired at each t_i and are indicated by a “1” in the matrix. The power spectral density of the signal is shown in Figure 2.2 (b). Also indicated is the firing order for each frequency. If the subperiod t_p (frequency duration) is constant, the cycle density or number of cycles per frequency varies as $t_p f_j$.

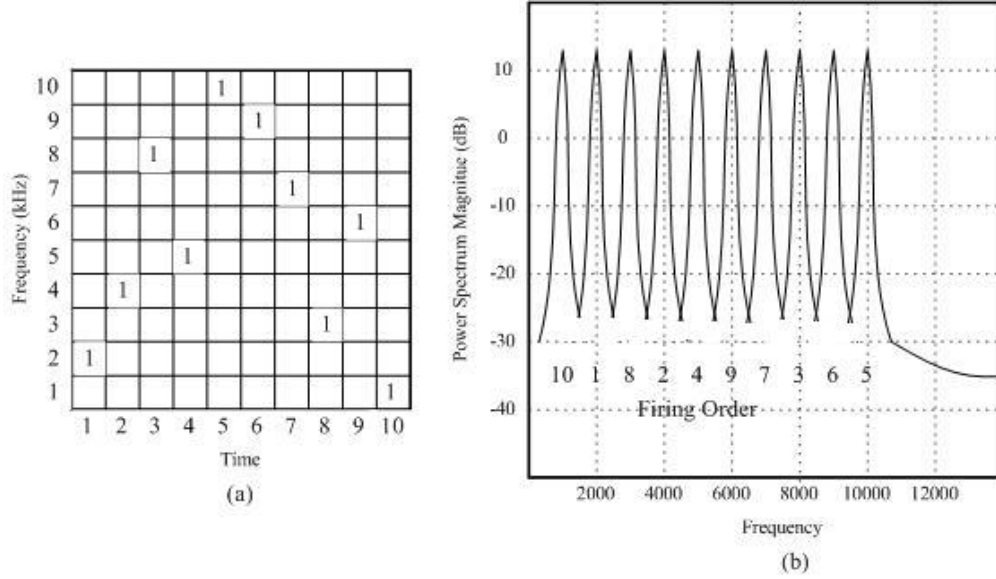


Figure 2. 2: Costas sequence $f_j = \{2, 4, 8, 5, 10, 9, 7, 3, 6, 1\}$ kHz, showing (a) the binary time-frequency matrix, and (b) the power spectrum magnitude for several code periods

2.5.2 Computing the Difference Triangle

The first step to verifying (2.43) and deriving the AF is to form a difference triangle. To form the difference triangle, we start by writing the N_F frequency values in the sequence $(f_j \text{ where } j = 1, \dots, N_F)$ as column headers across the top as illustrated in Figure 2.3. The $N_F - 1$ rows in the difference triangle correspond to the delays, with each row number i representing the delay value. To calculate each cell value in the difference triangle $\Delta_{i,j}$

$$\Delta_{i,j} = f_{j+i} - f_j \quad (2.44)$$

where $i = 1 \dots N_F - 1$, $j = 1 \dots N_F - 1$, and $i + j \leq N_F$. For example, the first row (delay

$i=1$) is formed by taking differences between adjacent frequencies. By (2.44), all results in this row must be unique. The second row in the difference matrix is formed by taking differences between next adjacent terms (delay $i=2$). Results in this row must also be unique. The process is repeated until the $i=N_F-1$ delay is computed. All values of $\Delta_{i,j}$ must be unique within each row, and is the defining criterion of a Costas sequence.

		f_i									
		2	4	8	5	10	9	7	3	6	1
i	1	2	4	-3	5	-1	-2	-4	3	-5	
	2	6	1	2	4	-3	-6	-1	-2		
	3	3	6	1	2	-7	-3	-6			
	4	8	5	-1	-2	-4	-8				
	5	7	3	-5	1	-9					
	6	5	-1	-2	-4						
	7	1	2	-7							
	8	4	-3								
	9	-1									

Figure 2. 3: Difference triangle for a $N_F = 10$ Costas sequence

2.5.3 Deriving the Costas Sequence AF

The AF can be approximated by overlaying the binary time frequency matrix upon itself, and shifting one relative to the other according to a particular delay (horizontal shifts) and a particular Doppler (vertical shifts). At each combination of shifts, the sum of coincidences between points of the fixed and the shifted matrix, represents the relative height of the AF. An easier way to derive the AF is using the difference triangle as shown in Figure 2.4. In Figure 2.4 the AF of the 10-frequency Costas signal is derived from the difference triangle. The AF is constructed by considering each row (delay) in the difference triangle, and placing a “1” in the AF delay-

Doppler cell corresponding to each $\Delta_{i,j}$.

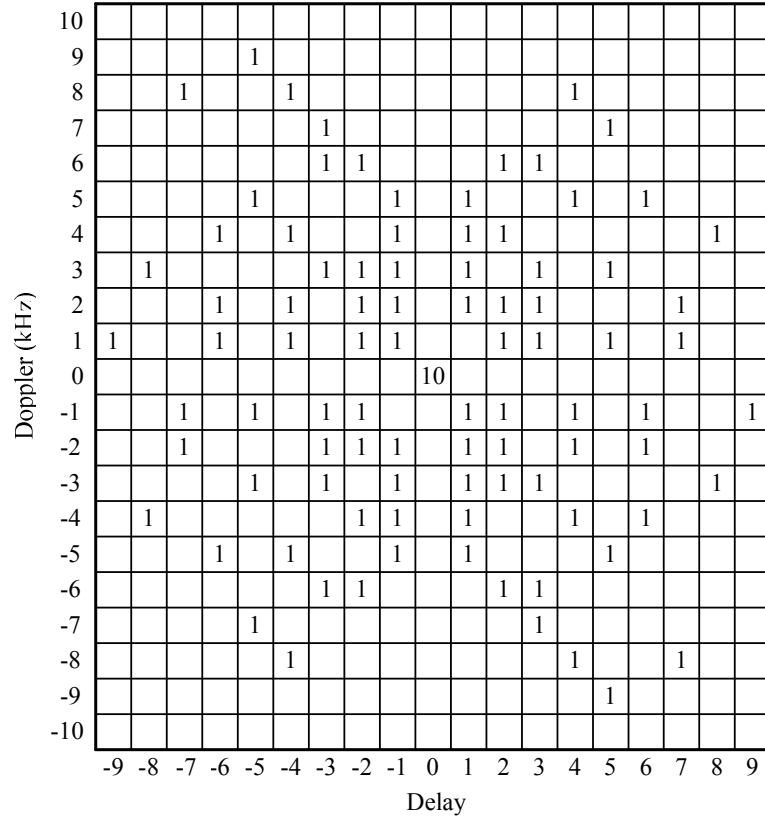


Figure 2. 4: The AF derive from the difference triangle for a $N_F = 10$ Costas sequence

CHAPTER 3

AMBIGUITY FUNCTION

3.1 Introduction

Time-frequency signal representations (TFRs) characterize signals over the time-frequency plane. They thus combine time-domain and frequency-domain analyses to yield a potentially more revealing picture of the temporal localization of a signal's spectral components. They may also serve as a basis for signal synthesis, coding, and processing. In general, TFRs map a one-dimensional signal of time, $x(t)$, into a two-dimensional function of time and frequency, $T_x(t, f)$. The values of the TFR surface above the time-frequency plane give an indication as to which spectral components are present at which times.

TFRs are particularly useful to analyze, modify, and synthesize non-stationary signals. Three dimensional plots of TFR surface have been used as pictorial representations enabling a signal processor to analyze how spectral components of a signal or system vary with time. TFRs are widely used mathematical tools for efficient coding of signals and as a statistics for signal detection and parameter estimation [13].

Ambiguity Function (AF), which is a quadratic TFR, has been used extensively for signal processing in various fields such as radar, sonar, radio astronomy,

communications and optics. In radar signal processing, the problem is the estimation of the range and radial velocity of a moving target where the range is proportional to the round-trip travel time, i.e. the delay time τ , of the radar signal while the radial velocity is proportional to the Doppler frequency shift ν .

In radar, signal estimation is maximized when the receive filter is matched to the transmit waveform. The output of the matched filter is equal to the cross-correlation between the received signal and the transmitted signal, and may be written as

$$Output = \int_{-\infty}^{\infty} s_r(t) s^*(t - \tau) dt \quad (3. 1)$$

where $s_r(t)$ is the received signal, $s(t)$ is the transmitted signal, the asterisk denotes complex conjugation, and τ is the time delay. The transmitted signal can be expressed as

$$s(t) = u(t) e^{j2\pi f_0 t} \quad (3. 2)$$

where $u(t)$ is the complex (baseband) modulation, and f_0 is the carrier frequency. The received signal is assumed to be the same as the transmitted signal except for the time delay τ_0 and a Doppler frequency shift ν and it is given as

$$s_r(t) = u(t - \tau_0) e^{j2\pi(f_0 + \nu)(t - \tau_0)} \quad (3. 3)$$

The output can be determined by substituting equations (3.2) and (3.3) into (3.1). It is customary to set $\tau_0 = 0$ (that is, to “center” the filter response at the target delay) and to set $f_0 = 0$ (that is, to remove the effect of carrier and consider the situation at the

baseband). Assigning the symbol χ to represent the matched filter output, we get

$$\chi(\tau, \nu) = \int_{-\infty}^{\infty} u(t) u^*(t - \tau) e^{j2\pi\nu t} dt \quad (3.4)$$

We see from equation (3.4) that the matched filter response, $\chi(\tau, \nu)$, is obtained by correlating a signal with its Doppler-shifted and time shifted version; that is, $\chi(\tau, \nu)$ is the two dimensional correlation function in delay and Doppler [5] .

The magnitude $|\chi(\tau, \nu)|$ is called the Ambiguity Function that is given as

$$|\chi(\tau, \nu)| = \left| \int_{-\infty}^{\infty} u(t) u^*(t + \tau) \exp(j2\pi\nu t) dt \right| \quad (3.5)$$

The detailed extraction of the Ambiguity Function from the matched filter response is given in Appendix B.

3.2 Main Properties of the Ambiguity Function

The first two properties assume that the energy E of $u(t)$ is normalized to unity.

Property 1: Maximum at (0,0)

$$|\chi(\tau, \nu)| \leq |\chi(0, 0)| = 1 \quad (3.6)$$

This property says that the ambiguity function can nowhere be higher than at the

origin (where it is normalized to unity by normalizing the signal energy).

To prove this property, we apply the Schwarz inequality to the AF squared:

$$\begin{aligned}
|\chi(\tau, v)|^2 &= \left| \int_{-\infty}^{\infty} u(t) u^*(t + \tau) \exp(j2\pi vt) dt \right|^2 \\
&\leq \int_{-\infty}^{\infty} |u(t)|^2 dt \int_{-\infty}^{\infty} |u^*(t + \tau) \exp(j2\pi vt)|^2 dt \\
&= \int_{-\infty}^{\infty} |u(t)|^2 dt \int_{-\infty}^{\infty} |u^*(t + \tau)|^2 dt = E \cdot E = 1 \cdot 1 = 1 \\
\therefore |\chi(\tau, v)|^2 &\leq 1, \quad \therefore |\chi(\tau, v)| \leq 1,
\end{aligned} \tag{3.7}$$

Equality [i.e., $|\chi(\tau, v)|^2 = 1$] will replace the inequality (3.7) when the functions in the two integrals [second expression in (3.7)] are conjugates of each other: namely, when

$$u(t) = [u^*(t + \tau) \exp(j2\pi vt)]^* = u(t + \tau) \exp(-j2\pi vt) \tag{3.8}$$

which obviously happens when $\tau = 0$, $v = 0$. Thus, we can conclude that

$$|\chi(\tau, v)| \leq |\chi(0, 0)| = 1 \tag{3.9}$$

Property2: Constant volume

$$\int_{-\infty}^{\infty} \int_{-\infty}^{\infty} |\chi(\tau, v)|^2 d\tau dv = 1 \tag{3.10}$$

Property 2 states that the total volume under the normalized ambiguity surface

(squared) equals unity, independent of the signal waveform.

Properties 1 and 2 imply that if we attempt to squeeze the ambiguity function to a narrow peak at the origin, the peak can not exceed a value of 1, and the volume squeezed out of that peak must reappear somewhere else.

To prove this property, we rewrite $\chi(\tau, \nu)$, replacing ν with $-f$:

$$\chi(\tau, -f) = \int_{-\infty}^{\infty} [u(t)u^*(t + \tau)] \exp(-j2\pi ft) dt \quad (3.11)$$

which is recognized as the Fourier transform

$$\chi(\tau, -f) = F[\beta(\tau, t)] \quad (3.12)$$

of the function

$$\beta(\tau, t) = u(t)u^*(t + \tau) \quad (3.13)$$

The energy in the time domain is equal to the energy in the frequency domain (Parseval's theorem):

$$\int_{-\infty}^{\infty} |\beta(\tau, t)|^2 dt = \int_{-\infty}^{\infty} |\chi(\tau, -f)|^2 df = \int_{-\infty}^{\infty} |\chi(\tau, \nu)|^2 d\nu \quad (3.14)$$

Integrating both sides with respect to τ yields the volume V under the ambiguity function squared

$$\begin{aligned}
\int_{-\infty}^{\infty} \int_{-\infty}^{\infty} |\beta(\tau, t)|^2 dt d\tau &= \int_{-\infty}^{\infty} \int_{-\infty}^{\infty} |\chi(\tau, -f)|^2 df d\tau \\
&= \int_{-\infty}^{\infty} \int_{-\infty}^{\infty} |\chi(\tau, v)|^2 dv d\tau = V
\end{aligned} \tag{3.15}$$

We will now evaluate the integral on the left-hand side, starting with a change of variables:

$$t = t_1, \quad t + \tau = t_2 \tag{3.16}$$

Using (3.13) and (3.16) in (3.15) yields

$$\int_{-\infty}^{\infty} \int_{-\infty}^{\infty} |u(t)u^*(t + \tau)|^2 dt d\tau = \int_{-\infty}^{\infty} \int_{-\infty}^{\infty} |u(t_1)u^*(t_2)| |\mathbf{J}(t_1, t_2)| dt_1 dt_2 = V \tag{3.17}$$

where the Jacobian is given by

$$\mathbf{J}(t_1, t_2) = \begin{vmatrix} \frac{\partial t_1}{\partial t} & \frac{\partial t_1}{\partial \tau} \\ \frac{\partial t_2}{\partial t} & \frac{\partial t_2}{\partial \tau} \end{vmatrix} = \begin{vmatrix} 1 & 0 \\ 1 & 1 \end{vmatrix} = 1 \tag{3.18}$$

Using (3.18) in (3.17), we get

$$\begin{aligned}
V &= \int_{-\infty}^{\infty} \int_{-\infty}^{\infty} |u(t_1)u^*(t_2)|^2 |1| dt_1 dt_2 \\
&= \int_{-\infty}^{\infty} |u(t_1)|^2 dt_1 \int_{-\infty}^{\infty} |u^*(t_2)|^2 dt_2 = E \cdot E = 1 \cdot 1 = 1
\end{aligned} \tag{3.19}$$

Property 3: Symmetry with respect to the origin

$$|\chi(-\tau, -v)| = |\chi(\tau, v)| \quad (3.20)$$

Property 3 suggests that it is sufficient to study and plot only two adjacent quadrants of the AF. The remaining two can be deduced from the symmetry property.

To prove this property, we set $-\tau$ and $-v$ in the equation for $|\chi(\tau, v)|$:

$$\chi(-\tau, -v) = \int_{-\infty}^{\infty} u(t) u^*(t - \tau) \exp(-j2\pi vt) dt \quad (3.21)$$

and make one change of variable, $t_1 = t - \tau$, which yields

$$\begin{aligned} \chi(-\tau, -v) &= \int_{-\infty}^{\infty} u(t_1 + \tau) u^*(t_1) \exp[-j2\pi v(t_1 + \tau)] dt_1 \\ &= \exp(-j2\pi v\tau) \int_{-\infty}^{\infty} u(t_1 + \tau) u^*(t_1) \exp(-j2\pi vt_1) dt_1 \\ &= \exp(-j2\pi v\tau) \int_{-\infty}^{\infty} u(t + \tau) u^*(t) \exp(-j2\pi vt) dt \end{aligned} \quad (3.22)$$

Because integration is a linear operation, the integral of a conjugate is equal to the conjugate of the integral; hence,

$$\begin{aligned} \chi(-\tau, -v) &= \exp(-j2\pi v\tau) \left[\int_{-\infty}^{\infty} u^*(t + \tau) u(t) \exp(j2\pi vt) dt \right]^* \\ &= \exp(-j2\pi v\tau) \chi^*(\tau, v) \end{aligned} \quad (3.23)$$

Taking the absolute value yields property 3,

$$|\chi(-\tau, -v)| = |\chi(\tau, v)| \quad (3.24)$$

Property 4: Linear FM effect

If a given complex envelope $u(t)$ has an ambiguity function $|\chi(\tau, v)|$: namely,

$$u(t) \Leftrightarrow |\chi(\tau, v)| \quad (3.25)$$

Then adding linear frequency modulation (LFM), which is equivalent to quadratic-phase modulation, implies that

$$u(t) \exp(j\pi k t^2) \Leftrightarrow |\chi(\tau, v - k\tau)| \quad (3.26)$$

Property 4 says that adding LFM modulation shears the resulting ambiguity function. The meaning of the shear will be demonstrated following the proof of property 4. This important property is the basis for an important pulse compression technique.

To prove this property, we define a new complex envelope, in which quadratic phase was added to the original envelope $u(t)$:

$$u_1(t) = u(t) \exp(j\pi k t^2) \quad (3.27)$$

The ambiguity function of $u_1(t)$,

$$u_1(t) \Leftrightarrow |\chi_l(\tau, v)| \quad (3.28)$$

is what we look for. This new ambiguity function (without the absolute value) is

$$\begin{aligned}
\chi_l(\tau, \nu) &= \int_{-\infty}^{\infty} u_l(t) u_l^*(t + \tau) \exp(j2\pi \nu t) dt \\
&= \int_{-\infty}^{\infty} u(t) \exp(j\pi k t^2) u^*(t + \tau) \exp[-j\pi k(t + \tau)^2] \exp(j2\pi \nu t) dt \quad (3.29) \\
&= \exp(-j\pi k \tau^2) \int_{-\infty}^{\infty} u(t) u^*(t + \tau) \exp[j2\pi(\nu - k\tau)t] dt \\
&= \exp(-j\pi k \tau^2) \chi(\tau, \nu - k\tau)
\end{aligned}$$

Taking the absolute value, we get property 4:

$$|\chi_l(\tau, \nu)| = |\chi(\tau, \nu - k\tau)| \quad (3.30)$$

3.3 Cuts Through the Ambiguity Function

Some insight into the two-dimensional ambiguity function (AF) can be obtained from its one-dimensional cuts. Consider the first cut along the delay axis. Setting $\nu = 0$ in (3.5) gives

$$|\chi(\tau, 0)| = \left| \int_{-\infty}^{\infty} u(t) u^*(t + \tau) dt \right| = |R(\tau)| \quad (3.31)$$

where $R(\tau)$ is the autocorrelation function (ACF) of $u(t)$. We got that zero-Doppler cut of the AF, known as the range window for a matched-filter receiver, is the ACF. On the other hand, the ACF equals the inverse Fourier transform of the power spectral density. Thus, we get the relationship

$$\text{range window} \Leftrightarrow \text{autocorrelation} \Leftrightarrow \mathbf{F}^{-1}\{\text{power spectrum}\}$$

The second interesting cut is along the Doppler frequency axis. Setting $\tau = 0$ in (3.5) results in

$$|\chi(0, \nu)| = \left| \int_{-\infty}^{\infty} |u(t)|^2 \exp(j2\pi\nu t) dt \right| \quad (3.32)$$

Equation (3.32) says that the zero-delay cut is the Fourier transform of the magnitude squared of the complex envelope $u(t)$. In other words, this cut is indifferent to any phase or frequency modulation in $u(t)$; it is a function only of the amplitude.

CHAPTER 4

TARGET DETECTION WITH AMBIGUITY FUNCTION AND CONVENTIONAL FFT METHOD

4.1 Construction of Complex Envelopes of Radar Signals for Ambiguity Function Process

Recall ambiguity function equation (3.5) from chapter 3. We can write this equation as:

$$|\chi(\tau, \nu)| = \left| \int_{-\infty}^{\infty} u_1(t) u_2^*(t + \tau) \exp(j2\pi \nu t) dt \right| \quad (4.1)$$

For auto-ambiguity function $u_1(t)$ and $u_2(t)$ is taken as the complex envelope of the transmitted signal. For cross-ambiguity function $u_1(t)$ is taken as the complex envelope of the transmitted signal and $u_2(t)$ is taken as the complex envelope of the received signal.

The resolution capabilities for a given waveform can be examined through the use of the auto-ambiguity function. The ability of a signal to resolve a target can be estimated based on the width of the main lobe of the auto-ambiguity function. The sidelobes of this function will also help determine how well a signal can resolve

multiple targets, or a target within a noisy environment [6].

The cross-ambiguity function is used in sonar and radar systems to locate a signal with an unknown time delay and Doppler shift. In an active surveillance system where a signal is transmitted and returns with additive noise, the time delay corresponds to range and Doppler shift corresponds to the line of sight target velocity. Provided that the Doppler effect can be approximated by a frequency shift, the presence of a target is indicated by a prominent peak in the cross-ambiguity function [14].

When the operation is cross-ambiguity, the additive noises associated with $u_1(t)$ and $u_2(t)$ are usually independent and do not correlate at any values of τ, ν . Then ambiguity function provides ambiguity lobes characteristic of only the signal component, along with an additive random component that limits the accuracy of estimation of the τ, ν values at which the lobe peaks. When the operation is an auto-ambiguity, so that $u_1(t)$ and $u_2(t + \tau)$ represent output from a single receiver, both the signal and noise components have an auto-ambiguity lobe that peaks at $\tau = 0, \nu = 0$ [15].

For using auto-ambiguity and cross-ambiguity function with FMCW radar waveform we must model transmitted and received signal's complex envelopes. In appendix B from equation (B.1) a bandpass signal can be written in several forms and the basic representation is

$$s(t) = g(t) \cos[\omega_c t + \phi(t)] \quad (4.2)$$

where $g(t)$ is the natural envelope of $s(t)$ and $\phi(t)$ is the instantaneous phase. In

appendix B from equation (B.2) another form is

$$s(t) = g_c(t) \cos \omega_c t - g_s(t) \sin \omega_c t \quad (4.3)$$

where $g_c(t)$ and $g_s(t)$ are in-phase and quadrature components, respectively, given by

$$\begin{aligned} g_c(t) &= g(t) \cos \phi(t) \\ g_s(t) &= g(t) \sin \phi(t) \end{aligned} \quad (4.4)$$

In appendix B from equation (B.5) the complex envelope $u(t)$ of the signal $s(t)$ is defined as

$$u(t) = g_c(t) + jg_s(t) \quad (4.5)$$

Let take $g(t) = 1$

$$u(t) = \cos \phi(t) + j \sin \phi(t) = e^{j\phi(t)} \quad (4.6)$$

In FMCW radar for triangular waveform modulation the transmitting signal is defined by frequency expression. From frequency expression of the signal the instantaneous phase is found and from the instantaneous phase the signal is generated.

Recall from equation (2.1) frequency of the transmitted waveform for the first section is

$$f_1(t) = f_0 - \frac{\Delta F}{2} + \frac{\Delta F}{T}t \quad (4.7)$$

Recall from equation (2.10) frequency of the transmitted waveform for the second section is

$$f_2(t) = f_0 + \frac{\Delta F}{2} - \frac{\Delta F}{T}t \quad (4.8)$$

For the remaining part of the analysis, only the first section of the transmitted waveform is considered. Second section of the transmitted waveform can be extracted easily.

Recall from the equation (2.8) the phase of the transmitted signal is

$$\phi(t) = 2\pi \left[\left(f_0 - \frac{\Delta F}{2} \right) t + \frac{\Delta F}{2T} t^2 \right] \quad (4.9)$$

Then recall from equation (2.9), the transmitted signal is given by,

$$s(t) = a_0 \cos 2\pi \left[\left(f_0 - \frac{\Delta F}{2} \right) t + \frac{\Delta F}{2T} t^2 \right] \quad (4.10)$$

If we rearrange equation (4.10), the transmitted signal can be written as

$$s(t) = a_0 \cos \left[2\pi f_0 t + 2\pi \left(-\frac{\Delta F}{2} t + \frac{\Delta F}{2T} t^2 \right) \right] \quad (4.11)$$

If we look at equations (4.2) and (4.11) they are the same expressions with

$$\begin{aligned}\omega_c &= 2\pi f_0 \\ \phi(t) &= 2\pi\left(-\frac{\Delta F}{2}t + \frac{\Delta F}{2T}t^2\right)\end{aligned}\tag{4.12}$$

Then from equation (4.6) we can write complex envelope of the transmitted waveform as

$$u(t) = \exp\left[j2\pi\left(-\frac{\Delta F}{2}t + \frac{\Delta F}{2T}t^2\right)\right]\tag{4.13}$$

In FMCW radar for triangular waveform modulation f_d Doppler shifted and t_d delayed received signal's frequency can be modeled as

$$f_r(t) = f_0 + f_d - \frac{\Delta F}{2} + \frac{\Delta F}{T}(t - t_d)\tag{4.14}$$

The phase of the received signal is

$$\phi_r(t) = 2\pi\left[\left(f_0 + f_d - \frac{\Delta F}{2} - \frac{\Delta F}{T}t_d\right)t + \frac{\Delta F}{2T}t^2\right]\tag{4.15}$$

Then the received signal is

$$s_r(t) = a_0 \cos\left[2\pi f_0 t + 2\pi\left(f_d t - \frac{\Delta F}{2}t - \frac{\Delta F}{T}t_d t + \frac{\Delta F}{2T}t^2\right)\right]\tag{4.16}$$

From equation (4.16) the complex envelope of the received signal can be written as

$$u_r(t) = \exp \left[j2\pi \left(f_d t - \frac{\Delta F}{2} t - \frac{\Delta F}{T} t_d t + \frac{\Delta F}{2T} t^2 \right) \right] \quad (4.17)$$

Construction of complex envelope of Costas signal is the same as the FMCW signal. From frequency expressions of the transmitted and received Costas signals, instantaneous phase expressions are extracted and with the instantaneous phase and frequency expressions complex envelope of the Costas signal is constructed.

4.2 Construction of Modified Costas Signal

A Costas array [11] is an $N \times N$ binary array, filled with N "ones" and $N(N-1)$ "zeros." There is exactly one "1" in each row and in each column.

In a Costas signal the N rows of the array represent N frequencies spaced Δf apart, and the N columns represent N contiguous subpulses ("bits"), each of duration t_b . A 1 in the (i, j) element of the array indicates that during the j th time interval the i th frequency is transmitted. A Costas signal dictates a specific relationship between the frequency spacing and the bit duration

$$\Delta f = \frac{1}{t_b} \quad (4.18)$$

This crucial relationship results in orthogonality between the different frequencies, when the integration time is equal to t_b .

Lower frequency spacing ($\Delta f < 1/t_b$) degrades the delay resolution. The AF main lobe widens. Higher frequency spacing ($\Delta f > 1/t_b$) narrows the AF mainlobe (because the signal bandwidth has increased) but results in additional high AF peaks

within the delay interval $-t_b < \tau < t_b$, known as grating lobes. When

$$\Delta f = a / t_b, \quad a > 1 \quad (4.19)$$

the grating lobe(s) appear at

$$\tau_g = \pm g \frac{t_b}{a}, \quad g = 1, 2, \dots, \lfloor a \rfloor \quad (4.20)$$

where $\lfloor a \rfloor$ indicates the largest integer smaller than a .

Figure 4.1 shows the Costas signal parameters for the relationship in equation (4.1) i.e., frequency spacing equals the inverse of the sub-code period, and Figure 4.2 and Figure 4.3 shows the resulting Ambiguity Function diagrams.

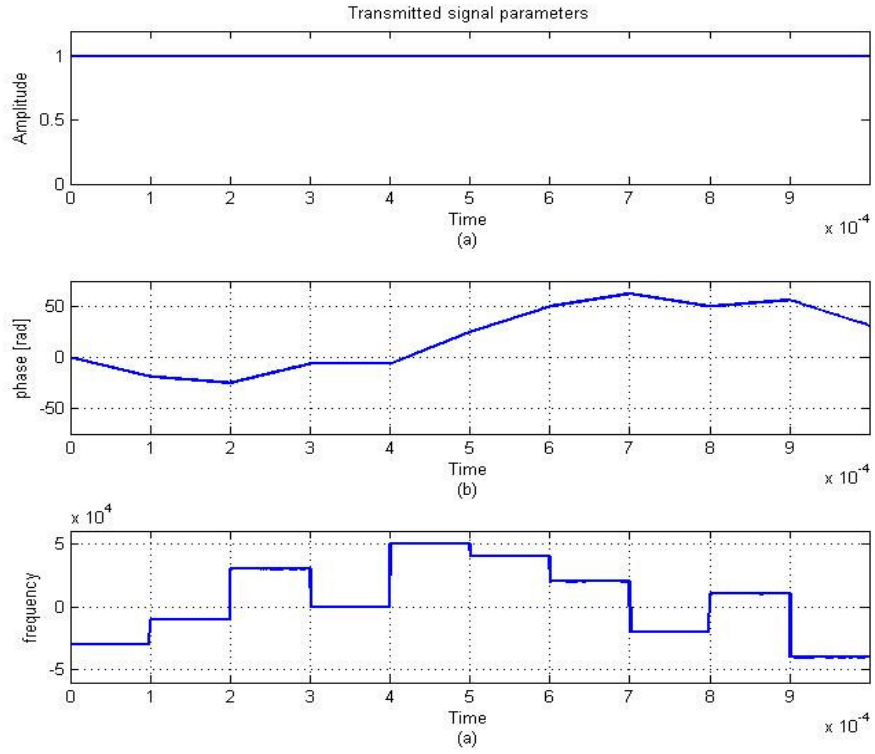


Figure 4. 1: (a) amplitude (b) phase (c) frequency parameters of $N=10$ $t_b = 1$ ms, and $\Delta f = 10$ kHz Costas signal

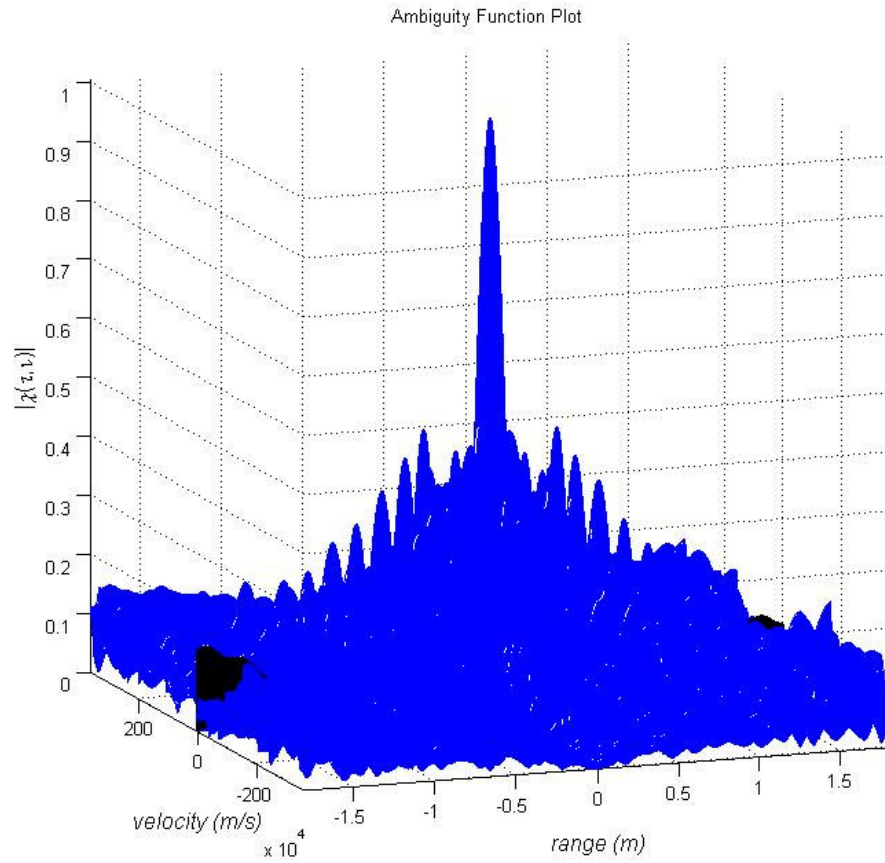


Figure 4. 2: 3-D Ambiguity Function plot of the $N=10$ $t_b = 1$ ms, and $\Delta f = 10$ kHz Costas signal

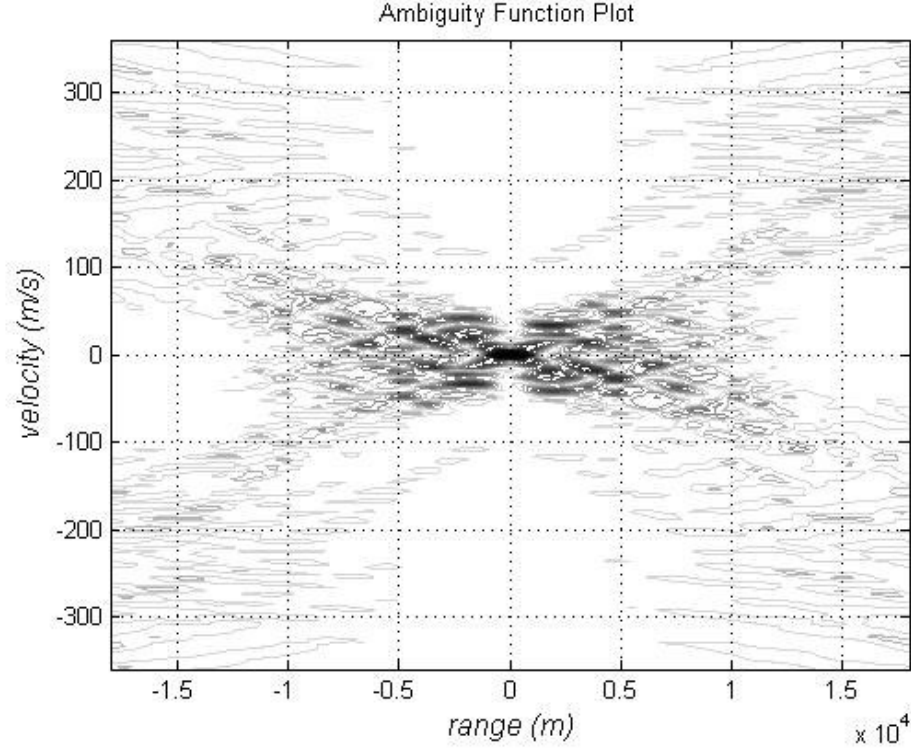


Figure 4. 3: 2-D Ambiguity Function plot of the $N=10$ $t_b = 1$ ms, and $\Delta f = 10$ kHz Costas signal

From Figure 4.2 and Figure 4.3 we can see that with these parameters the AF has a very large mainlobe. AF mainlobe gets smaller with the increase of Δf but it results additional grating lobes, as demonstrated in the next example with $\Delta f = 50$ kHz.

Figure 4.4 shows the Costas signal parameters for the relationship in equation (4.2) i.e., frequency spacing is larger than the inverse of the sub-code period, and Figure 4.5 and Figure 4.6 shows the resulting Ambiguity Function diagrams.

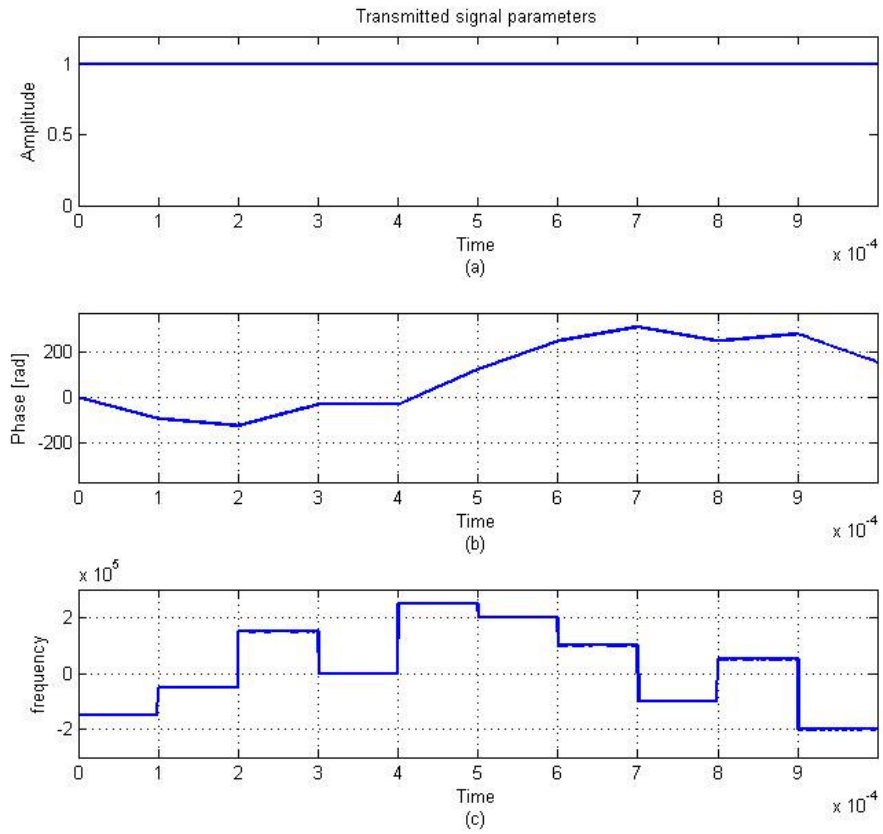


Figure 4. 4: (a) amplitude (b) phase (c) frequency parameters of $N=10$ $t_b = 1$ ms, and $\Delta f = 50$ kHz Costas signal

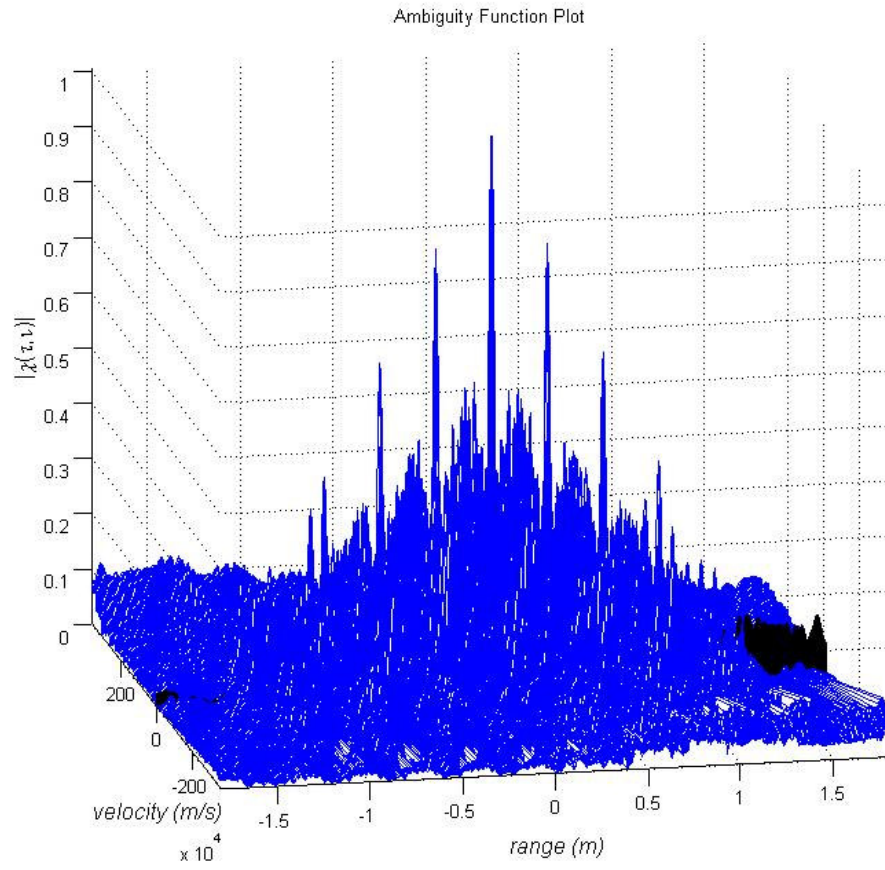


Figure 4. 5: 3-D Ambiguity Function plot of the $N=10$ $t_b = 1$ ms, and $\Delta f = 50$ kHz Costas signal

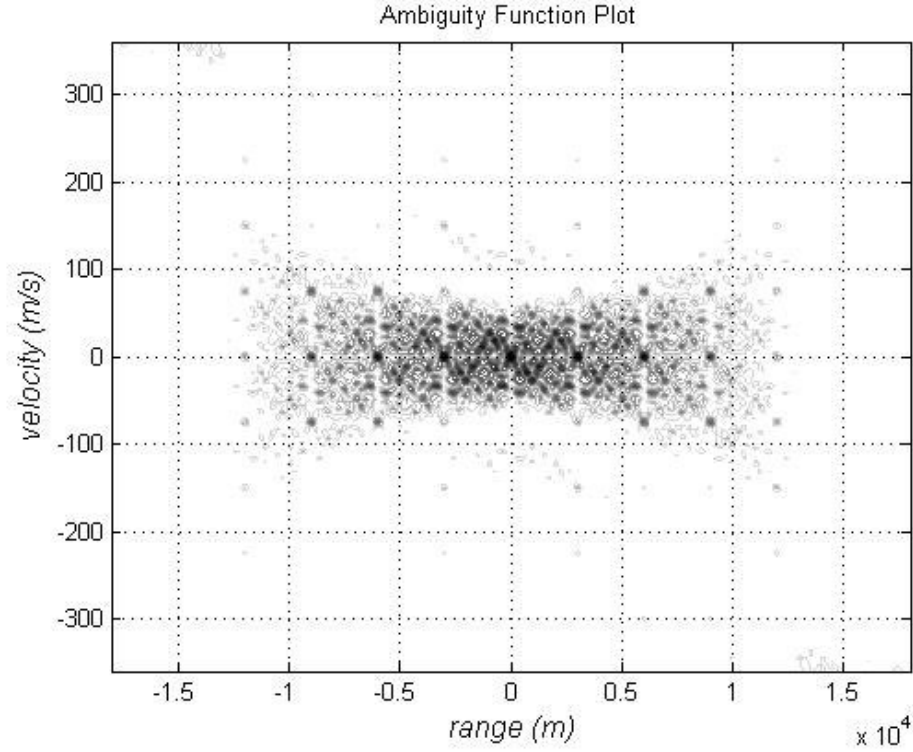


Figure 4. 6: 2-D Ambiguity Function plot of the $N=10$ $t_b = 1$ ms, and $\Delta f = 50$ kHz Costas signal

From Figure 4.5 and Figure 4.6 we can see that with these parameters AF has a smaller mainlobe but the penalty is the grating lobes. To nullify grating lobes while maintaining smaller mainlobe we add LFM to each frequency of the Costas signal as shown in Figure 4.7 (c). The bandwidth of the LFM is arranged by the each pulse duration that is inverse of the pulse duration. By this method we obtain the modified Costas signal [16].

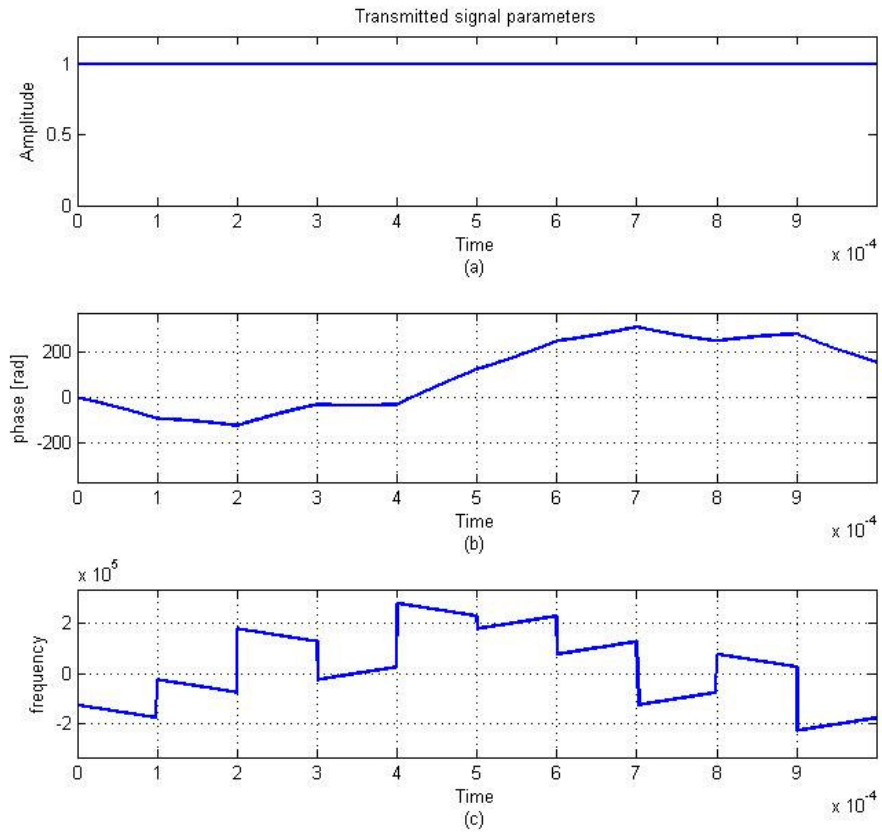


Figure 4. 7: (a) amplitude (b) phase (c) frequency parameters of $N=10$ $t_b = 1$ ms, and $\Delta f = 50$ kHz modified Costas signal

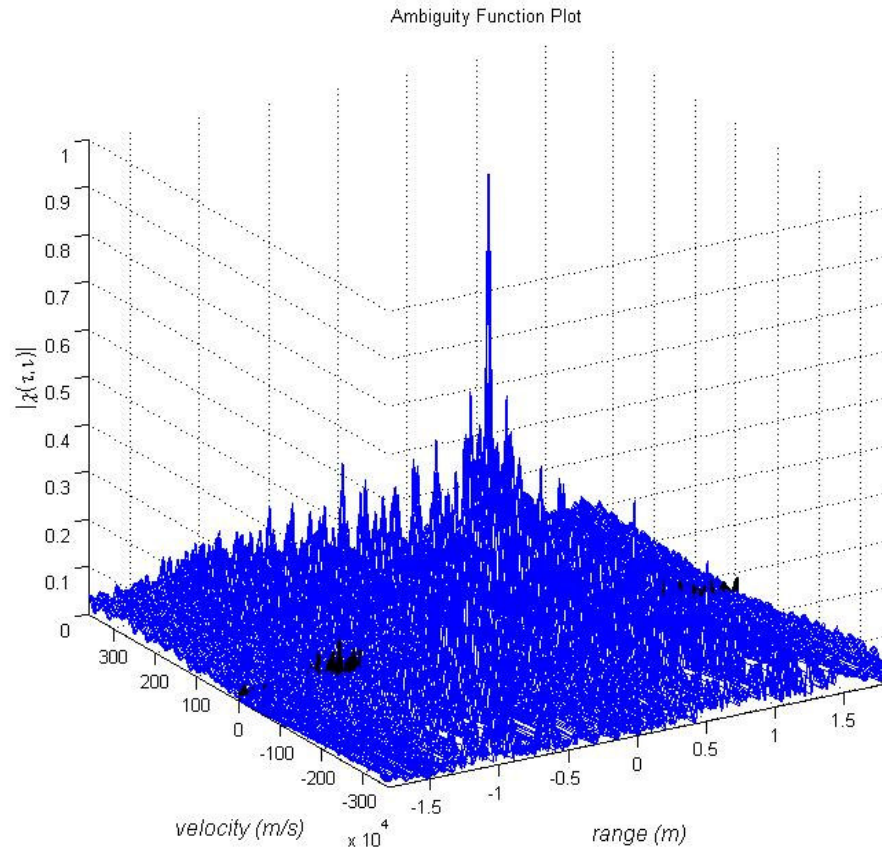


Figure 4. 8: 3-D Ambiguity Function plot of the $N=10$ $t_b = 1$ ms, and $\Delta f = 50$ kHz modified Costas signal

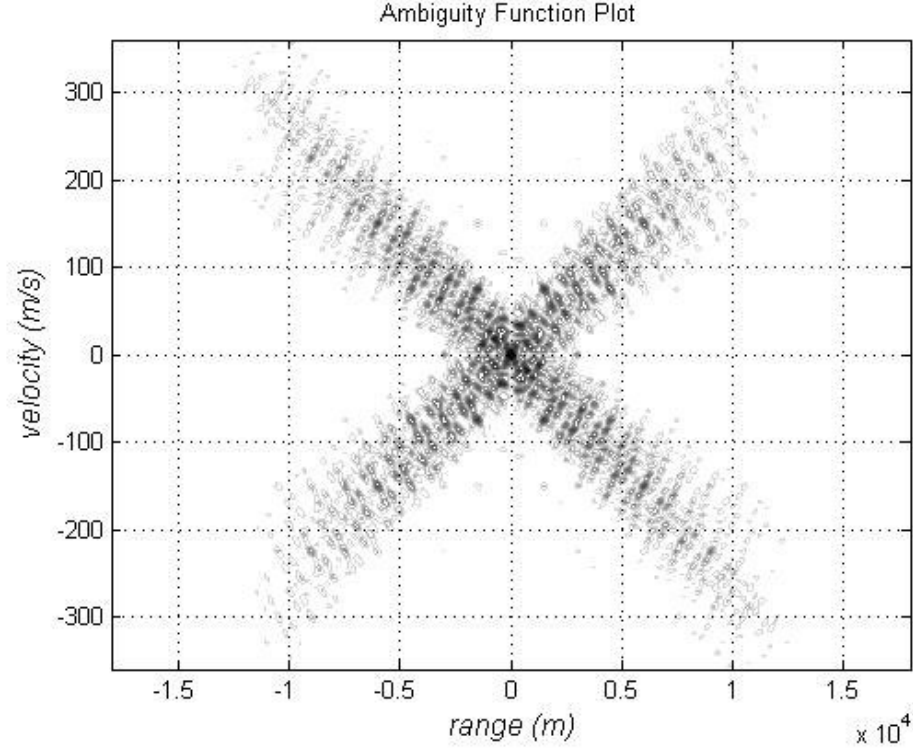


Figure 4. 9: 2-D Ambiguity Function plot of the $N=10$ $t_b = 1$ ms, and $\Delta f = 50$ kHz modified Costas signal

From Figure 4.8 and Figure 4.9 we can see that by the modified Costas signal we eliminate the grating lobes while maintaining the smaller mainlobe. In this thesis for analysis and simulations with Costas coding techniques modified Costas signal with $N=40$ is used.

4.3 Simulations

In this thesis unless otherwise stated simulations with FMCW coding technique are carried on with the following radar parameters for both Ambiguity Function and

conventional FFT method.

Maximum range: 15000 m.

Maximum velocity: 300 m/s.

Radar carrier frequency (f_0): 20 GHz.

FMCW modulation bandwidth (ΔF): 20 MHz.

FMCW modulation period (T): 1 ms.

In this thesis unless otherwise stated simulations with Costas coding technique are carried on with the following radar parameters.

Maximum range: 15000 m.

Maximum velocity: 300 m/s.

Radar carrier frequency (f_0): 20 GHz.

Costas code frequency number (N): 40.

Costas code frequency separation (Δf): 200 kHz.

Costas code modulation period (T): 1 ms.

4.3.1 Radar Resolution with Auto-Ambiguity Function

The Doppler and range resolution values of a radar signal can be found by using the

Auto-Ambiguity function. For Auto-Ambiguity function calculation, complex envelope of the transmitted signal is constructed and used for both $u_1(t)$ and $u_2(t)$ in equation (4.1).

4.3.1.1 Radar Resolution with FMCW Coding Technique

A simple simulation of radar resolution by using Auto-Ambiguity function technique with FMCW coding technique can be accomplished as follows.

Step 1: Generate frequency expression for the FMCW Transmitted waveform (see Figure 4.10 (c)).

Step 2: Generate phase expressions for the transmitted waveforms by using frequency expressions obtained in Step 1 above (see Figure 4.10 (b)).

Step 3: Generate complex envelopes for the transmitted waveform by using their frequency and phase expressions obtained in Step 1 and in Step 2 above, respectively.

Step 4: Compute the Auto-Ambiguity function by using transmitted waveform complex envelope obtained in Step 3 above and display the result to visualize the radar resolution values.

Simulation 1: Radar resolution values with FMCW coding technique

Figure 4.10 shows the transmitted signal parameters (amplitude, phase and frequency) of FMCW coded radar and Figure 4.11 and Figure 4.12 shows the resulting Auto-Ambiguity Function from this transmitted signal.

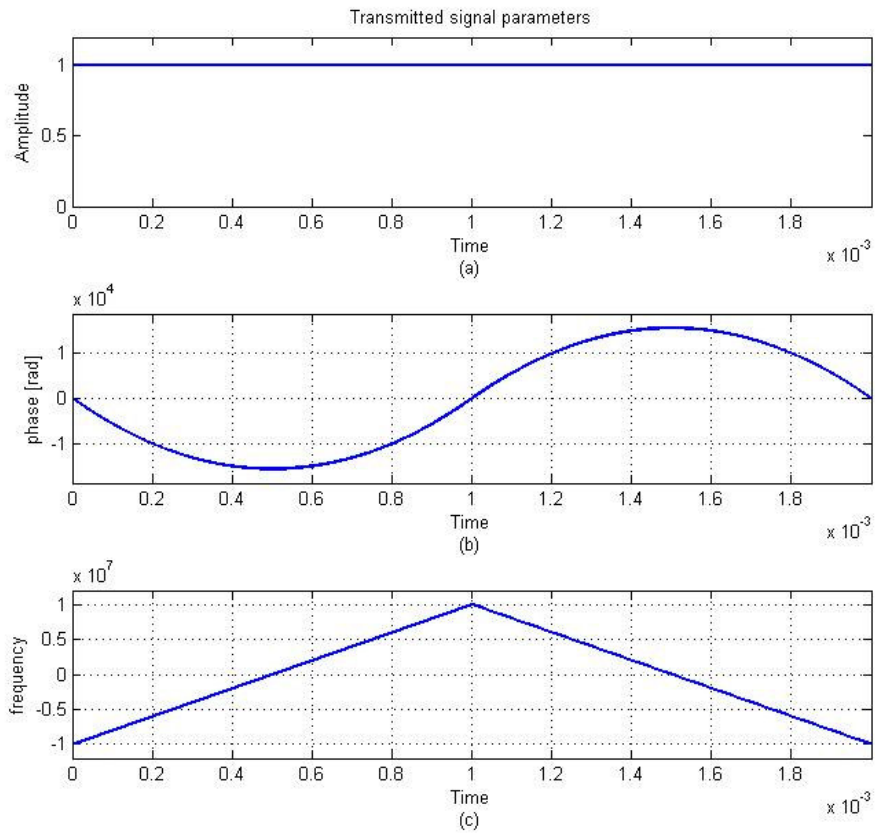


Figure 4. 10: (a) amplitude, (b) phase, and (c) frequency parameters of the transmitted signal with FMCW coding with triangular waveform used in the Auto-Ambiguity function calculation.

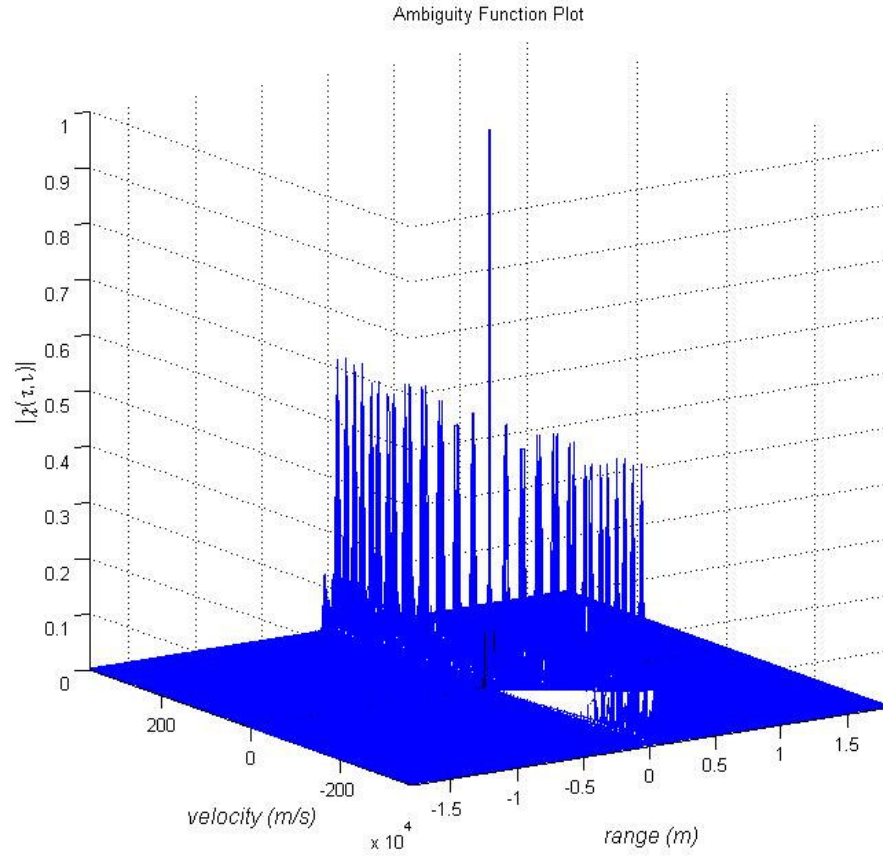


Figure 4. 11: 3-D Auto-Ambiguity function plot of FMCW coding technique

In Figure 4.11 the main lobe at the center of the graph gives the Doppler and range resolution values of the radar for the modulation technique and signal waveform used in the radar. In our case FMCW coding technique with triangular waveform modulation is used. Sidelobes in Figure 4.11 gives an idea for the false targets. Figure 4.12 gives a closer look in 2-D for the main lobe values.

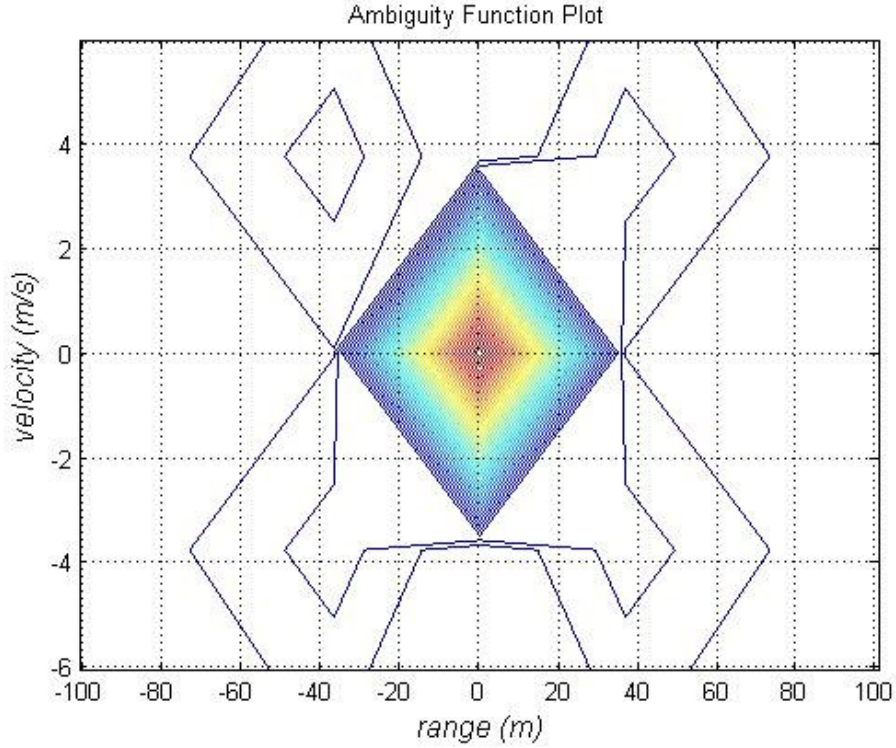


Figure 4. 12: 2-D Auto-Ambiguity function plot of FMCW coding technique

From Figure 4.12, Doppler resolution is extracted about 7 m/s and range resolution is extracted about 70 m for the radar with the operating parameters given in section 4.3, using FMCW coding technique with triangular waveform modulation.

4.2.1.2 Radar Resolution with Costas Coding Technique

A simple simulation of radar resolution by using Auto-Ambiguity function technique with Costas coding technique can be accomplished as follows.

Step 1: Generate frequency expression for the Costas coded transmitted waveform

(see Figure 4.13 (c)).

Step 2: Generate phase expressions for the transmitted waveforms by using frequency expressions obtained in Step 1 above (see Figure 4.13 (b)).

Step 3: Generate complex envelopes for the transmitted waveform by using their frequency and phase expressions obtained in Step 1 and in Step 2 above, respectively.

Step 4: Compute the Auto-Ambiguity function by using transmitted waveform complex envelope obtained in Step 3 above and display the result to visualize the radar resolution values.

Simulation 2: Radar resolution values with Costas coding technique

Figure 4.13 shows the transmitted signal parameters (amplitude, phase and frequency) of Costas coded radar and Figure 4.14 and Figure 4.15 shows the resulting Auto-Ambiguity Function from this transmitted signal.

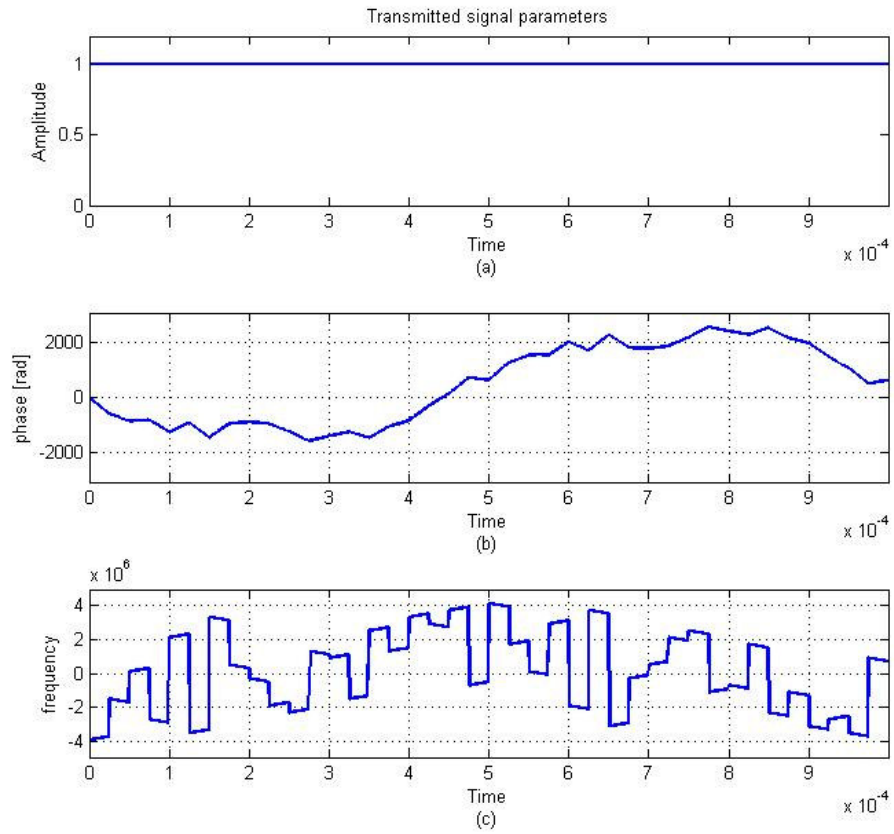


Figure 4. 13: (a) amplitude, (b) phase, and (c) frequency parameters of the transmitted signal with Costas coding used in the Auto-Ambiguity function calculation.

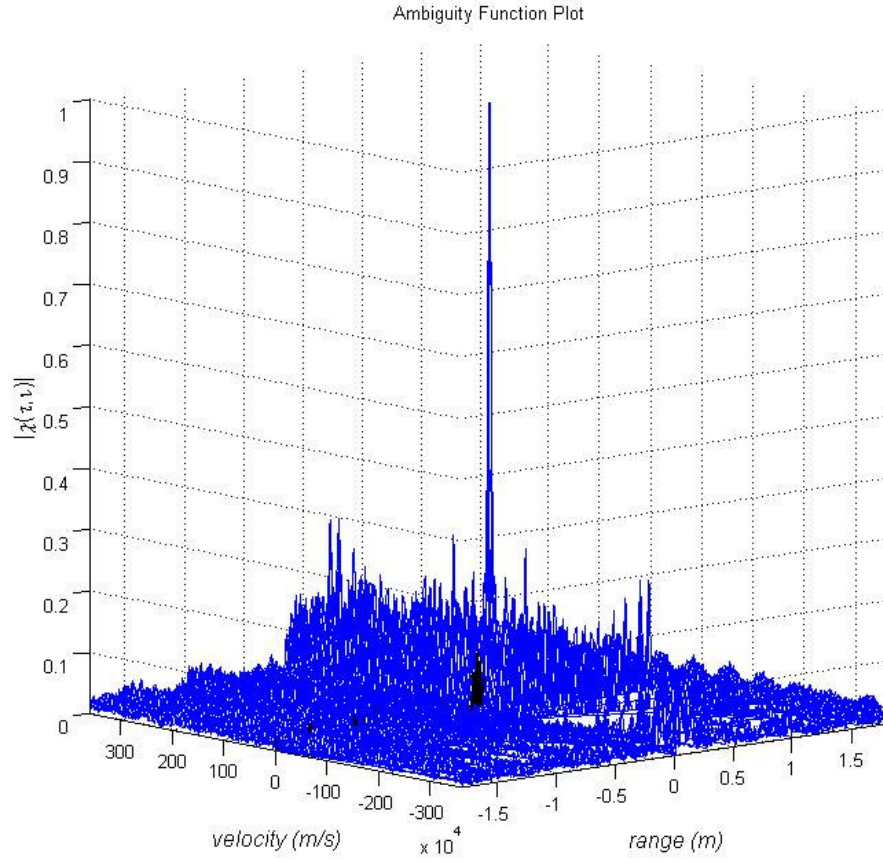


Figure 4. 14: 3-D Auto-Ambiguity function plot of Costas coding technique

In Figure 4.14 the main lobe at the center of the graph gives the Doppler and range resolution values of the radar for the modulation technique and signal waveform used in the radar. In our case Costas coding technique is used. Sidelobes in Figure 4.11 gives an idea for the false targets. Figure 4.15 gives a closer look in 2-D for the main lobe values.

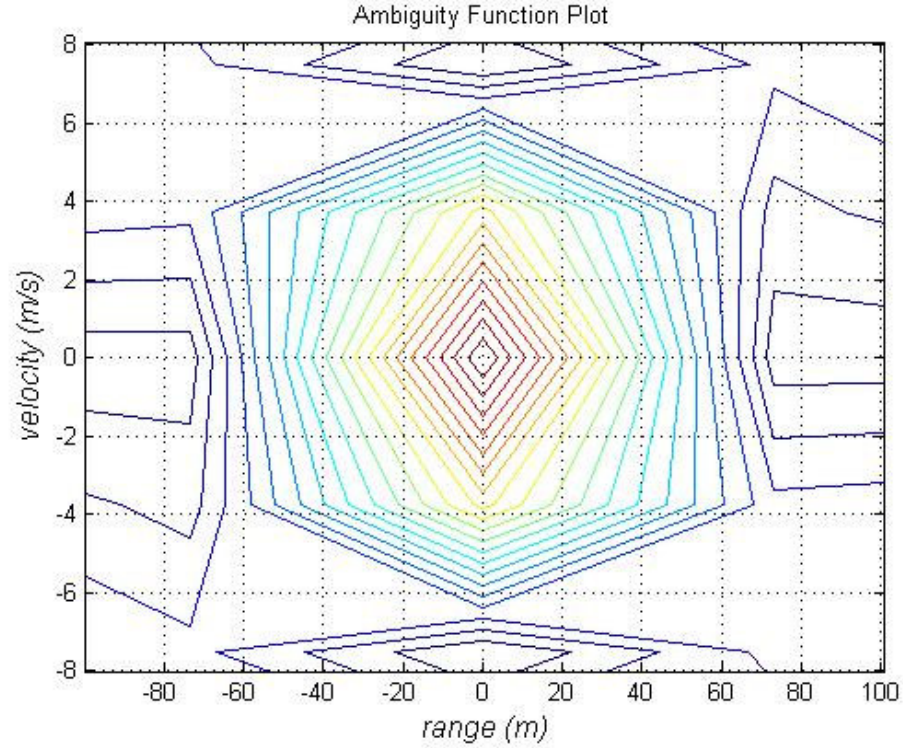


Figure 4. 15: 2-D Auto-Ambiguity function plot of Costas coding technique

From Figure 4.15, Doppler resolution is extracted about 12 m/s and range resolution is extracted about 120 m for the radar with the operating parameters given in section 4.3, using Costas coding technique with triangular waveform modulation.

From Auto-Ambiguity analysis of FMCW and Costas coding techniques we saw that FMCW coded radar has better resolution values than the Costas coded radar under the given operating parameters in section 4.3. But Costas coded radar has lower sidelobes than FMCW coded radar so Costas coded radar is robust than FMCW radar for the false targets.

4.3.2 Target Detection Scenarios

In this thesis for target detection conventional FFT method and Cross-Ambiguity function method are used. Using of Cross-Ambiguity function for target detection in the context of frequency modulation is firstly examined by this thesis on the open literature.

In conventional FFT method the range and the velocity information of the target is extracted from the mixing of the transmitted and received signal frequencies.

In Cross-Ambiguity function method the range and the velocity information of the target is extracted from the some kind of correlation process of the transmitted and received signal complex envelopes. For Cross-Ambiguity function calculation complex envelope of the transmitted signal is constructed and used as $u_1(t)$ in equation (4.1) and complex envelope of the received signal is constructed and used as $u_2(t)$ in equation (4.1).

4.3.2.1 Stationary Target Scenarios

4.3.2.1.1 Use of Conventional FFT Method in Stationary Target Scenario

A simple simulation of a FMCW Radar system using conventional FFT method with a stationary target can be accomplished as follows.

Step 1: Generate a FMCW Transmitted waveform.

Step 2: Introduce a delay (τ) to the transmitted waveform to obtain the received

waveform, under stationary target assumption.

Step 3: Multiply the transmitted and the received waveforms to obtain the mixer output signal.

Step 4: Pass the mixer output waveform through a low pass filter to obtain the low frequency sinusoidal signal component with beat frequency.

Step 5: Compute the FFT of the filtered output obtained in Step 4 above and display the result to visualize the beat frequency as shown in Figure 4.17.

Simulation 3: A stationary target at range $R = 10000$ meter away from the radar.

Figure 4.16 shows the theoretical beat frequency which is obtained by directly subtracting transmitted signal frequency from received signal frequency and Figure 4.17 shows the FFT of resulting mixer output.

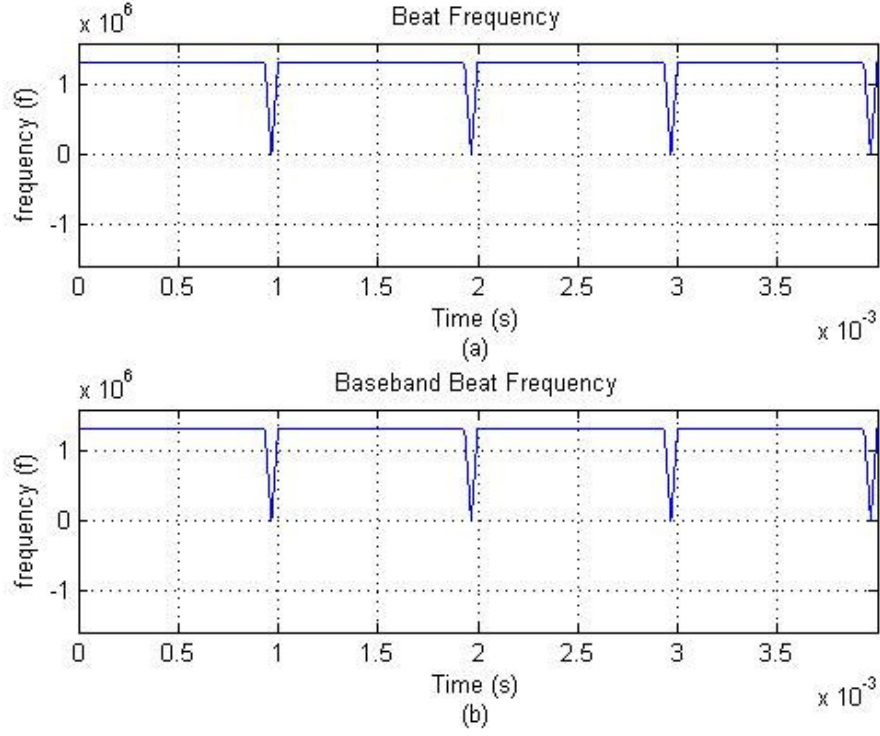


Figure 4. 16: Beat frequency of a stationary target (a) beat frequency extracted from RF signal (b) beat frequency extracted from baseband signal

For this simulation transmitted waveform is constructed in two different ways. First the transmitted waveform is constructed using (2.1) and (2.10) keeping the center frequency f_0 in the expressions. Then, secondly the transmitted waveform is constructed completely in the baseband by the following equations

$$f_1(t) = -\frac{\Delta F}{2} + \frac{\Delta F}{T}t \quad (4.21)$$

$$f_2(t) = \frac{\Delta F}{2} - \frac{\Delta F}{T}t \quad (4.22)$$

The beat frequency plots resulting for these two cases are shown in parts (a) and (b) of Figure 4.16. It is observed that both for the RF case and for the baseband case the resulting beat frequency is the same and measured as 1.338 MHz. Then, using (2.17) we can calculate the range of the target as 10035 meters.

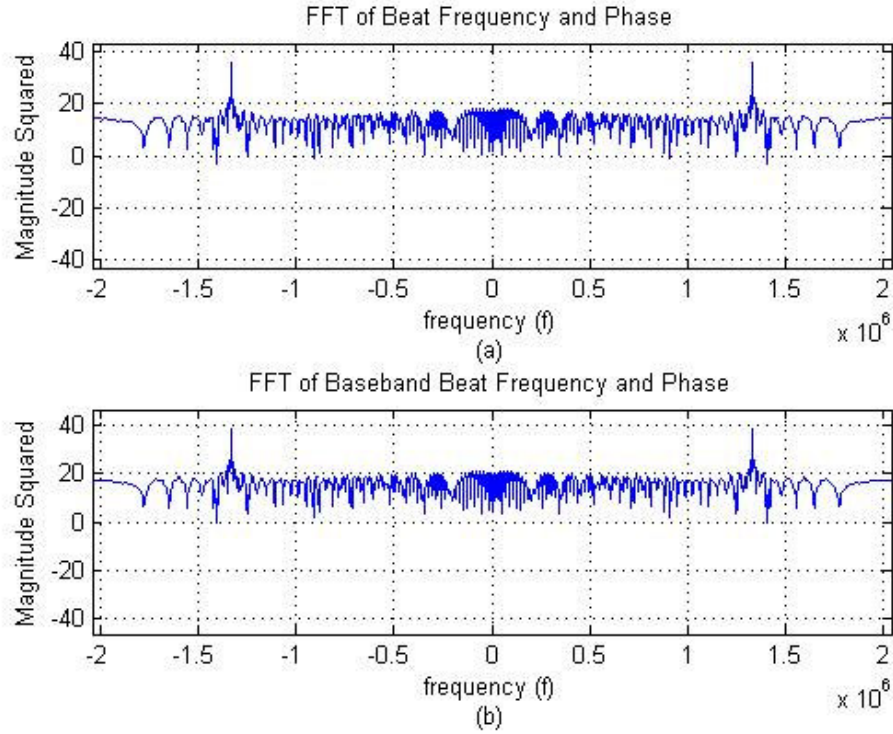


Figure 4. 17: FFT display of a stationary target (a) range extracted from RF signal (b) range extracted from baseband signal

Here we can see from Figure 4.17 that for RF case or for baseband case FFT display of beat frequency gives us the range of the target. The distance axis is adjusted according to (2.17) and target is 10037 meters far away from the radar.

4.3.2.1.2 Use of Cross-Ambiguity Function with FMCW Coding in Stationary Target Scenario

A simple simulation of a FMCW Radar system using Cross-Ambiguity function method with a stationary target can be accomplished as follows.

Step 1: Generate frequency expression for the FMCW coded transmitted waveform (see Figure 4.18 (c)).

Step 2: Introduce a delay (τ) to the frequency expression for the transmitted waveform to obtain the received waveform frequency expression, under stationary target assumption (see Figure 4.19 (c)).

Step 3: Generate phase expressions for the transmitted and received waveforms by using frequency expressions obtained in Step 2 above (see Figure 4.18 (b) for the transmitted signal phase and Figure 4.19 (b) for the received signal phase).

Step 4: Generate complex envelopes for the transmitted and received waveforms by using their frequency and phase expressions obtained in Step 2 and in Step 3 above, respectively.

Step 5: Compute the Cross-Ambiguity function by using transmitted and received complex envelopes obtained in Step 4 above and display the result to visualize the target in range.

Simulation 4: A stationary target at range $R = 10000$ meter away from the radar.

Figure 4.18 shows the transmitted signal parameters and Figure 4.19 shows the received signal parameters. Figure 4.20 and Figure 4.21 shows the resulting cross-

ambiguity function graphs from complex envelopes of these signals.

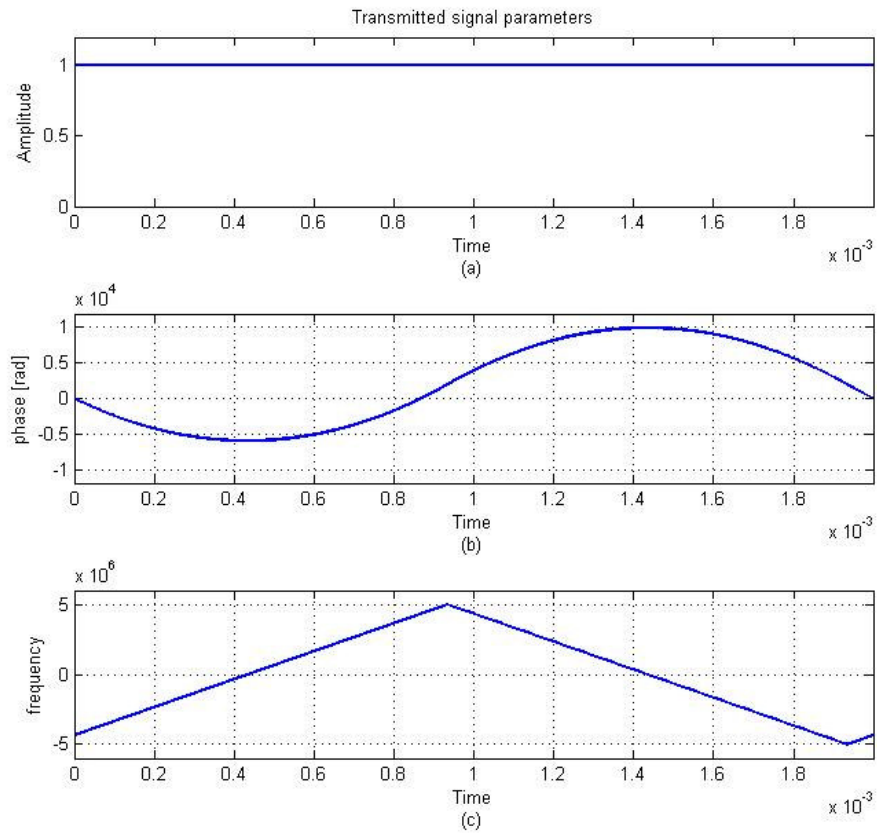


Figure 4. 18: (a) amplitude, (b) phase, and (c) frequency parameters for the FMCW coded transmitted signal used in stationary target simulation.

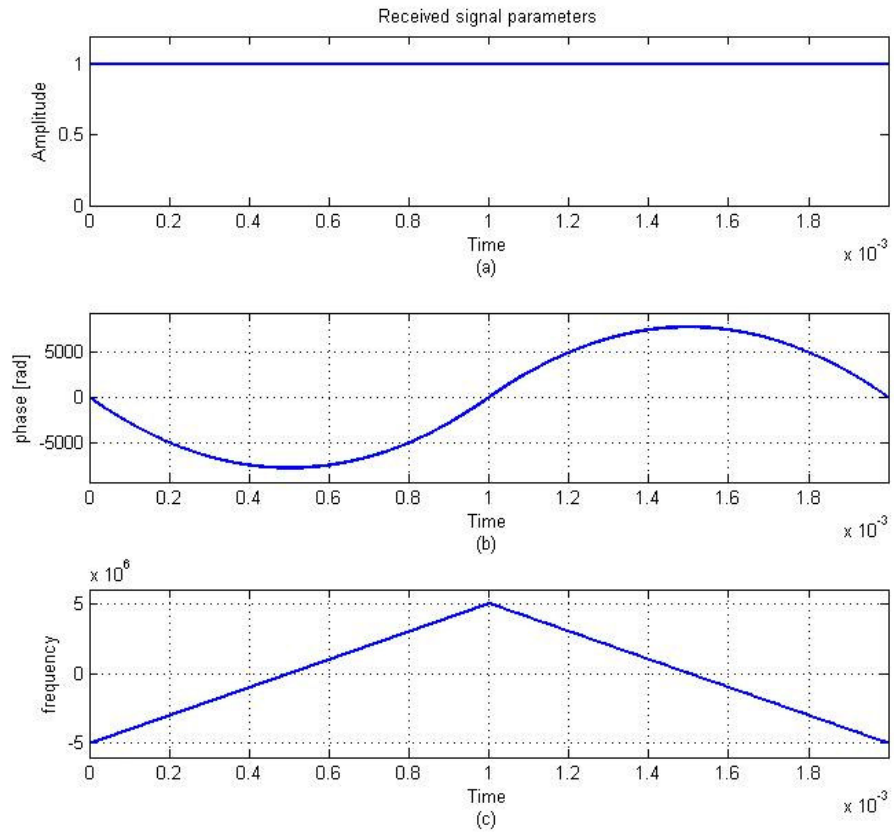


Figure 4. 19: (a) amplitude, (b) phase, and (c) frequency parameters for the FMCW coded received signal used in stationary target simulation.

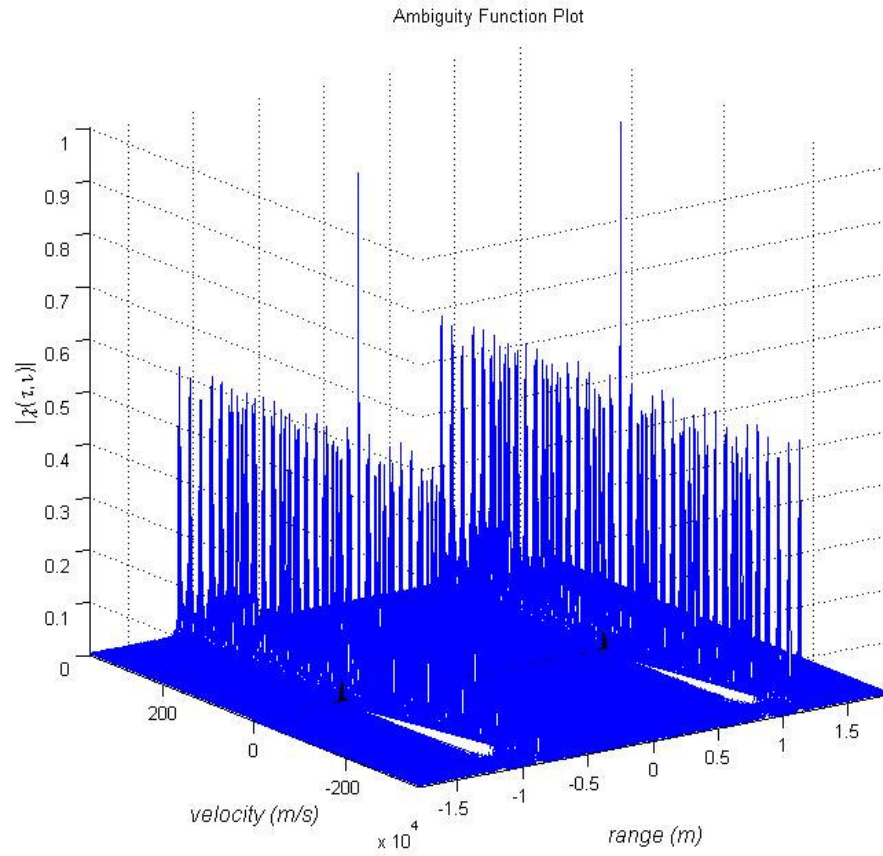


Figure 4. 20: 3-D Cross-Ambiguity function plot of FMCW coding technique ($\Delta R = 70$ m and $\Delta V = 7$ m/s) used in stationary target simulation

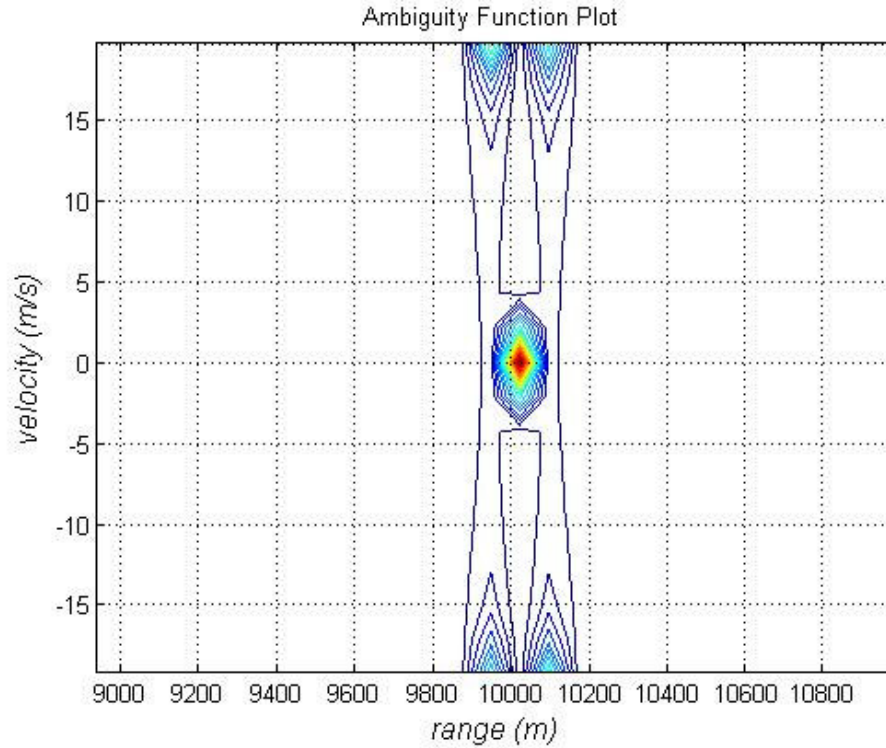


Figure 4. 21: Cross-Ambiguity function contour plot of FMCW coding technique ($\Delta R = 70$ m and $\Delta V = 7$ m/s) used in stationary target simulation

The results of this simulation are presented in Figure 4.20 and Figure 4.21 showing the target range as about 10000 meter and radial velocity as 0 m/s.

4.3.2.1.3 Use Cross-Ambiguity Function with Costas Coding in Stationary Target Scenario

A simple simulation of a Costas coded radar system using Cross-Ambiguity function method with a stationary target can be accomplished as follows.

Step 1: Generate frequency expression for the Costas coded transmitted waveform

(see Figure 4.22 (c)).

Step 2: Introduce a delay (τ) to the frequency expression for the transmitted waveform to obtain the received waveform frequency expression, under stationary target assumption (see Figure 4.23 (c)).

Step 3: Generate phase expressions for the transmitted and received waveforms by using frequency expressions obtained in Step 2 above (see Figure 4.22 (b) for the transmitted signal phase and Figure 4.23 (b) for the received signal phase).

Step 4: Generate complex envelopes for the transmitted and received waveforms by using their frequency and phase expressions obtained in Step 2 and in Step 3 above, respectively.

Step 5: Compute the Cross-Ambiguity function by using transmitted and received complex envelopes obtained in Step 4 above and display the result to visualize the target in range.

Simulation 5: A stationary target at range $R = 10000$ meter away from the radar.

Figure 4.22 shows the transmitted signal parameters and Figure 4.23 shows the received signal parameters. Figure 4.24 and Figure 4.25 shows the resulting cross-ambiguity function graphs from complex envelopes of these signals.

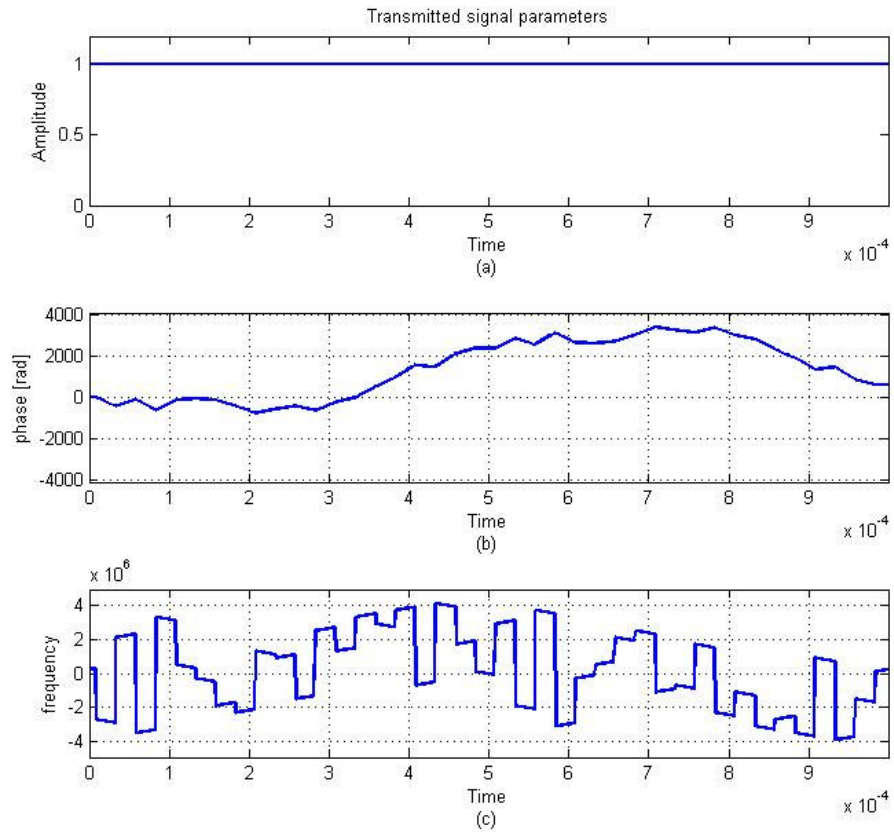


Figure 4. 22: (a) amplitude, (b) phase, and (c) frequency parameters for the Costas coded transmitted signal used in stationary target simulation.

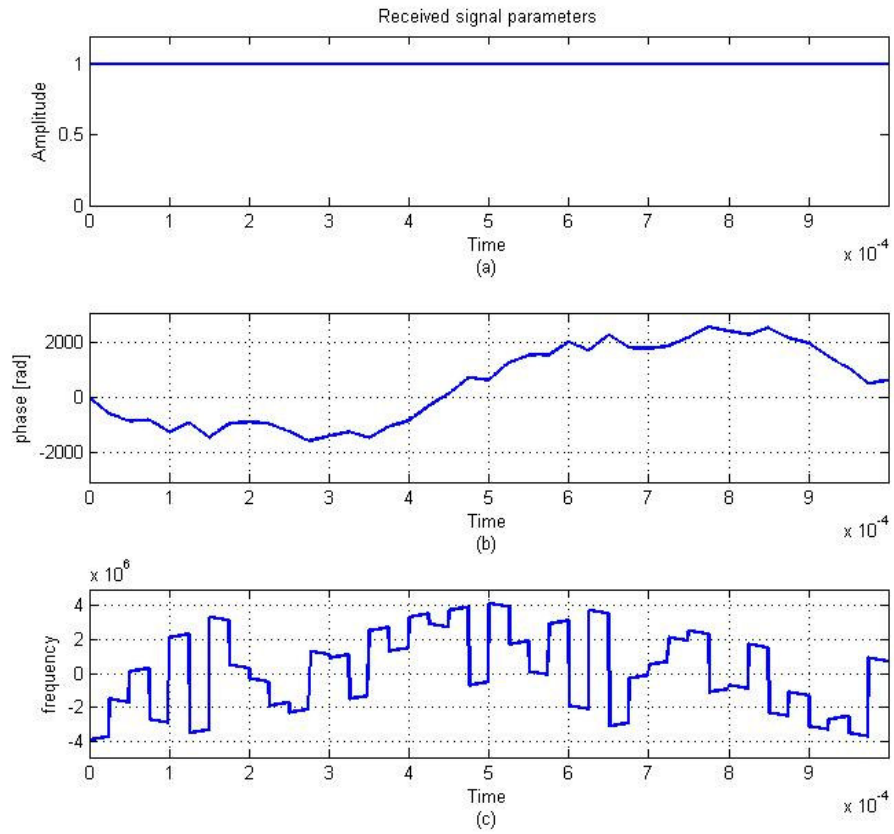


Figure 4. 23: (a) amplitude, (b) phase, and (c) frequency parameters for the Costas coded received signal used in stationary target simulation.

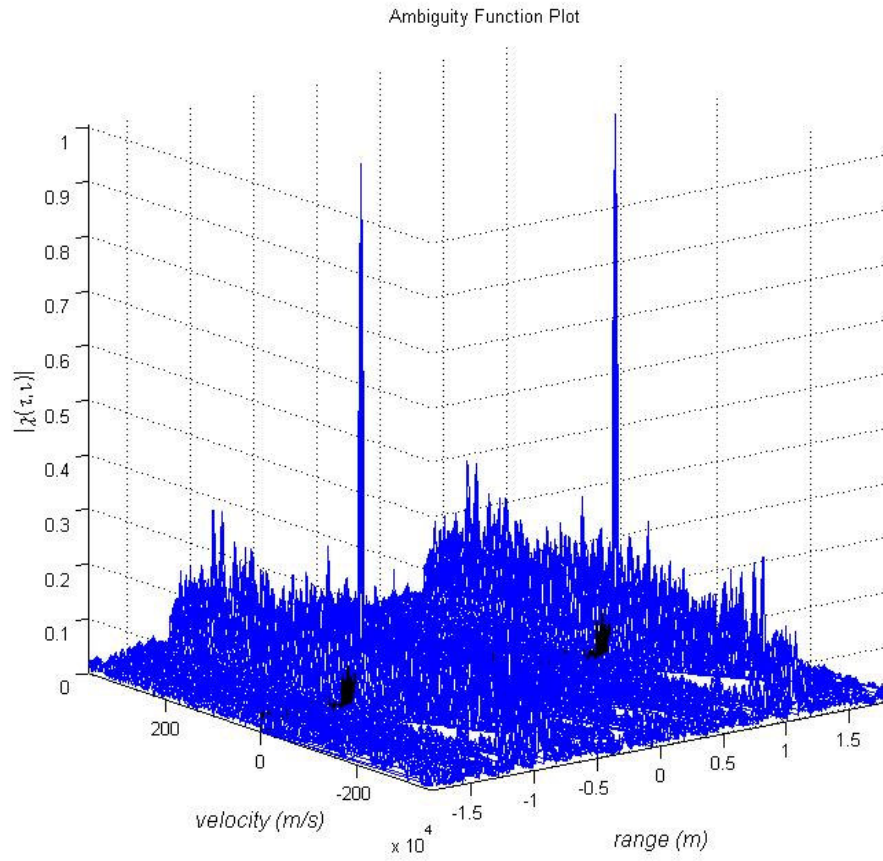


Figure 4. 24: 3-D Cross-Ambiguity function plot of Costas coding technique ($\Delta R = 120$ m and $\Delta V = 12$ m/s) used in stationary target simulation

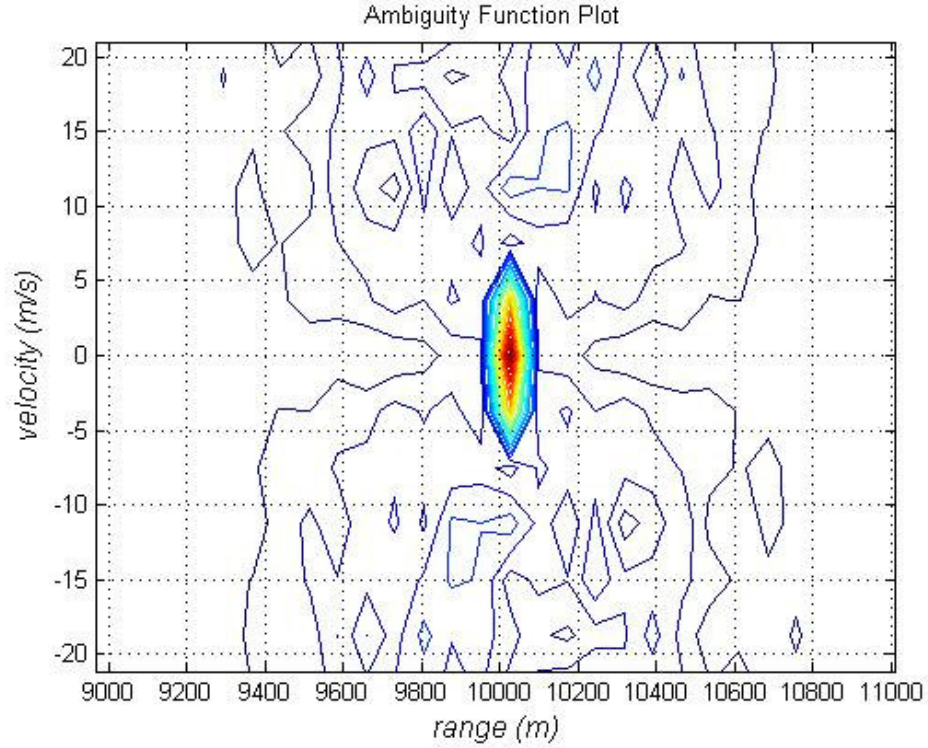


Figure 4. 25: Cross-Ambiguity function contour plot of Costas coding technique ($\Delta R = 120$ m and $\Delta V = 12$ m/s) used in stationary target simulation

The results of this simulation are presented in Figure 4.24 and Figure 4.25 showing the target range as about 10000 meter and radial velocity as 0 m/s.

In stationary target scenarios conventional FFT method and the Ambiguity Function method give the successful results in simulations.

4.3.2.2 Moving Target Scenarios

4.3.2.2.1 Use of Conventional Spectrogram Method in Moving Target Scenario

A simple simulation of a FMCW Radar system using conventional spectrogram method with a moving target can be accomplished as follows.

Step 1: Generate a FMCW coded transmitted waveform.

Step 2: Introduce a delay (τ) and a Doppler shift (f_d) to the transmitted waveform to get the received waveform.

Step 3: Multiply the received waveform with the transmitted waveform to obtain the mixer output signal.

Step 4: Pass the mixer output signal through a low pass filter to get signal with beat frequencies.

Step 5: Compute the spectrogram of the filtered output and display the result.

Simulation 6: For this target detection simulation the target range is 10000 meter and the target's velocity is 300 m/s.

Figure 4.26 shows the theoretical beat frequency which is obtained by directly subtracting transmitted signal frequency from received signal frequency and Figure 4.27 shows the spectrogram of resulting mixer output.

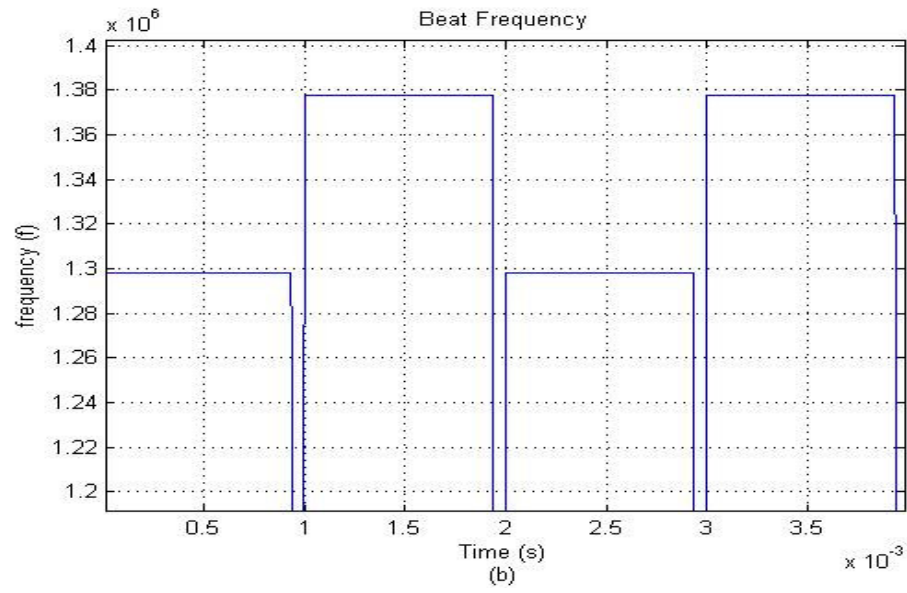
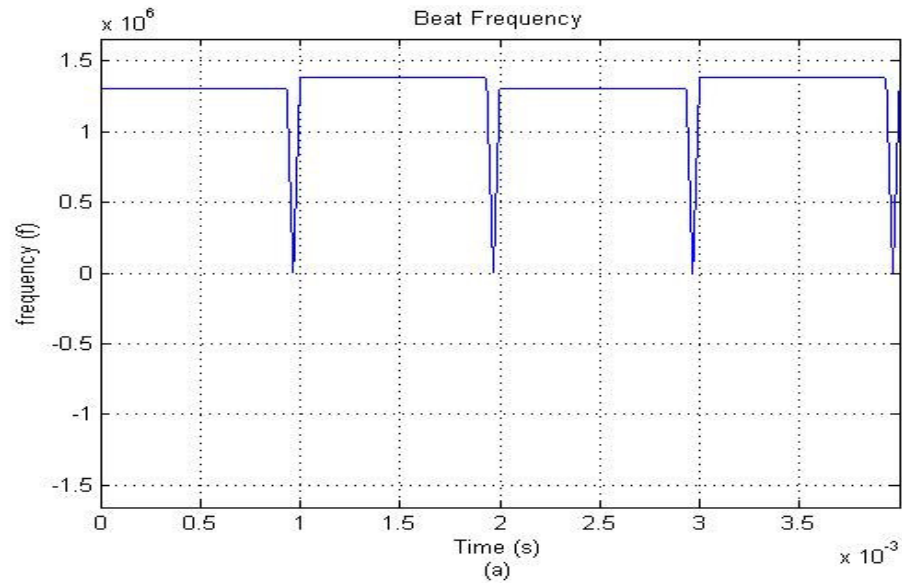


Figure 4. 26: (a)Beat frequency of a moving target obtained from the differences between the received and transmitted waveform frequency expressions directly. (b) Zoom in into Figure 4.26 (a) about beat frequencies

From beat frequency values observed in Figure 4.26 (1.298 MHz and 1.378 MHz) we can calculate the range as 10035 meter and the radial velocity of the target as 300 m/s by using (2.18) and (2.19).

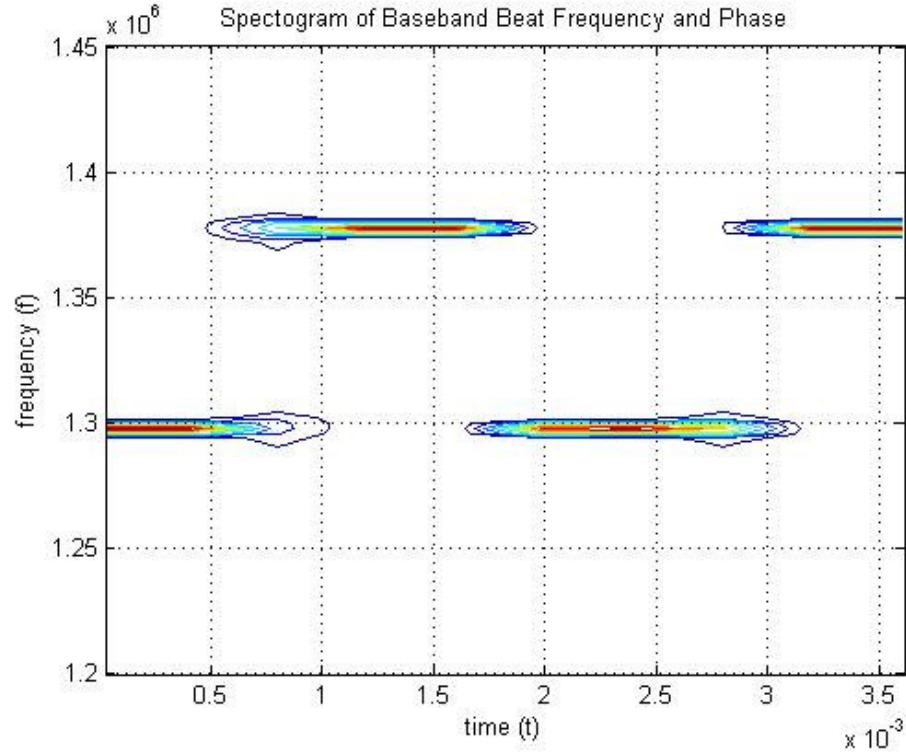


Figure 4. 27: Contour plot of the spectrogram of the filtered mixer output for moving target simulation

Similarly, from the beat frequency values observed in Figure 4.27 (1.298 MHz and 1.378 MHz), we can calculate the range as 10035 meter and the radial velocity of the target as 300 m/s by using (2.18) and (2.19).

For moving targets, beat frequencies for the first segment (upsweep) and for the second segment (downsweep) can be found by using FFT for each segment

separately. This approach is theoretically acceptable but in implementation it is very difficult for a receiver to separate a received signal to its segments truly. By using the spectrogram technique the received signal is processed as a whole with up-sweep and down-sweep segments together.

Figure 4.28 shows the FFT of filtered mixer output for the up-sweep and down-sweep segments separately, in the case of a moving target simulation.

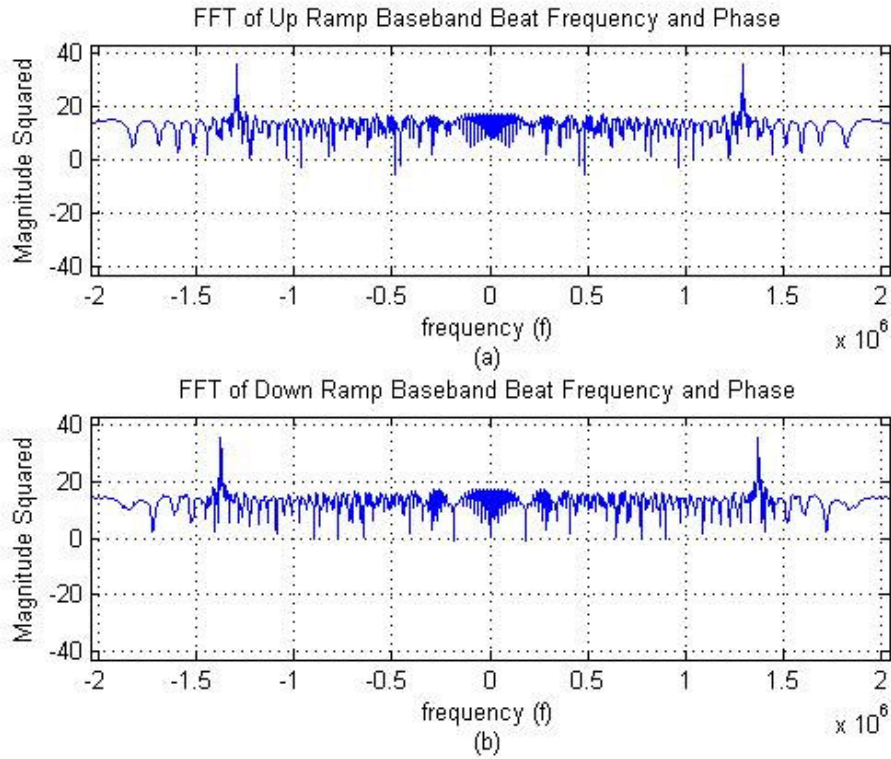


Figure 4. 28: FFT results of (a) up-sweep and (b) down-sweep segments separately.

From Figure 4.28 (a) the beat frequency for up-sweep segment is observed as 1.298 MHz and from Figure 4.28 (b) the beat frequency for down-sweep segment is observed as 1.378 MHz then we can calculate the range as 10035 meter and the

radial velocity of the target as 300 m/s by using (2.18) and (2.19).

4.3.2.2.2 Use of Cross-Ambiguity Function with FMCW Coding in Moving Target Scenario

A simple simulation of a FMCW Radar system using Cross-Ambiguity function method with a moving target can be accomplished as follows.

Step 1: Generate frequency expression for the FMCW coded transmitted waveform (see Figure 4.29 (c)).

Step 2: Introduce a delay (τ) and a Doppler shift (f_d) to the frequency expression for the transmitted waveform to obtain the received waveform frequency expression (See Figure 4.30 (c)).

Step 3: Generate phase expressions for the transmitted and received waveforms by using frequency expressions obtained in Step 2 above (See Figure 4.29 (b) for transmitted signal phase and Figure 4.30 (b) for received signal phase).

Step 4: Generate complex envelopes for the transmitted and received waveforms by using their frequency and phase expressions obtained in Step 2 and in Step 3 above, respectively.

Step 5: Compute the Cross-Ambiguity function by using transmitted and received complex envelopes obtained in Step 4 above and display the results to visualize the target both in range and in radial velocity.

Simulation 7: For this target detection simulation the target range is 10000 meter

and the target's radial velocity is 300 m/s.

Figure 4.29 shows the transmitted signal parameters and Figure 4.30 shows the received signal parameters. Figure 4.21 and Figure 4.32 shows the resulting cross-ambiguity function graphs from complex envelopes of these signals.

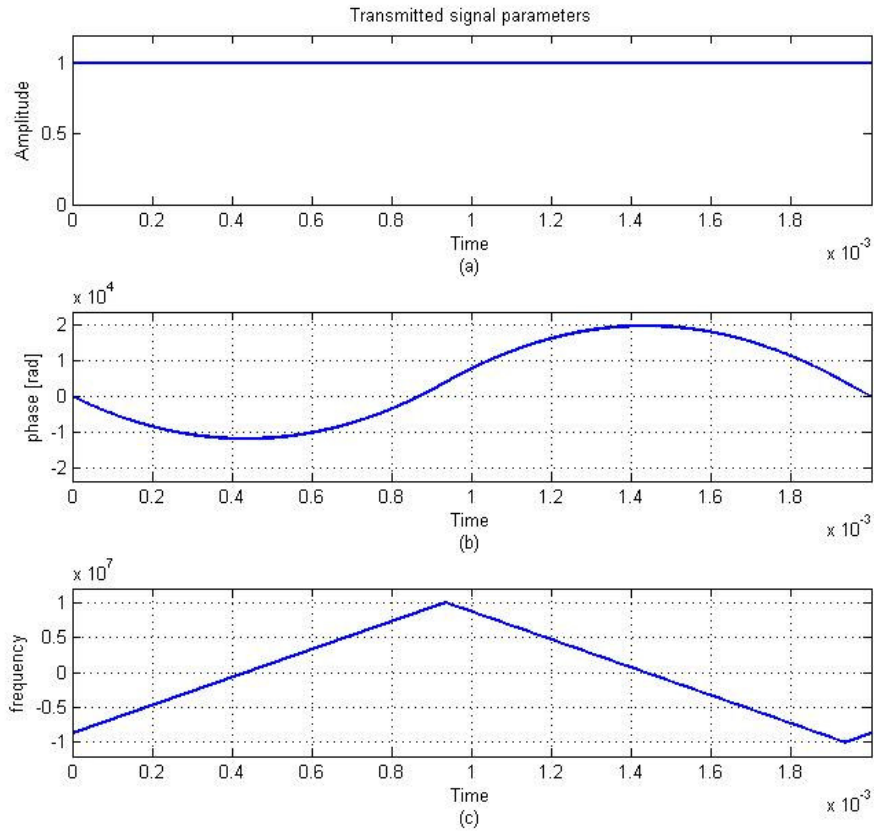


Figure 4. 29: (a) amplitude, (b) phase, and (c) frequency parameters for the FMCW coded transmitted signal used in moving target simulation.

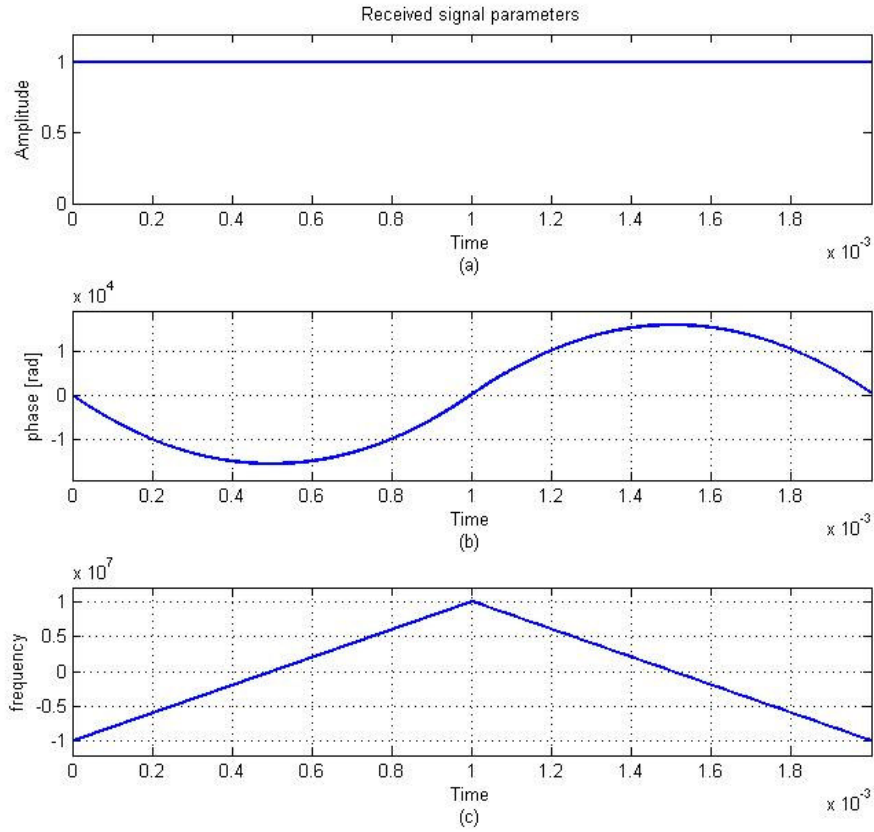


Figure 4. 30: (a) amplitude, (b) phase, and (c) frequency parameters for the FMCW coded received signal used in moving target simulation.

Figure 4.29 (c) and Figure 4.30 (c) shows the time delay and Doppler shift between the transmitted and received signals. Time delay can be seen from figures but since the Doppler frequency is very small compared to ΔF we could not see Doppler shift

from these figures ($\Delta F = 20$ MHz and $f_d = \frac{2V_r}{\lambda} = 400$ kHz)

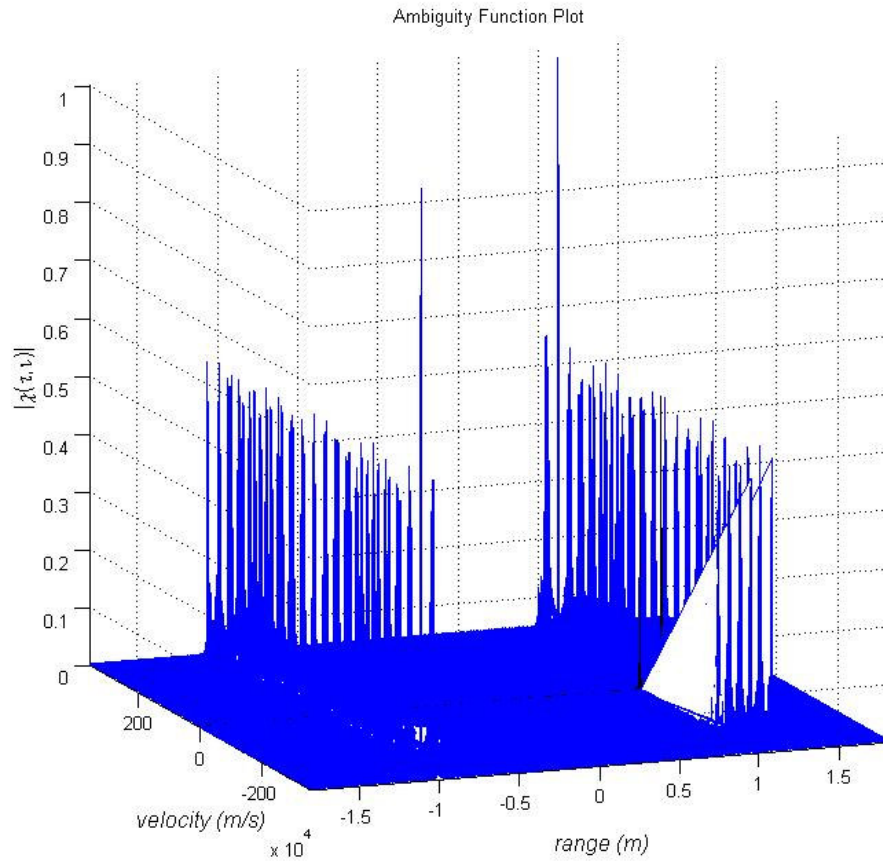


Figure 4. 31: 3-D Cross-Ambiguity function plot of FMCW coding technique ($\Delta R = 70$ m and $\Delta V = 7$ m/s) used in moving target simulation

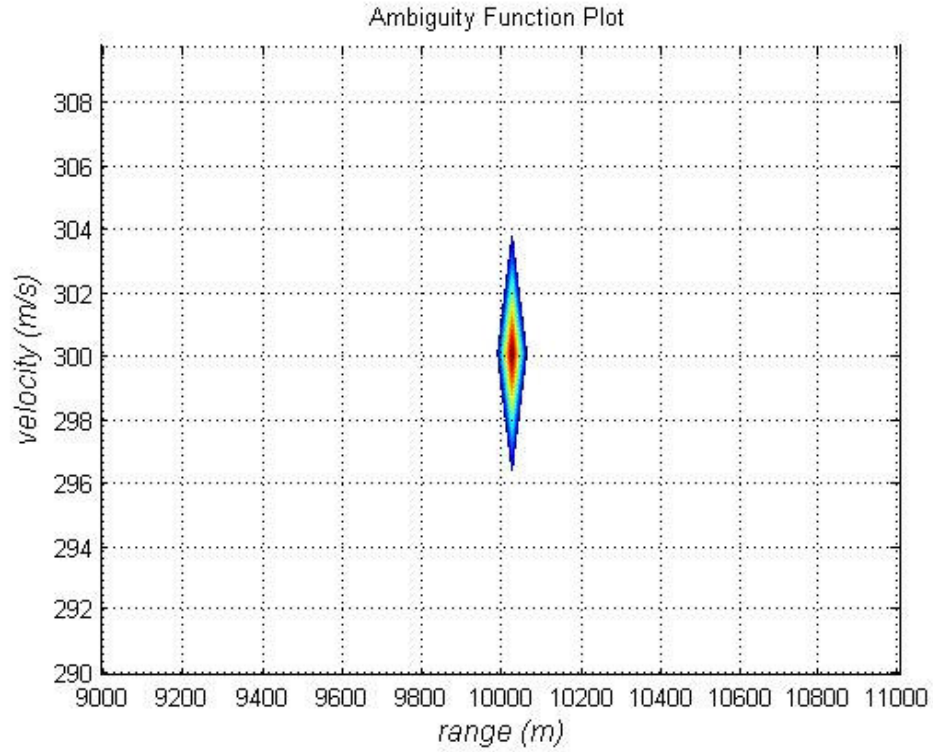


Figure 4. 32: Cross-Ambiguity function contour plot of FMCW coding technique ($\Delta R = 70$ m and $\Delta V = 7$ m/s) used in moving target simulation

The results of this simulation are presented in Figure 4.31 and Figure 4.32 showing the target range as 10025 meter and radial velocity as 300 m/s.

4.3.2.2.3 Use of Cross-Ambiguity Function with Costas Coding in Moving Target Scenario

A simple simulation of a Costas coded radar system using Cross-Ambiguity function method with a moving target can be accomplished as follows.

Step 1: Generate frequency expression for the Costas coded transmitted waveform

(see Figure 4.33 (c)).

Step 2: Introduce a delay (τ) and a Doppler shift (f_d) to the frequency expression for the transmitted waveform to obtain the received waveform frequency expression (see Figure 4.34 (c)).

Step 3: Generate phase expressions for the transmitted and received waveforms by using frequency expressions obtained in Step 2 above (see Figure 4.33 (b) for the transmitted signal phase and Figure 4.34 (b) for the received signal phase).

Step 4: Generate complex envelopes for the transmitted and received waveforms by using their frequency and phase expressions obtained in Step 2 and in Step 3 above, respectively.

Step 5: Compute the Cross-Ambiguity function by using transmitted and received complex envelopes obtained in Step 4 above and display the results to visualize the target both in range and in radial velocity.

Simulation 8: For this target detection simulation the target range is 10000 meter and the target's radial velocity is 300 m/s.

Figure 4.33 shows the transmitted signal parameters and Figure 4.34 shows the received signal parameters. Figure 4.35 and Figure 4.36 shows the resulting cross-ambiguity function graphs from complex envelopes of these signals.

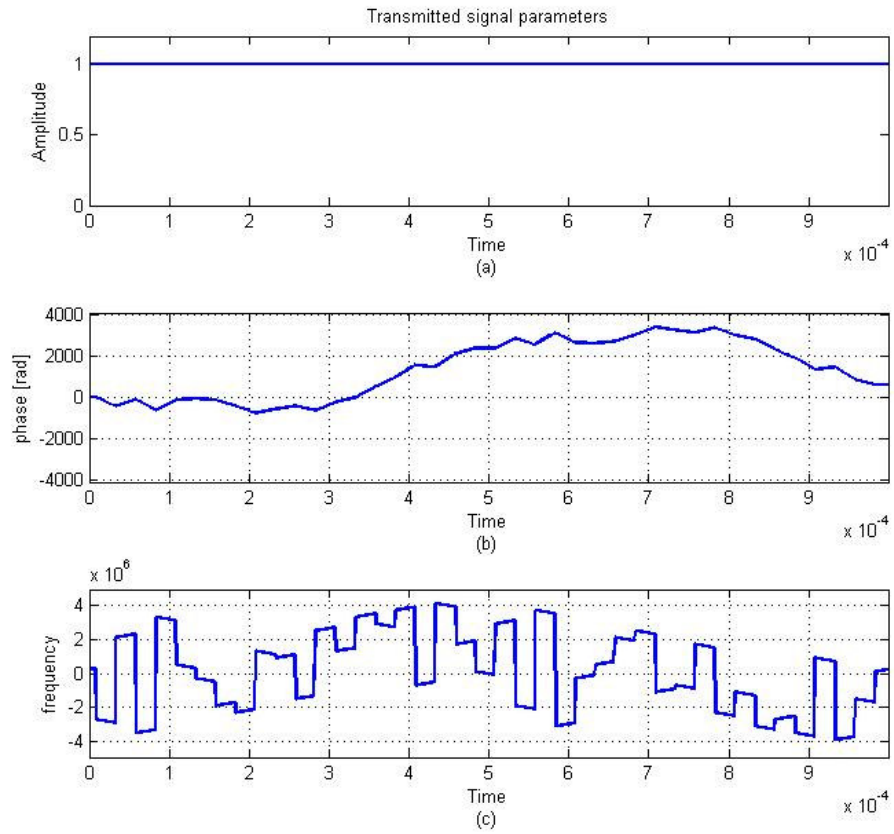


Figure 4. 33: (a) amplitude, (b) phase, and (c) frequency parameters for the Costas coded transmitted signal used in moving target simulation.

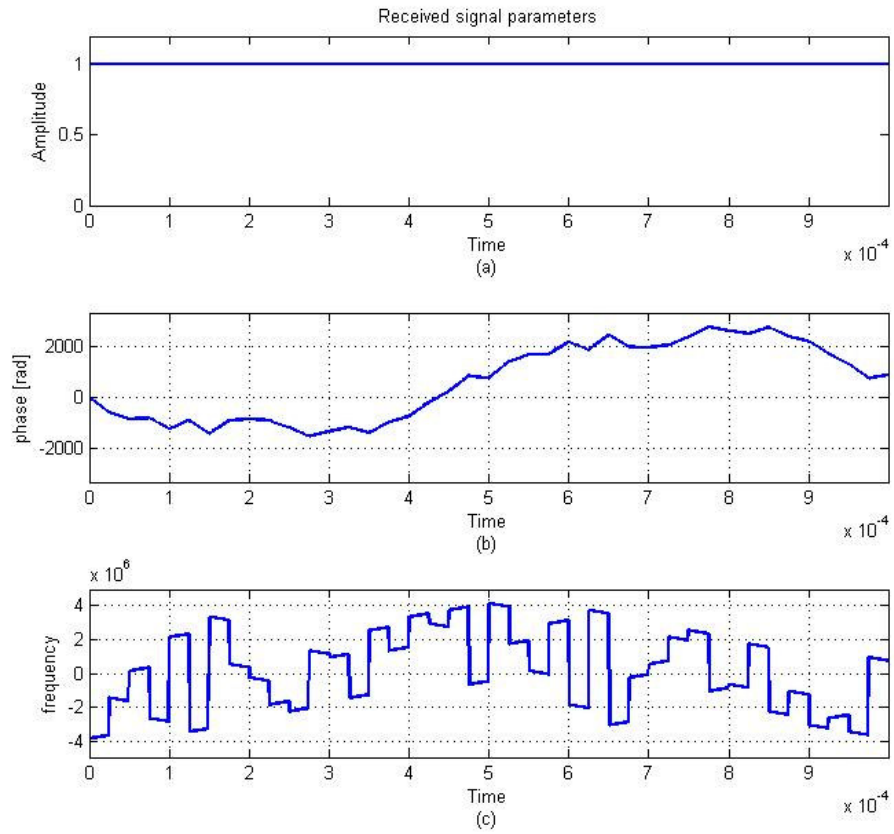


Figure 4. 34: (a) amplitude, (b) phase, and (c) frequency parameters for the Costas coded received signal used in moving target simulation.

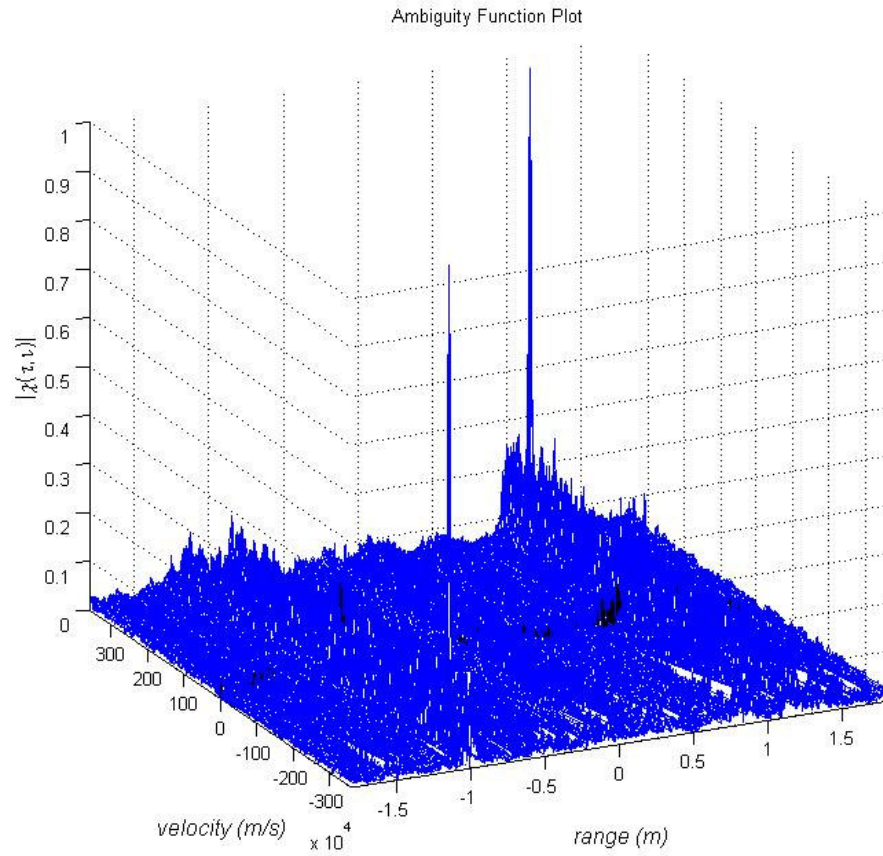


Figure 4. 35: 3-D Cross-Ambiguity function plot of Costas coding technique ($\Delta R = 120$ m and $\Delta V = 12$ m/s) used in moving target simulation

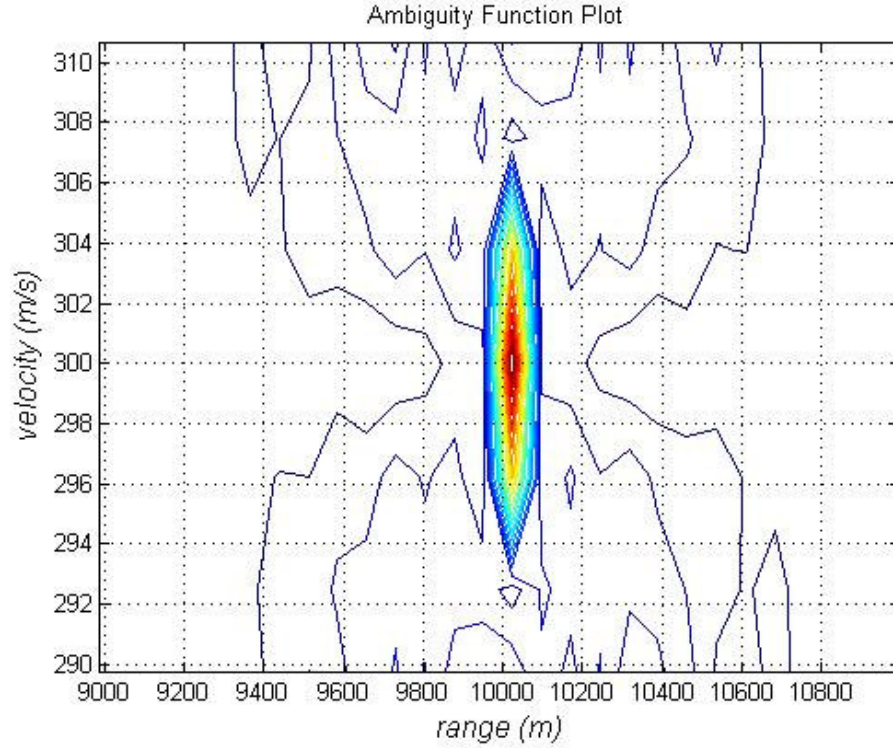


Figure 4. 36: Cross-Ambiguity function contour plot of Costas coding technique ($\Delta R = 120$ m and $\Delta V = 12$ m/s) used in moving target simulation

The results of this simulation are presented in Figure 4.35 and Figure 4.36 showing the target range as 10020 meter and radial velocity as 300 m/s.

In moving target scenarios conventional spectrogram method and the Ambiguity Function method give the successful results in simulations. For a moving target while plot of Ambiguity Function method gives the exact target information (range and velocity) conventional spectrogram method needs one more iteration. Beat frequencies are extracted from the spectrogram graph and the target information is obtained by solving equations (2.18) and (2.19) simultaneously.

4.3.2.3 Multiple Target Scenarios

A simple simulation of a FMCW Radar system using conventional spectrogram method with multiple targets can be accomplished as follows.

Step 1: Generate a FMCW coded transmitted waveform.

Step 2: Introduce a proper delay (τ) and a proper Doppler shift (f_d) to the transmitted signal for each of the targets to obtain individual received signals and then superpose all these received signal components to obtain the effective received signal.

Step 3: Multiply the received signal with the transmitted signal to obtain the mixer output signal.

Step 4: Pass the mixer output signal through the low pass filter to obtain the beat frequency information.

Step 5: Compute the spectrogram of the filtered mixer output and display the result.

A simple simulation of a FMCW/Costas coded radar system using Cross-Ambiguity function method with multiple targets can be accomplished as follows.

Step 1: Generate frequency expression for the FMCW/Costas coded transmitted waveform.

Step 2: Introduce a delay (τ) and a Doppler shift (f_d) to the frequency expression for the transmitted waveform for each of the targets to obtain individual received waveform frequency expression and then superpose all these received signal

components to obtain the effective received signal waveform.

Step 3: Generate phase expressions for the transmitted and received waveforms by using frequency expressions obtained in Step 2 above.

Step 4: Generate complex envelopes for the transmitted and received waveforms by using their frequency and phase expressions obtained in Step 2 and in Step 3 above, respectively.

Step 5: Compute the Cross-Ambiguity function by using transmitted and received complex envelopes obtained in Step 4 above and display the result to visualize the targets both in range and in radial velocity.

4.3.2.3.1 Different Range and Different Velocity Scenario

4.3.2.3.1.1 Use of Conventional Spectrogram Method

Simulation 9: In this multiple target simulation by conventional spectrogram method, targets in different range and in different velocity are observed. In the scenario, first target range is used as 10000 meter and radial velocity is used as 300 m/s, second target range is used as 5000 meter and radial velocity is used as 200 m/s.

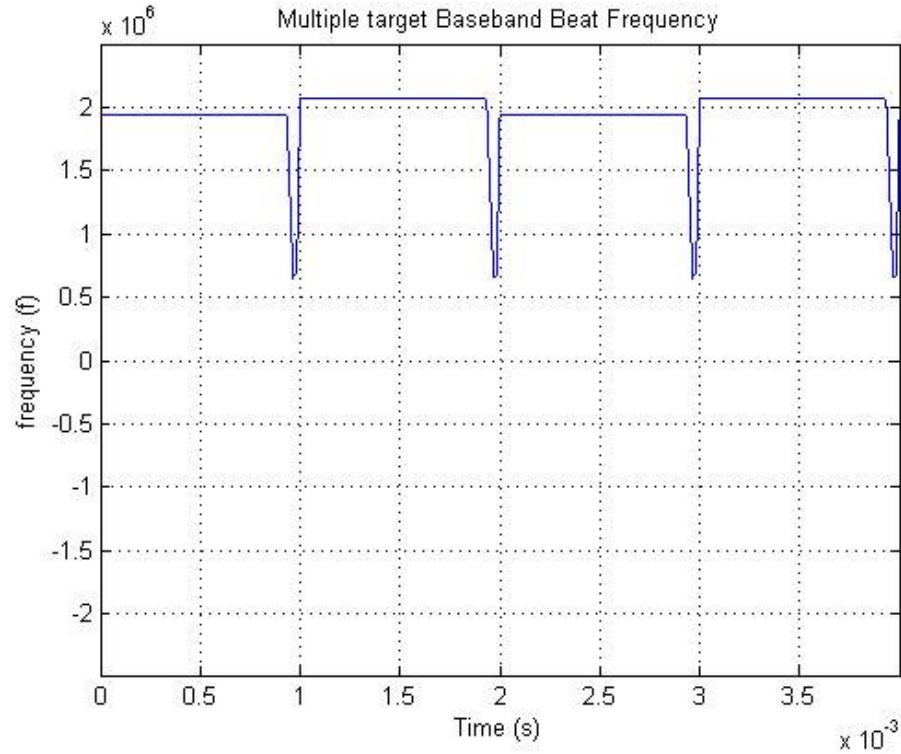


Figure 4. 37: Beat frequency of multiple targets in different range and in different velocity, obtained from the differences between the received and transmitted waveform frequency expressions directly.

From Figure 4.37 which is obtained by extracting the transmitted signal frequency from the received signal frequency directly, it is very hard to understand that this beat frequency comes from two targets. One can realize that this frequency comes from a farther and faster target. Even if one realizes that this beat frequency comes from multiple targets it is impossible to extract real values from this graph.

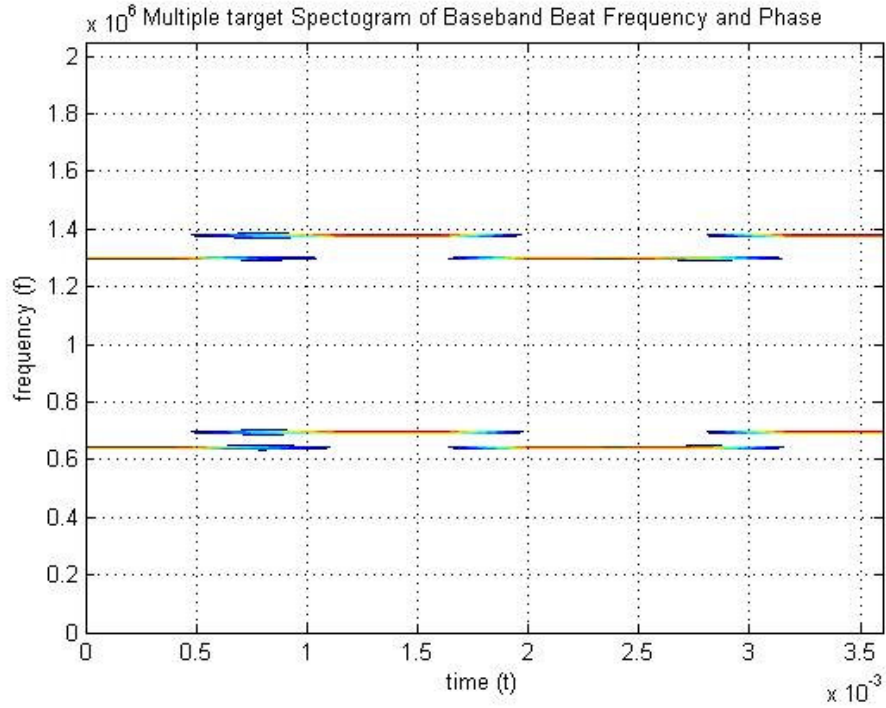


Figure 4. 38: Contour plot of the spectrogram of the filtered mixer output for multiple targets in different range and in different velocity simulation

From Figure 4.38, with beat frequency expressions extracted by spectrogram technique, we can calculate range and velocity of the targets by using (2.18) and (2.19). From Figure 4.38 beat frequencies for the first target is observed as 1.298 MHz and 1.378 MHz and beat frequencies for the second target is observed as 642 kHz and 696 kHz. With this beat frequencies we can calculate the first target range as 10035 meter and the radial velocity as 300 m/s and the second target range as 5017.5 meter and the radial velocity as 202.5 m/s.

4.3.2.3.1.2 Use of Cross-Ambiguity Method with FMCW Coding

Simulation 10: In this multiple target simulation by Cross-Ambiguity method with

FMCW coding, targets in different range and in different velocity are observed. In the scenario, first target range is used as 10000 meter and radial velocity is used as 300 m/s, second target range is used as 5000 meter and radial velocity is used as 200 m/s.

Figure 4.39 shows the transmitted signal parameters, Figure 4.40 shows the first target the received signal parameters and Figure 4.41 shows the second target the received signal parameters. Figure 4.42 and Figure 4.43 shows the resulting cross-ambiguity function graphs from complex envelopes of these signals.

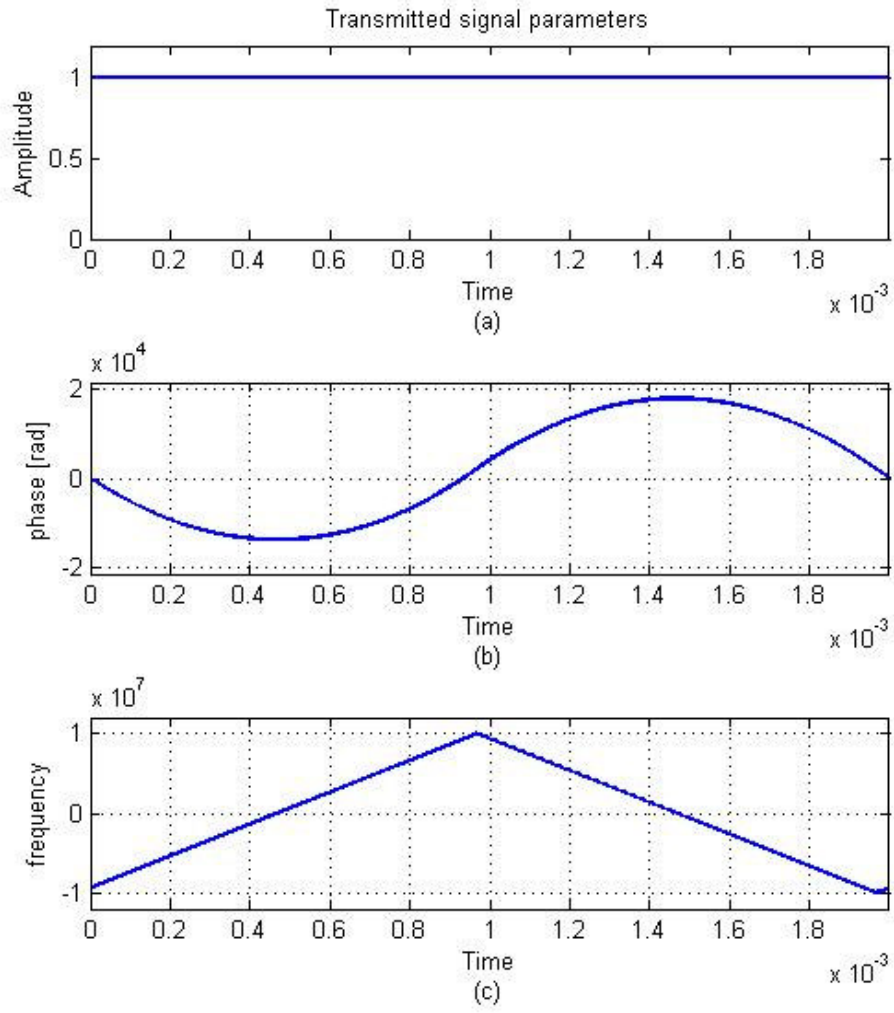


Figure 4. 39: (a) amplitude, (b) phase, and (c) frequency parameters for the FMCW coded transmitted signal used in multiple targets in different range and in different velocity simulation.

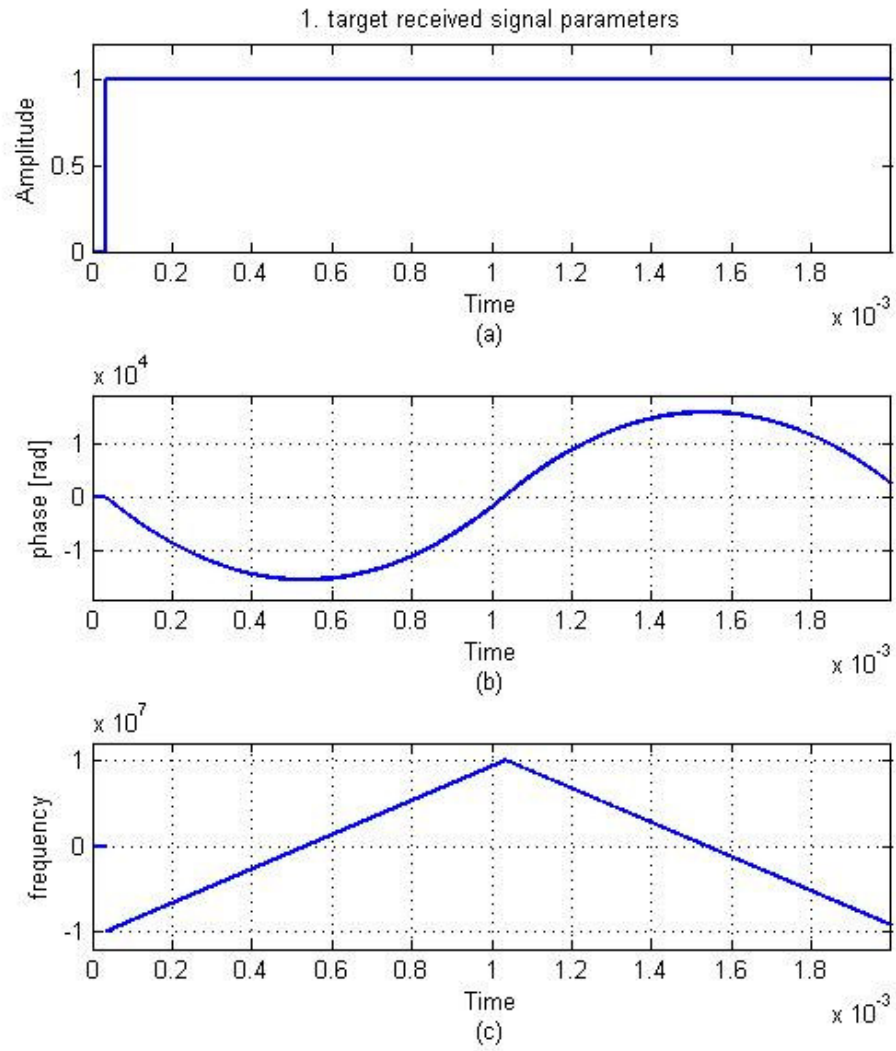


Figure 4. 40: (a) amplitude, (b) phase, and (c) frequency parameters for the FMCW coded 1.st target received signal used in multiple targets in different range and in different velocity simulation.

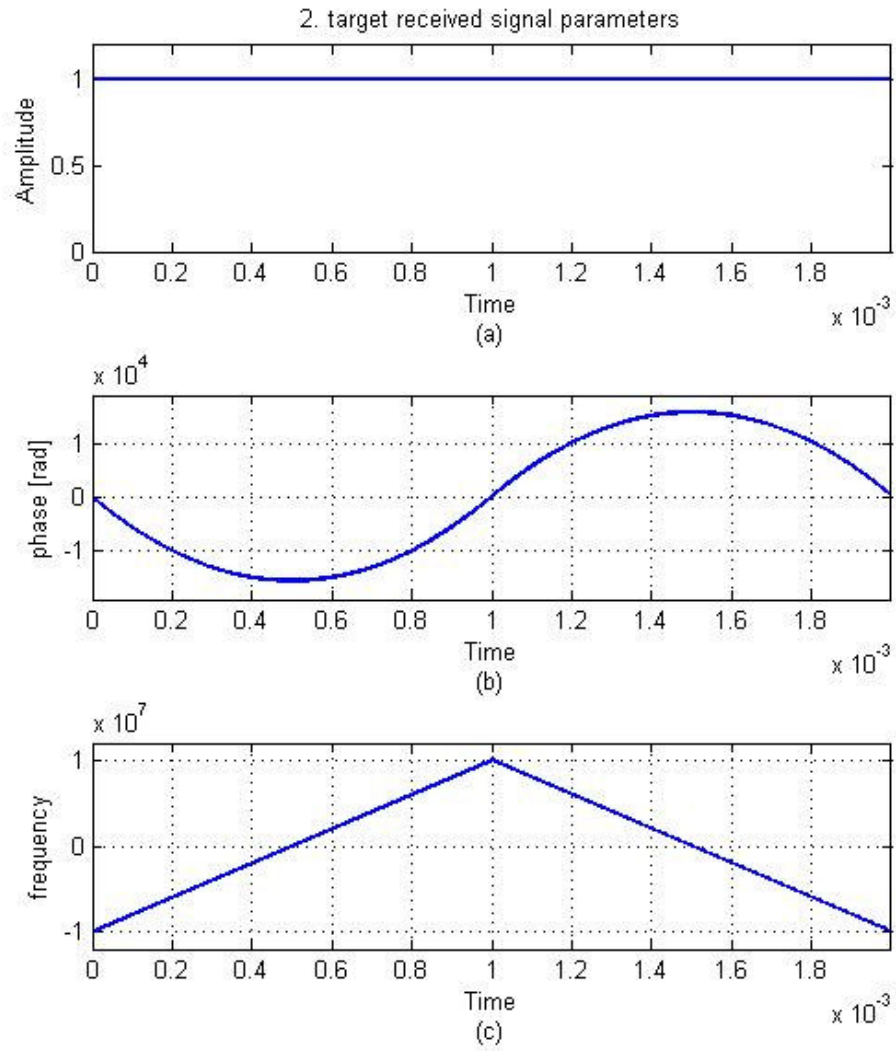


Figure 4. 41: (a) amplitude, (b) phase, and (c) frequency parameters for the FMCW coded 2.nd target received signal used in multiple targets in different range and in different velocity simulation.

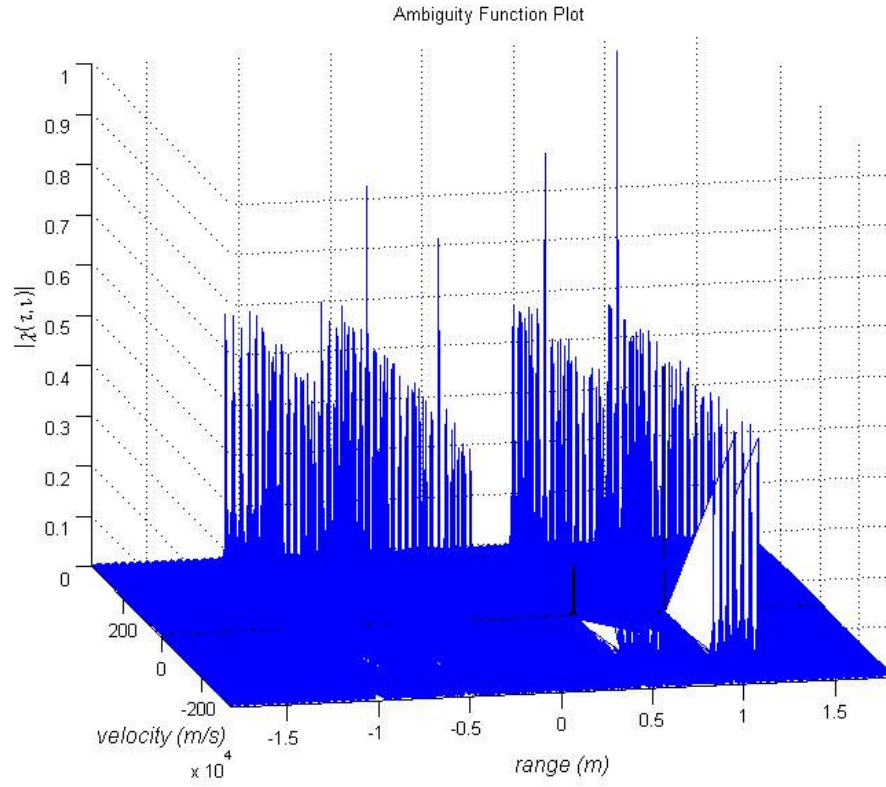


Figure 4. 42: 3-D Cross-Ambiguity function plot of FMCW coding technique ($\Delta R = 70$ m and $\Delta V = 7$ m/s) used in multiple targets in different range and in different velocity simulation.

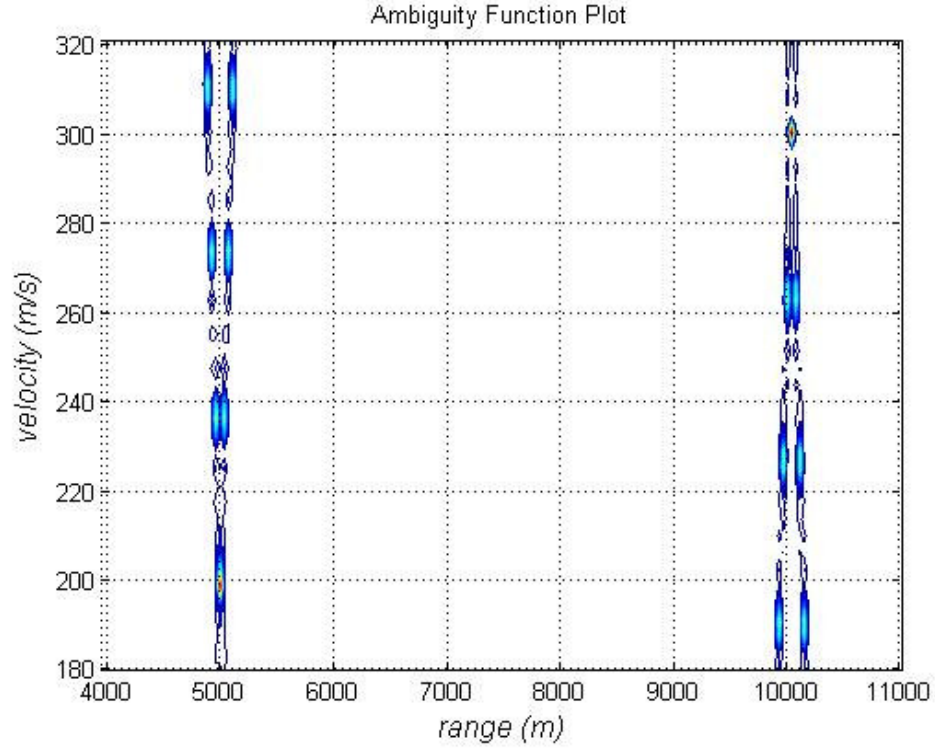


Figure 4. 43: Cross-Ambiguity function contour plot of FMCW coding technique ($\Delta R = 70$ m and $\Delta V = 7$ m/s) used in multiple targets in different range and in different velocity simulation.

The results of this simulation are presented in Figure 4.42 and Figure 4.43 showing the first target range as 10024 meter and radial velocity as 300 m/s and the second target range as 5012 meter and radial velocity as 199 m/s.

4.3.2.3.1.3 Use of Cross-Ambiguity Method with Costas Coding

Simulation 11: In this multiple target simulation by Cross-Ambiguity method with Costas coding, targets in different range and in different velocity are observed. In the scenario, first target range is used as 10000 meter and radial velocity is used as 300

m/s, second target range is used as 5000 meter and radial velocity is used as 200 m/s.

Figure 4.44 shows the transmitted signal parameters, Figure 4.45 shows the first target the received signal parameters and Figure 4.46 shows the second target the received signal parameters. Figure 4.47 and Figure 4.48 shows the resulting cross-ambiguity function graphs from complex envelopes of these signals.

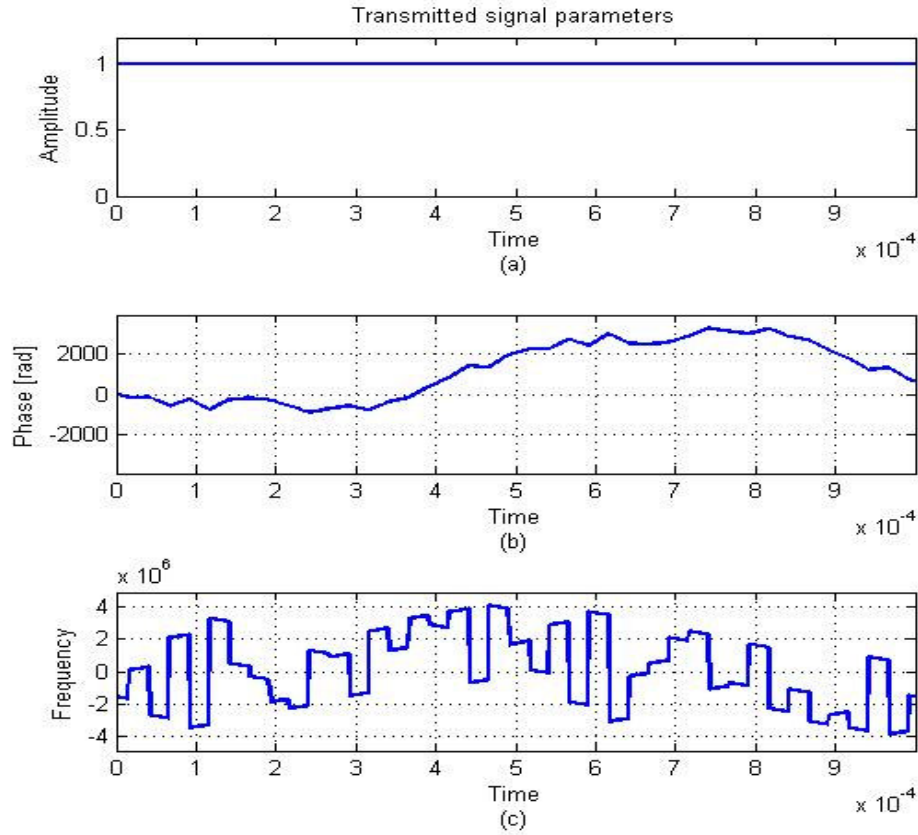


Figure 4. 44: (a) amplitude, (b) phase, and (c) frequency parameters for the Costas coded transmitted signal used in multiple targets in different range and in different velocity simulation.

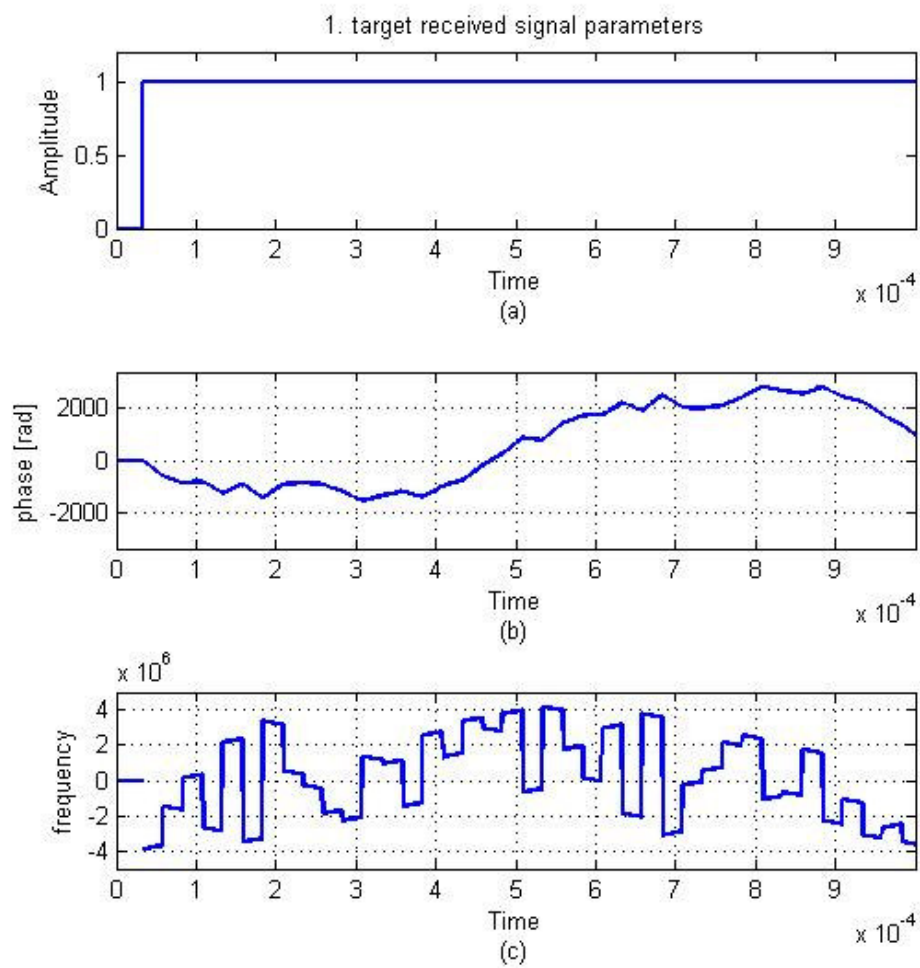


Figure 4. 45: (a) amplitude, (b) phase, and (c) frequency parameters for the Costas coded 1.st target received signal used in multiple targets in different range and in different velocity simulation.

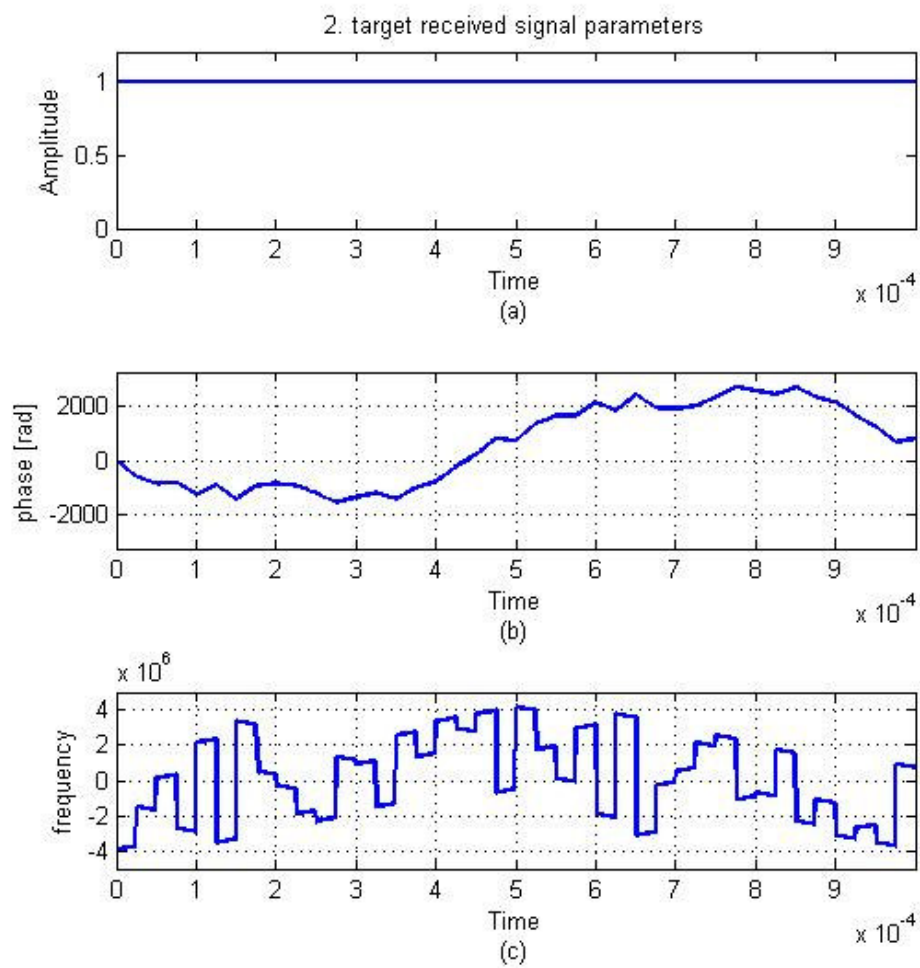


Figure 4. 46: (a) amplitude, (b) phase, and (c) frequency parameters for the Costas coded 2.nd target received signal used in multiple targets in different range and in different velocity simulation.

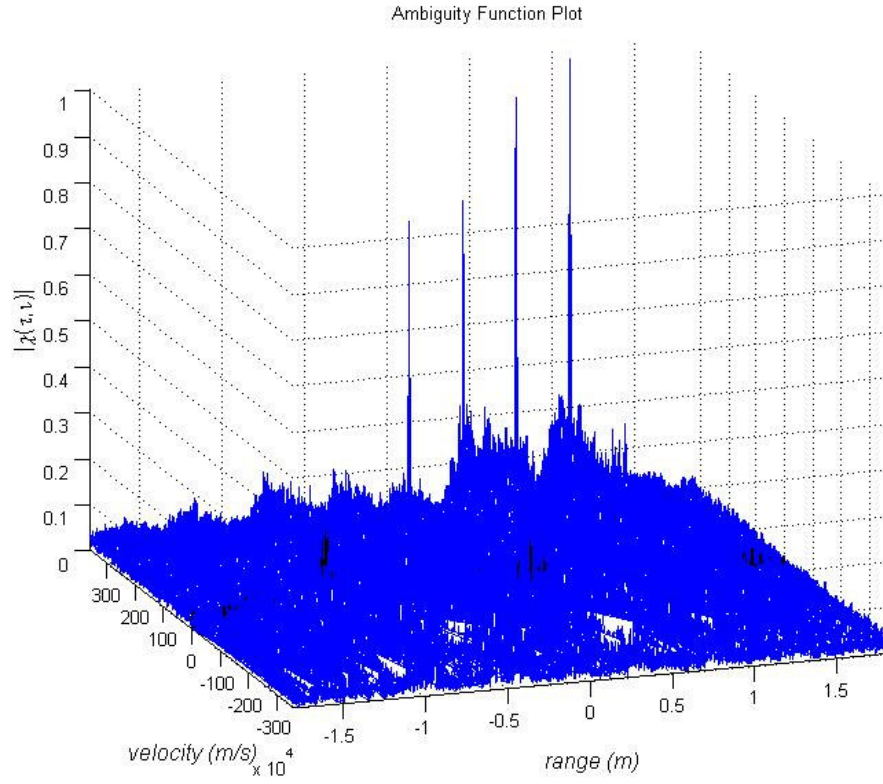


Figure 4. 47: 3-D Cross-Ambiguity function plot of Costas coding technique ($\Delta R = 120$ m and $\Delta V = 12$ m/s) used in multiple targets in different range and in different velocity simulation.

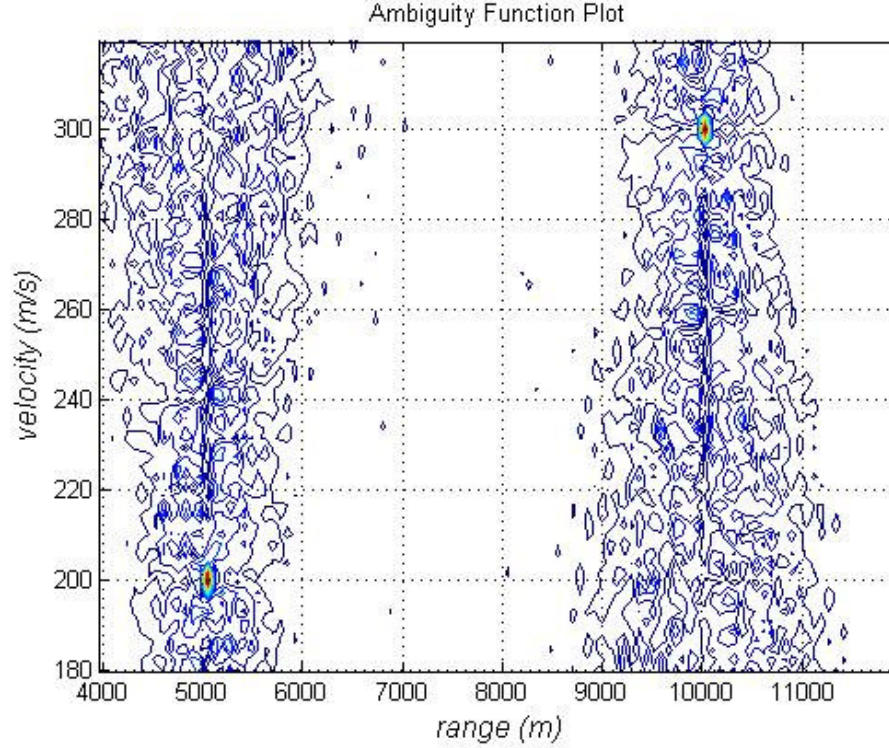


Figure 4. 48: Cross-Ambiguity function contour plot of Costas coding technique ($\Delta R = 120$ m and $\Delta V = 12$ m/s) used in multiple targets in different range and in different velocity simulation.

The results of this simulation are presented in Figure 4.47 and Figure 4.48 showing the first target range as 10024 meter and radial velocity as 300 m/s and the second target range as 5049 meter and radial velocity as 199 m/s.

In multiple target scenarios for targets in different range and in different velocity situation conventional spectrogram method and the Ambiguity Function method give the successful results in simulations. For multiple targets while plot of Ambiguity Function method gives the exact target information (range and velocity) for each one separately, conventional spectrogram method needs more iterations. From the spectrogram graph firstly which beat frequency pair belongs to which target must be

chosen then for each target with these frequency pairs target information is extracted by solving equations (2.18) and (2.19) simultaneously. For the case targets are closer to each other it can be difficult to choose which frequency pair belongs to which target for the spectrogram method.

4.3.2.3.2 Same Range and Different Velocity Scenario

4.3.2.3.2.1 Use of Conventional Spectrogram Method

Simulation 12: In this multiple target simulation by conventional spectrogram method, targets in same range and in different velocity are observed. In the scenario, first target range is used as 10000 meter and radial velocity is used as 300 m/s, second target range is used as 10000 meter and radial velocity is used as 200 m/s.

Figure 4.49 shows the theoretical beat frequency which is obtained by directly subtracting transmitted signal frequency from received signal frequency and Figure 4.50 shows the spectrogram of resulting mixer output.

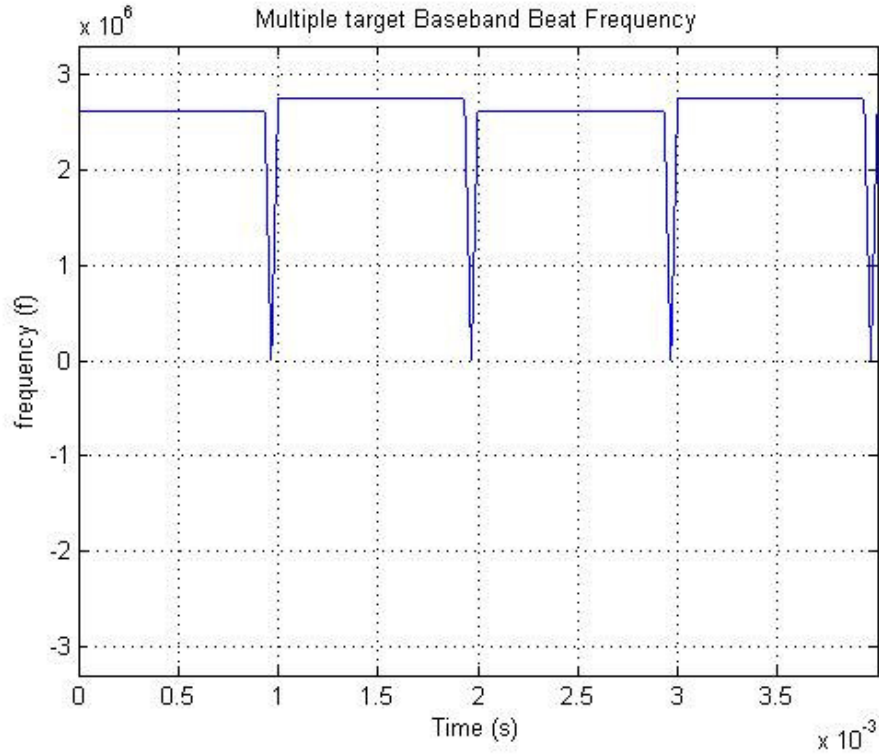


Figure 4. 49: Beat frequency of multiple targets in same range and in different velocity, obtained from the differences between the received and transmitted waveform frequency expressions directly.

From Figure 4.49 which is obtained by extracting the transmitted signal frequency from the received signal frequency directly, it is again very hard to understand that this beat frequency comes from two targets and it is impossible to extract real targets range and velocity values from this graph.

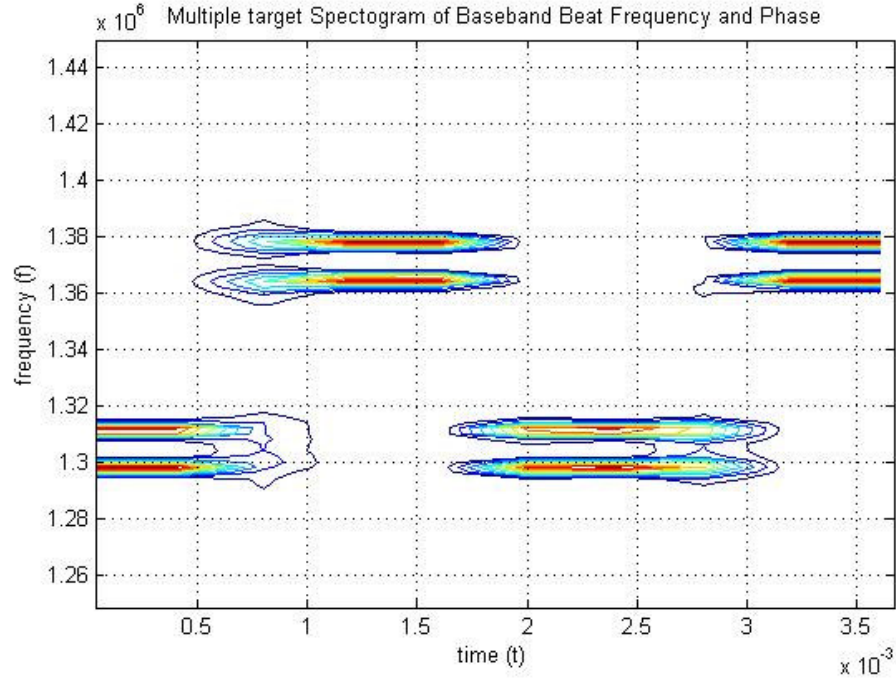


Figure 4. 50: Contour plot of the spectrogram of the filtered mixer output for multiple targets in different range and in different velocity simulation

As can be seen from the Figure 4.50 it is difficult to choose which beat frequency pair belongs to which target. If up-sweep and down-sweep beat frequencies can not be chosen correctly the correct range and velocity information for each target can not be calculated. So for the case where the targets are in the same range with different velocities, it is impossible to detect targets truly by using conventional spectrogram method. For this simulation beat frequencies belong to up-sweep are 1.312 MHz and 1.298 MHz, beat frequencies belong to down-sweep are 1.378 MHz and 1.364 MHz. With these beat frequency pairs four matching can be made i.e., 1.378-1.312 MHz, 1.364-1.298 MHz, 1.378-1.298 MHz and 1.364-1.312 MHz and by solving equation (2.18) and (2.19) simultaneously we obtain target values as 10088 m – 247.5 m/s, 9982.5 m – 247.5 m/s, 10035 m – 300 m/s, and 10035 m – 195 m/s respectively.

4.3.2.3.2.2 Use of Cross-Ambiguity Method with FMCW Coding

Simulation 13: In this multiple target simulation by Cross-Ambiguity method with FMCW coding, targets in same range and in different velocities are observed. In the scenario, first target range is used as 10000 meter and radial velocity is used as 300 m/s, second target range is used as 10000 meter and radial velocity is used as 200 m/s.

Figure 4.51 shows the transmitted signal parameters, Figure 4.52 shows the first target the received signal parameters and Figure 4.53 shows the second target the received signal parameters. Figure 4.54 and Figure 4.55 shows the resulting cross-ambiguity function graphs from complex envelopes of these signals.

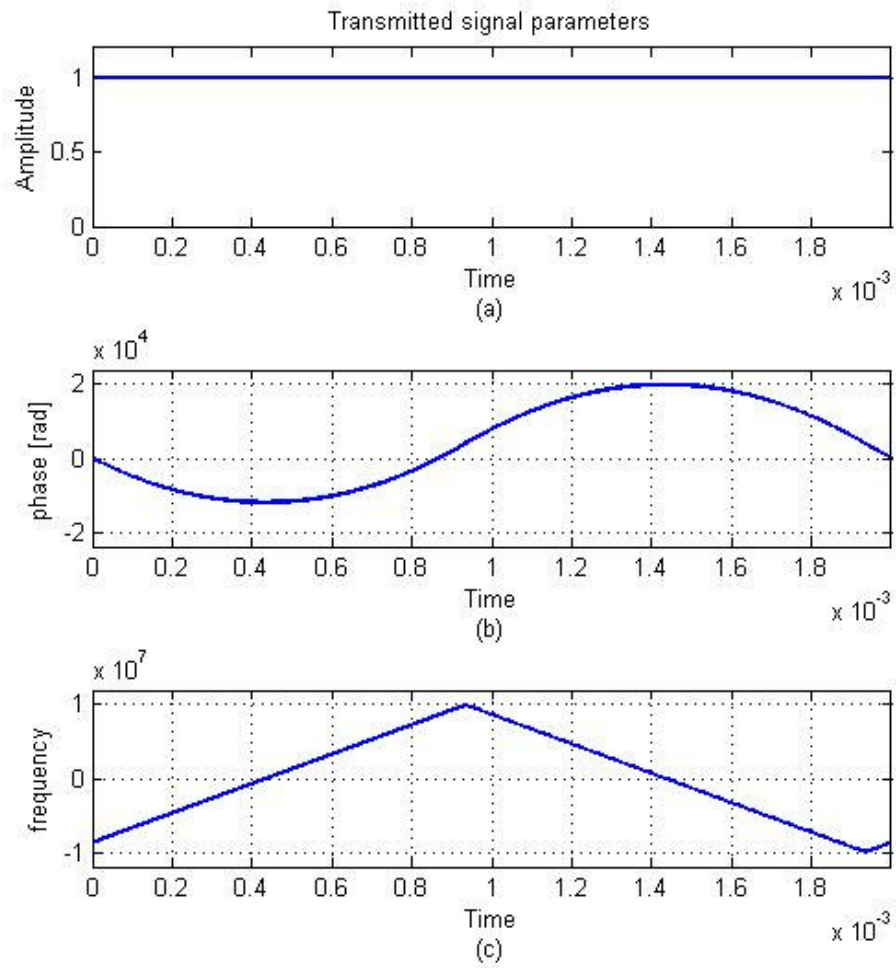


Figure 4. 51: (a) amplitude, (b) phase, and (c) frequency parameters for the FMCW coded transmitted signal used in multiple targets in same range and in different velocity simulation.

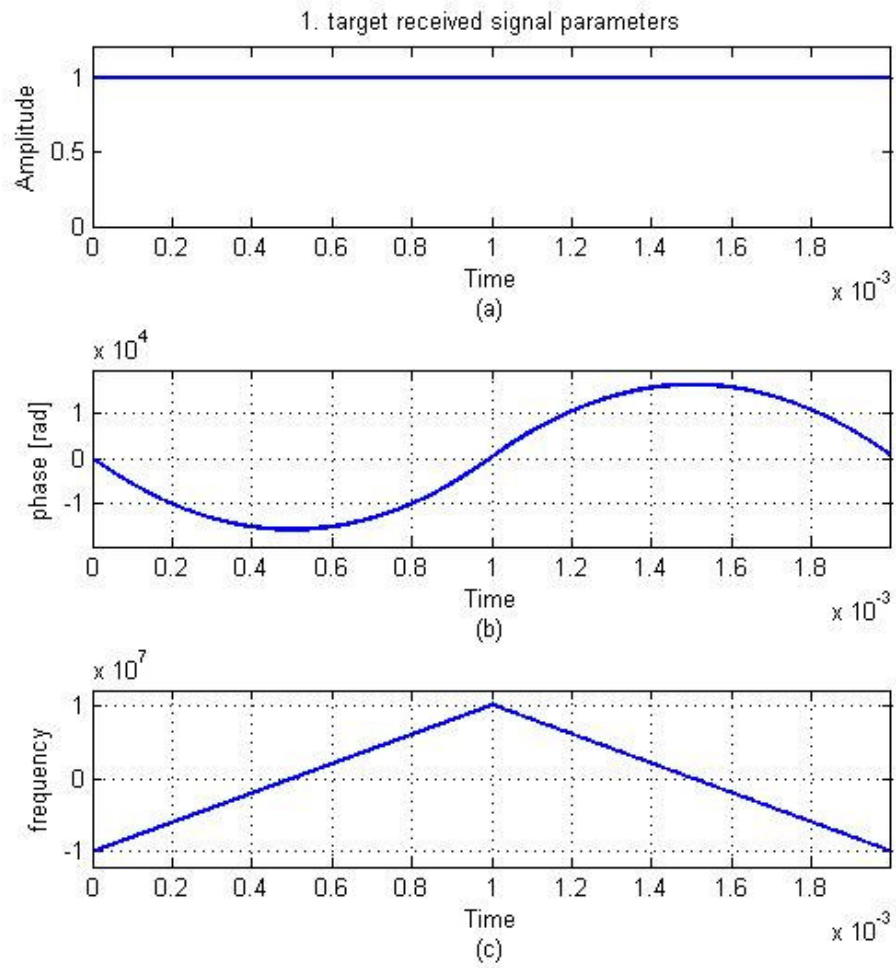


Figure 4. 52: (a) amplitude, (b) phase, and (c) frequency parameters for the FMCW coded 1.st target received signal used in multiple targets in same range and in different velocity simulation.

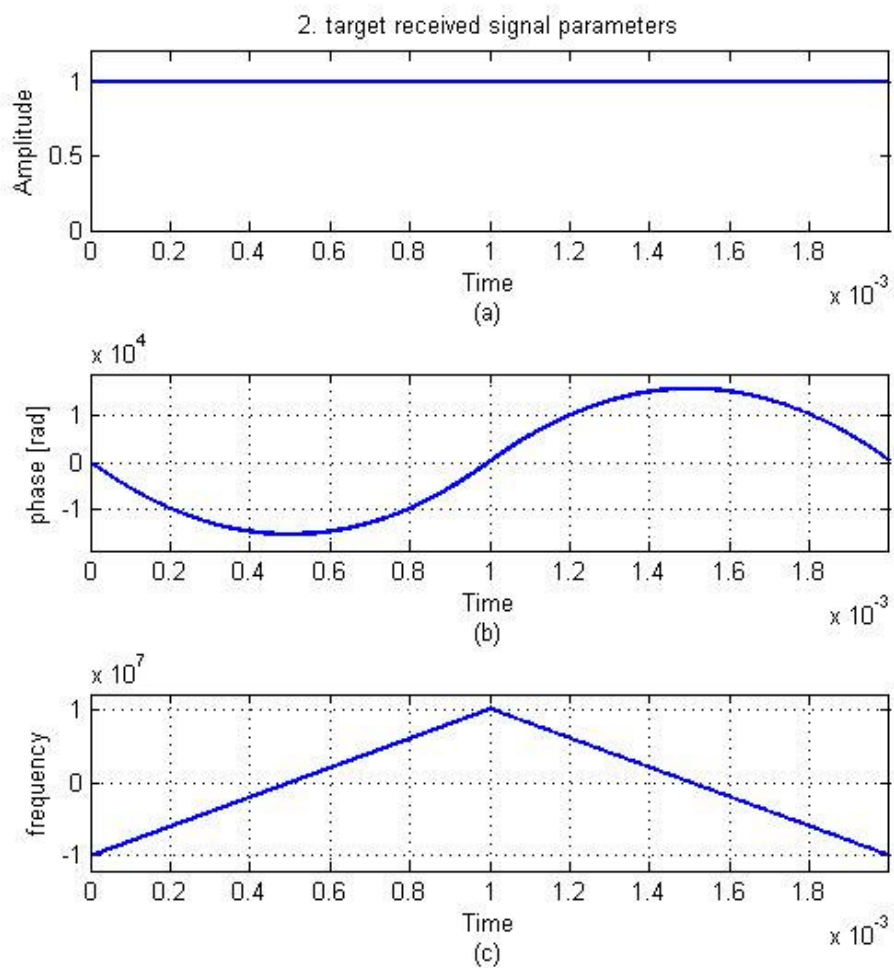


Figure 4. 53: (a) amplitude, (b) phase, and (c) frequency parameters for the FMCW coded 2.nd target received signal used in multiple targets in same range and in different velocity simulation.

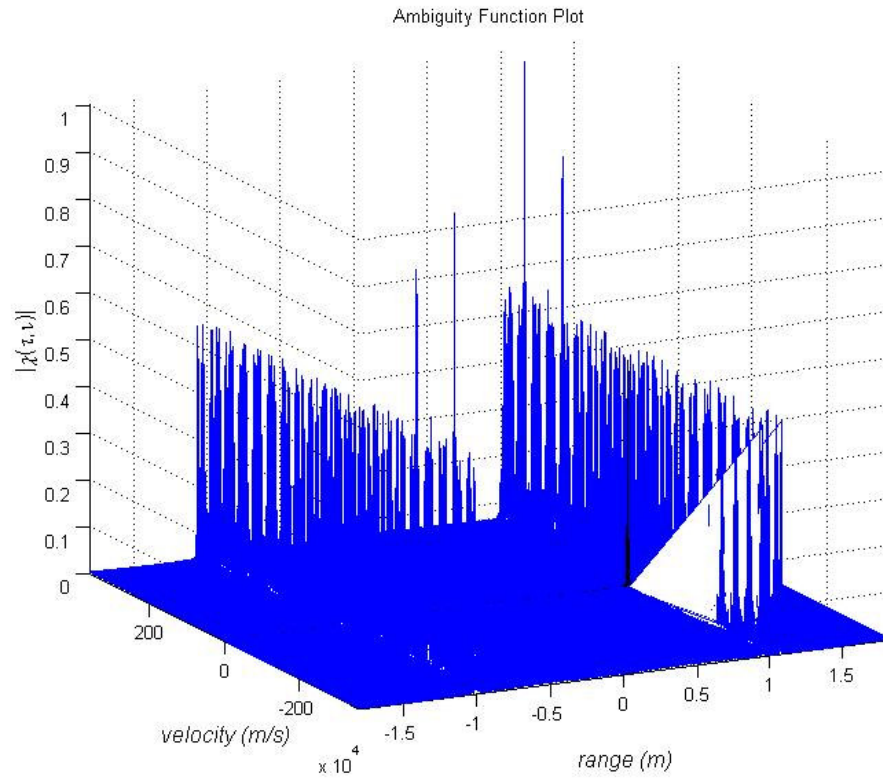


Figure 4. 54: 3-D Cross-Ambiguity function plot of FMCW coding technique ($\Delta R = 70$ m and $\Delta V = 7$ m/s) used in multiple targets in same range and in different velocity simulation.

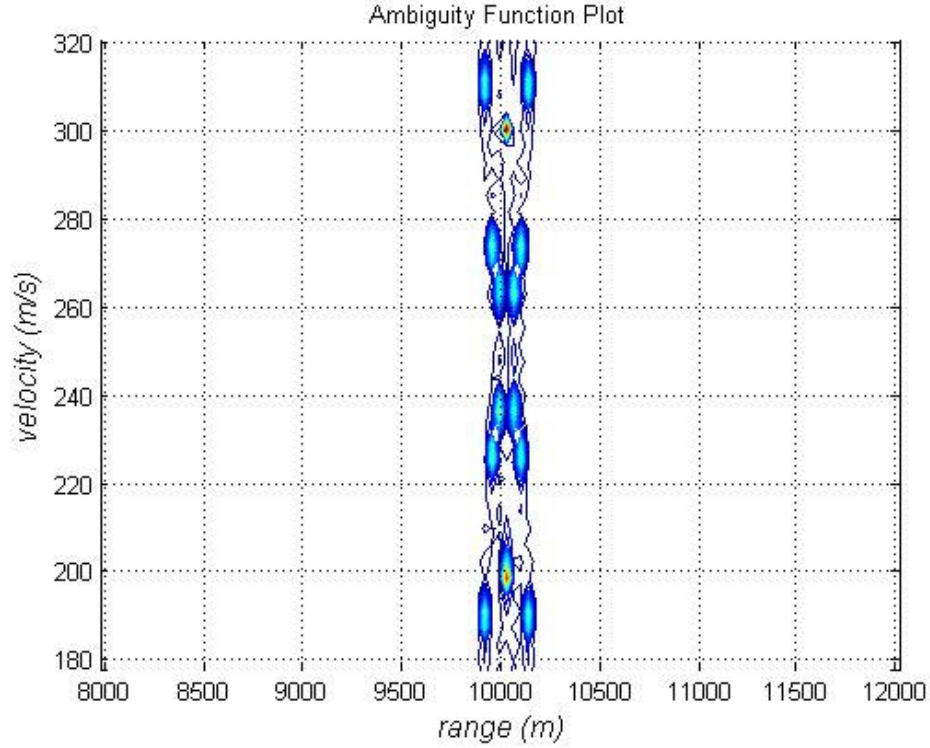


Figure 4. 55: Cross-Ambiguity function contour plot of FMCW coding technique ($\Delta R = 70$ m and $\Delta V = 7$ m/s) used in multiple targets in same range and in different velocity simulation.

The results of this simulation are presented in Figure 4.54 and Figure 4.55 showing the first target range as 10024 meter and radial velocity as 300 m/s and the second target range as 10024 meter and radial velocity as 199 m/s.

4.3.2.3.2.3 Use of Cross-Ambiguity Method with Costas Coding

Simulation 14: In this multiple target simulation by Cross-Ambiguity method with Costas coding, targets in same range and in different velocities are observed. In the scenario, first target range is used as 10000 meter and radial velocity is used as 300 m/s, second target range is used as 10000 meter and radial velocity is used as 200

m/s.

Figure 4.56 shows the transmitted signal parameters, Figure 4.57 shows the first target the received signal parameters and Figure 4.58 shows the second target the received signal parameters. Figure 4.59 and Figure 4.60 shows the resulting cross-ambiguity function graphs from complex envelopes of these signals.

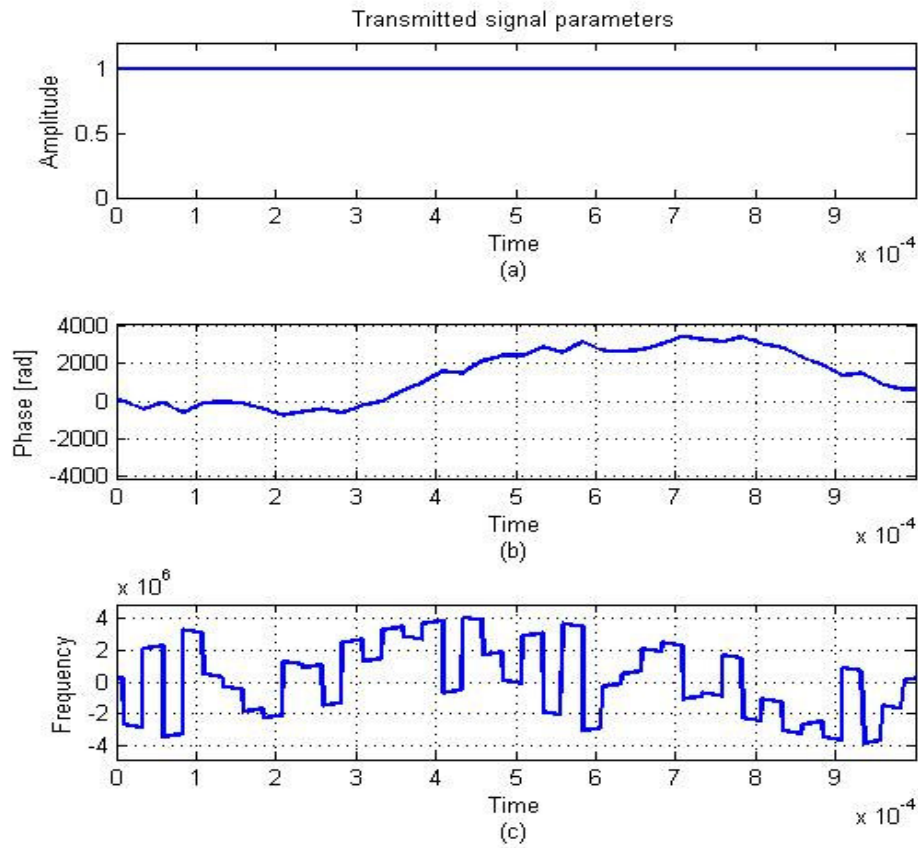


Figure 4. 56: (a) amplitude, (b) phase, and (c) frequency parameters for the Costas coded transmitted signal used in multiple targets in same range and in different velocity simulation.

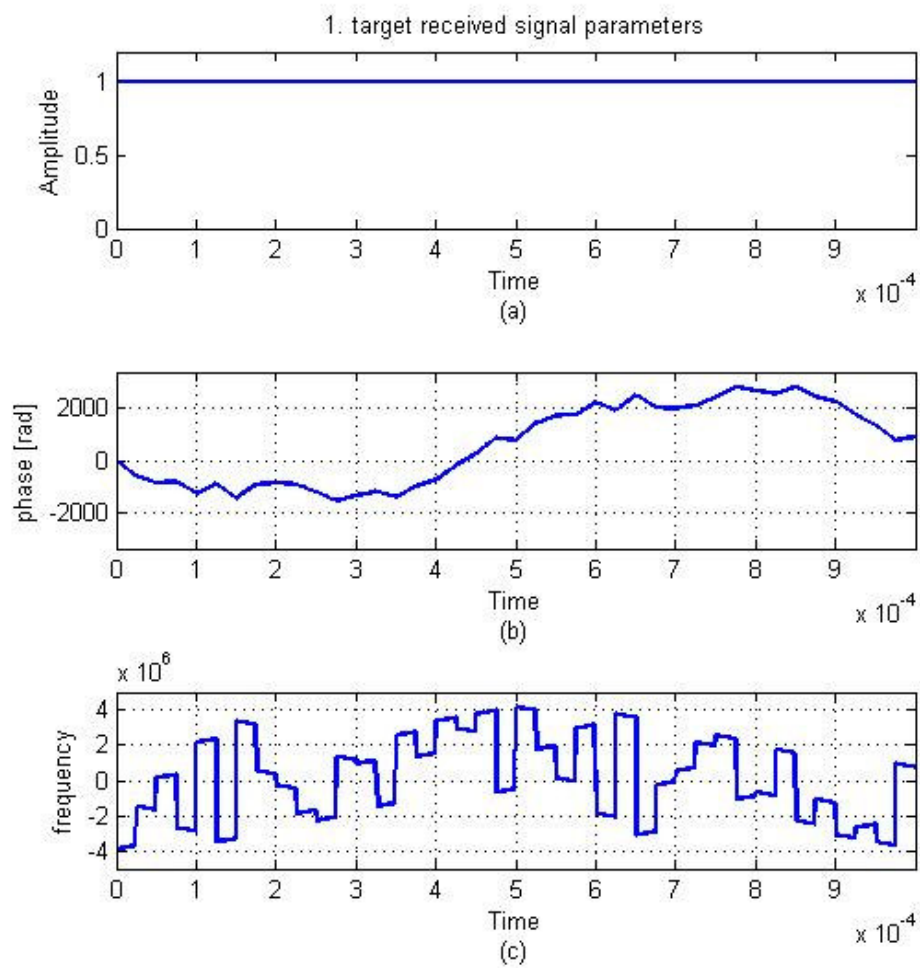


Figure 4. 57: (a) amplitude, (b) phase, and (c) frequency parameters for the Costas coded 1.st target received signal used in multiple targets in same range and in different velocity simulation.

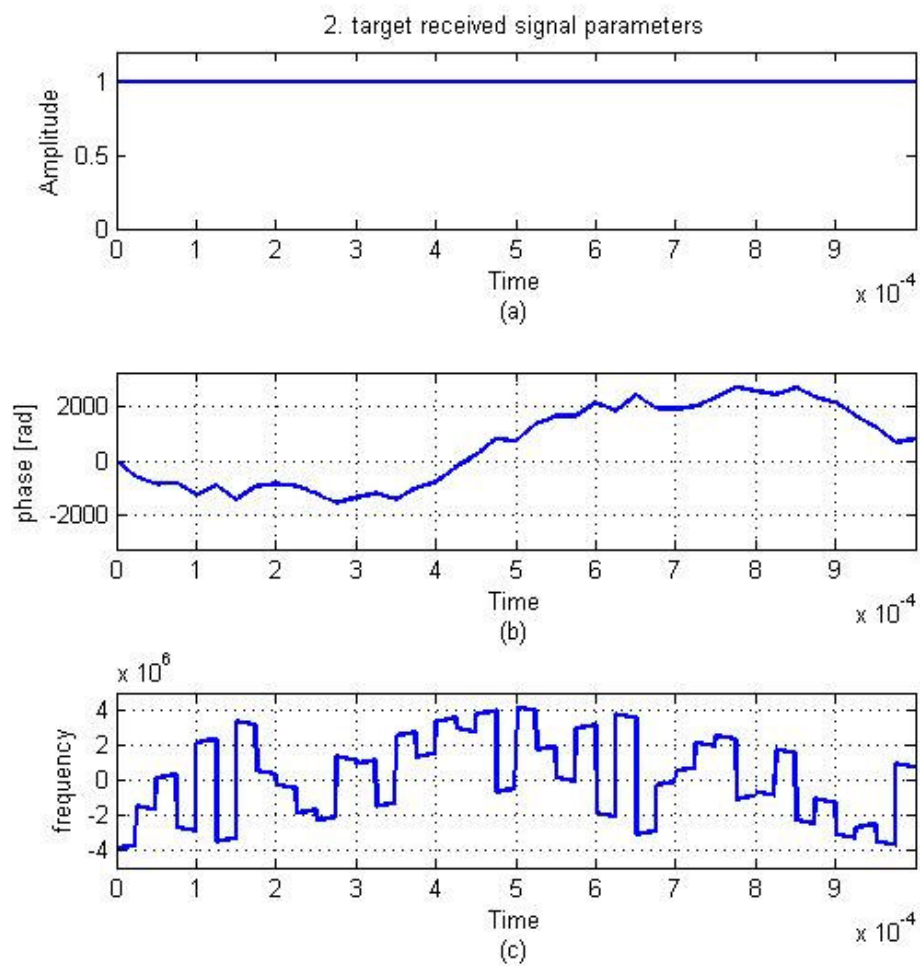


Figure 4. 58: (a) amplitude, (b) phase, and (c) frequency parameters for the Costas coded 2.nd target received signal used in multiple targets in same range and in different velocity simulation.

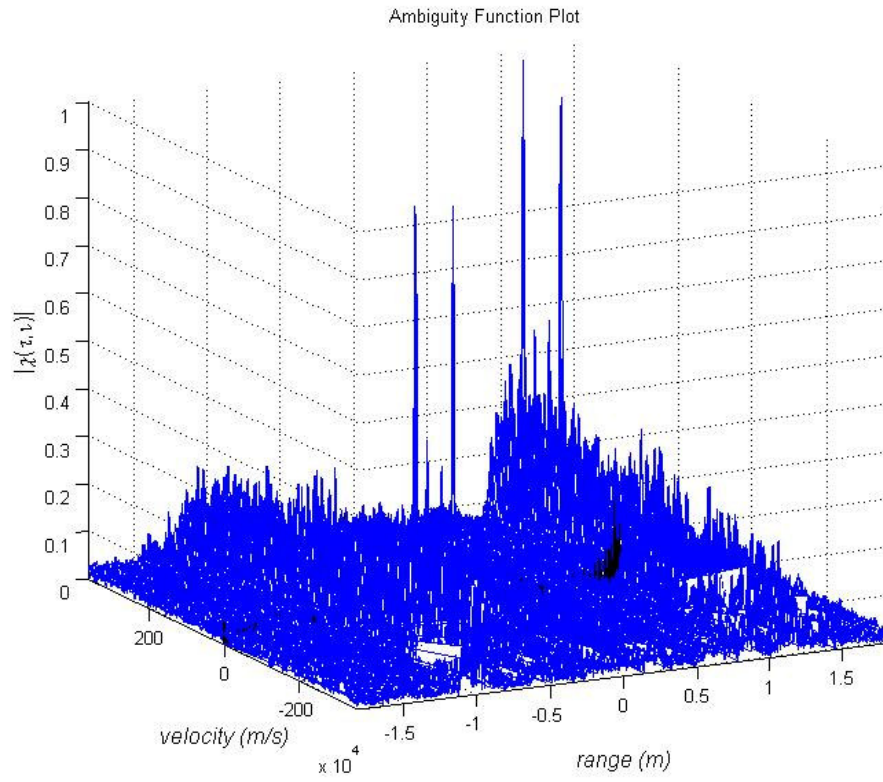


Figure 4. 59: 3-D Cross-Ambiguity function plot of Costas coding technique ($\Delta R = 120$ m and $\Delta V = 12$ m/s) used in multiple targets in same range and in different velocity simulation.

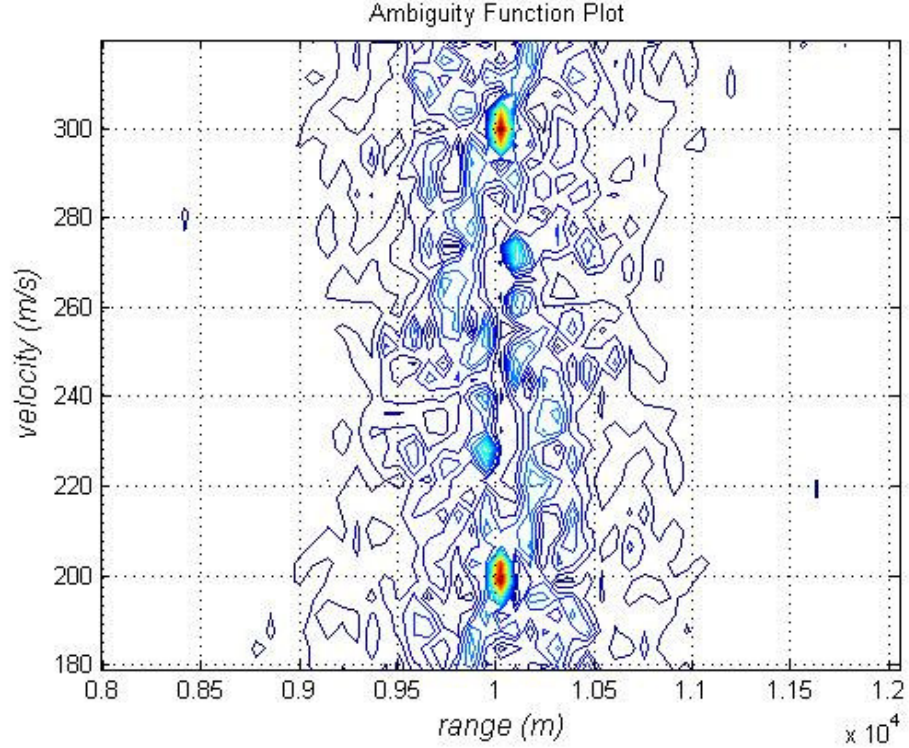


Figure 4. 60: Cross-Ambiguity function contour plot of Costas coding technique ($\Delta R = 120$ m and $\Delta V = 12$ m/s) used in multiple targets in same range and in different velocity simulation.

The results of this simulation are presented in Figure 4.59 and Figure 4.60 showing the first target range as 10024 meter and radial velocity as 300 m/s and the second target range as 10024 meter and radial velocity as 198 m/s.

In multiple target scenarios for targets in same range and in different velocity situation Ambiguity Function method give the successful results in simulations but we could not get exact results with the conventional spectrogram method. For this scenario the plot of Ambiguity function gives the exact target information (range and velocity) but the plot of spectrogram method gives unresolved results. It is impossible to choose which beat frequency pair belongs to which target from the

graph of spectrogram for this simulation.

4.3.2.3.3 Different Range and Same Velocity Scenario

4.3.2.3.3.1 Use of Conventional Spectrogram Method

Simulation 15: In this multiple target simulation by conventional spectrogram method, targets in different range and in same velocity are observed. In the scenario, first target range is used as 10000 meter and radial velocity is used as 200 m/s, second target range is used as 5000 meter and radial velocity is used as 200 m/s.

Figure 4.61 shows the theoretical beat frequency which is obtained by directly subtracting transmitted signal frequency from received signal frequency and Figure 4.62 shows the spectrogram of resulting mixer output.

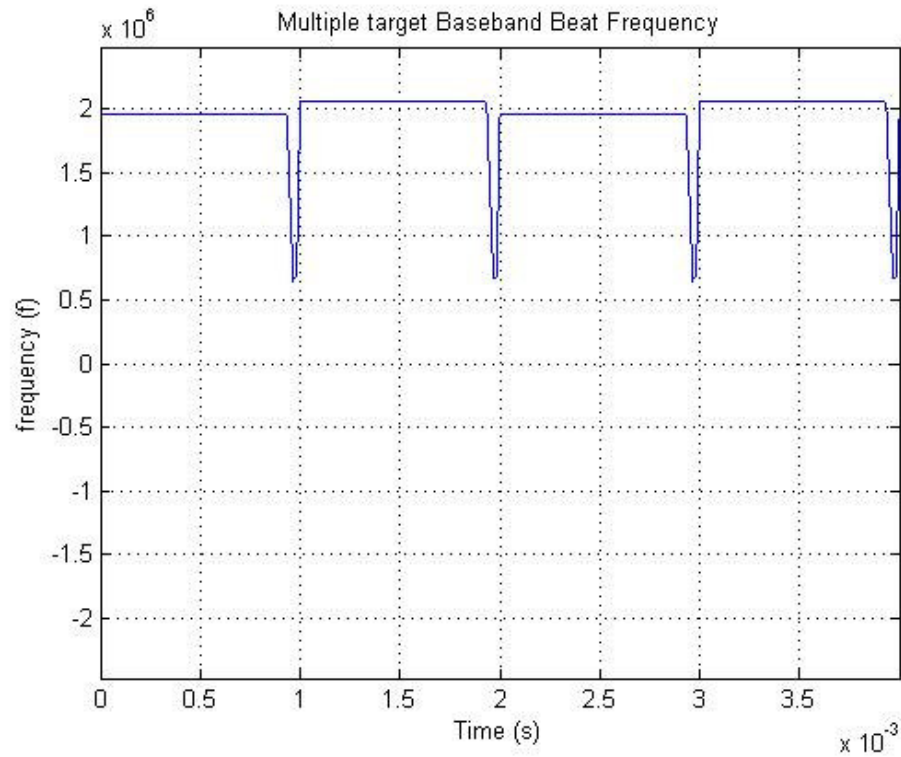


Figure 4. 61: Beat frequency of multiple targets in different range and in same velocity, obtained from the differences between the received and transmitted waveform frequency expressions directly.

From Figure 4.61 which is obtained by extracting the transmitted signal frequency from the received signal frequency directly, it is again very hard to understand that this beat frequency comes from two targets and it is impossible to extract real targets range and velocity values from this graph.

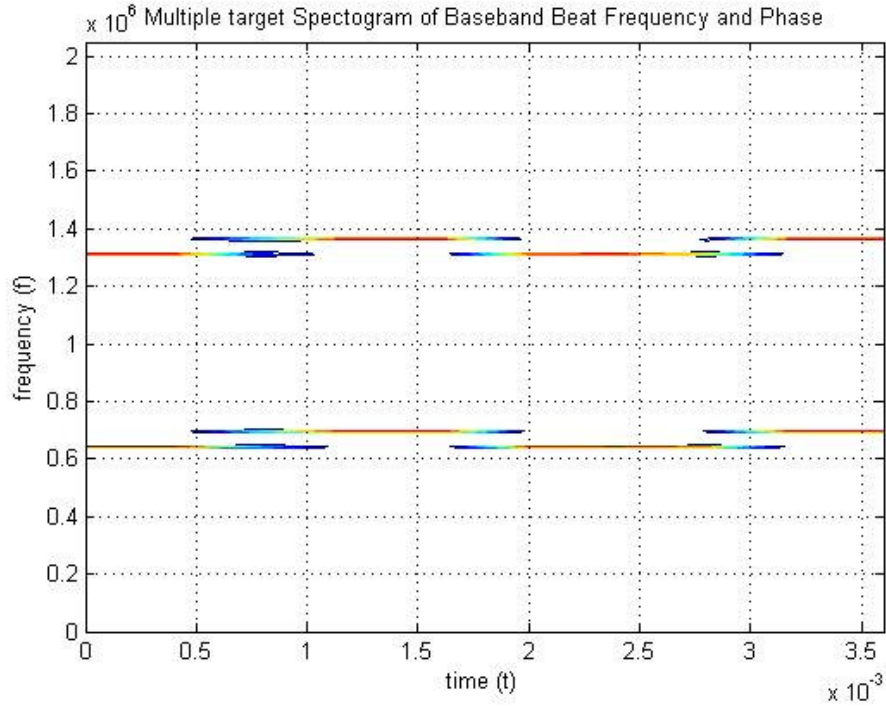


Figure 4. 62: Contour plot of the spectrogram of the filtered mixer output for multiple targets in different range and in same velocity simulation

From Figure 4.62, with beat frequency expressions extracted by spectrogram technique, we can calculate range and velocity of the targets by using (2.18) and (2.19). From Figure 4.62 beat frequencies for the first target is observed as 1.311 MHz and 1.365 MHz and beat frequencies for the second target is observed as 642 kHz and 696 kHz. With this beat frequencies we can calculate the first target range as 10035 meter and the radial velocity as 202.5 m/s and the second target range as 5017.5 meter and the radial velocity as 202.5 m/s.

4.3.2.3.3.2 Use of Cross-Ambiguity Method with FMCW Coding

Simulation 16: In this multiple target simulation by Cross-Ambiguity method with

FMCW coding, targets in different range and in same velocity are observed. In the scenario, first target range is used as 10000 meter and radial velocity is used as 200 m/s, second target range is used as 5000 meter and radial velocity is used as 200 m/s.

Figure 4.63 shows the transmitted signal parameters, Figure 4.64 shows the first target the received signal parameters and Figure 4.65 shows the second target the received signal parameters. Figure 4.66 and Figure 4.67 shows the resulting cross-ambiguity function graphs from complex envelopes of these signals.

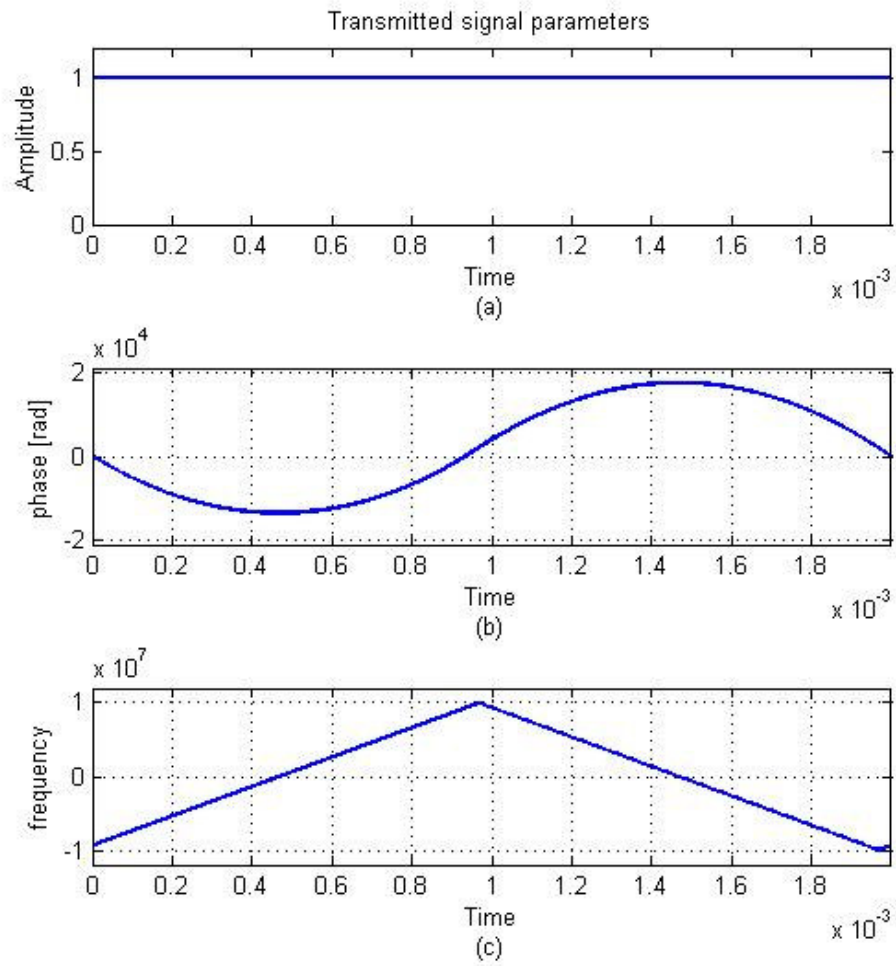


Figure 4. 63: (a) amplitude, (b) phase, and (c) frequency parameters for the FMCW coded transmitted signal used in multiple targets in different range and in same velocity simulation.

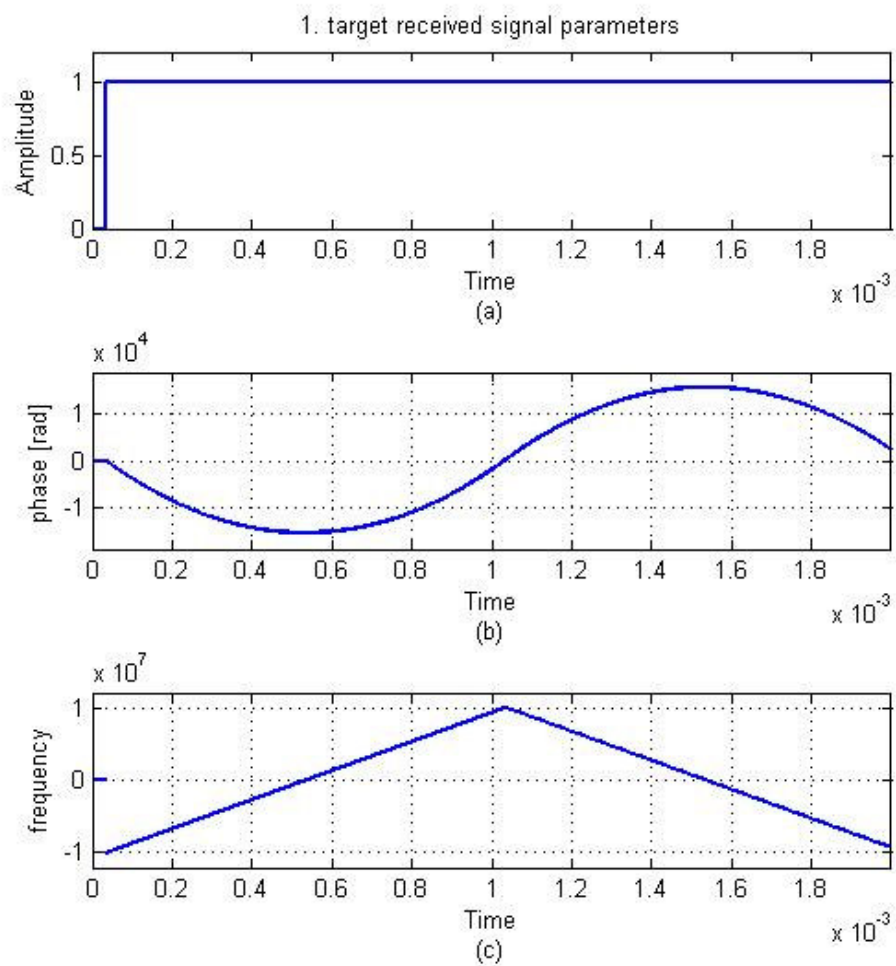


Figure 4. 64: (a) amplitude, (b) phase, and (c) frequency parameters for the FMCW coded 1.st target received signal used in multiple targets in different range and in same velocity simulation.

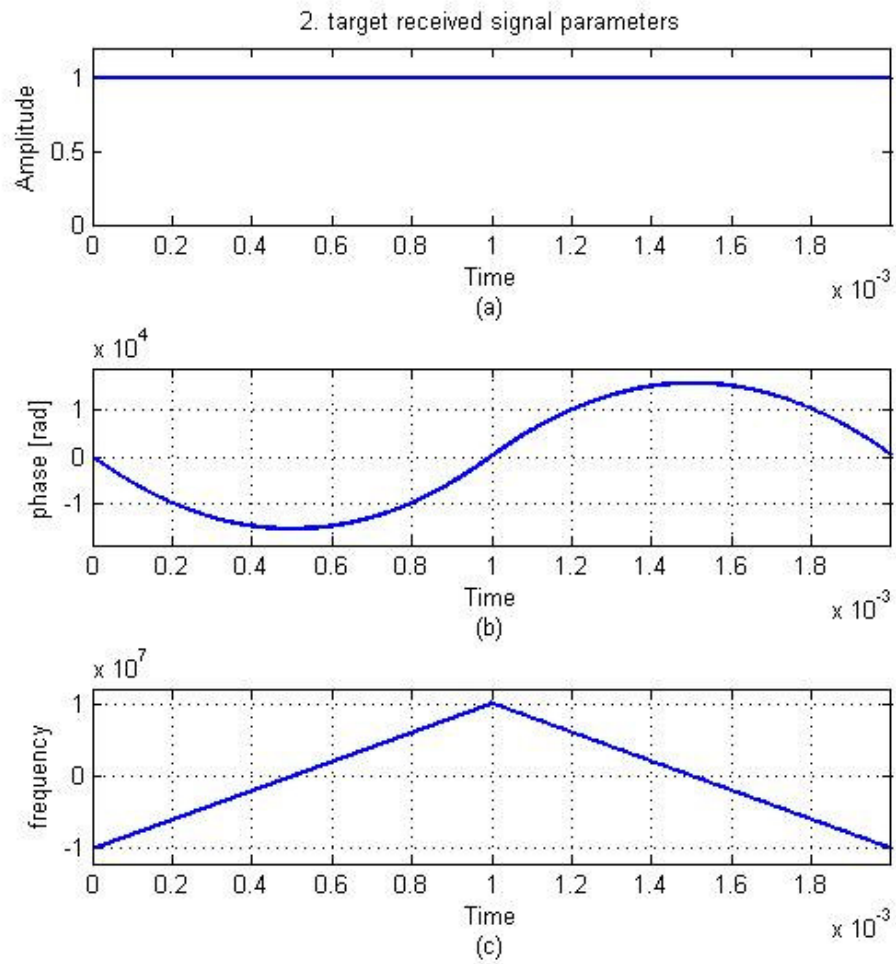


Figure 4. 65: (a) amplitude, (b) phase, and (c) frequency parameters for the FMCW coded 2.nd target received signal used in multiple targets in different range and in same velocity simulation.

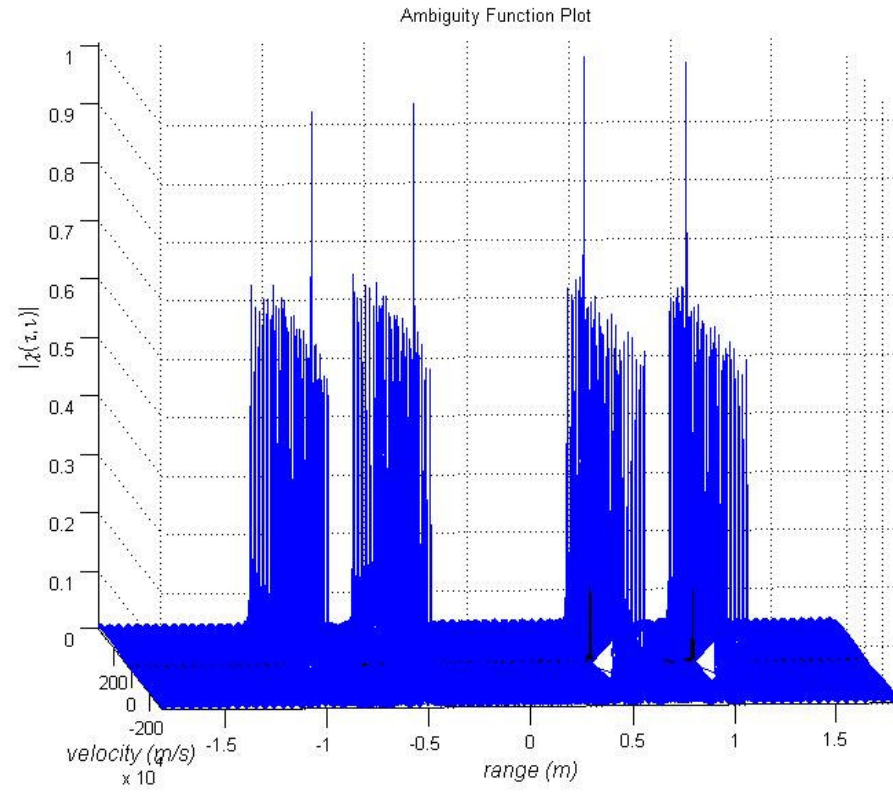


Figure 4. 66: 3-D Cross-Ambiguity function plot of FMCW coding technique ($\Delta R = 70$ m and $\Delta V = 7$ m/s) used in multiple targets in different range and in same velocity simulation.

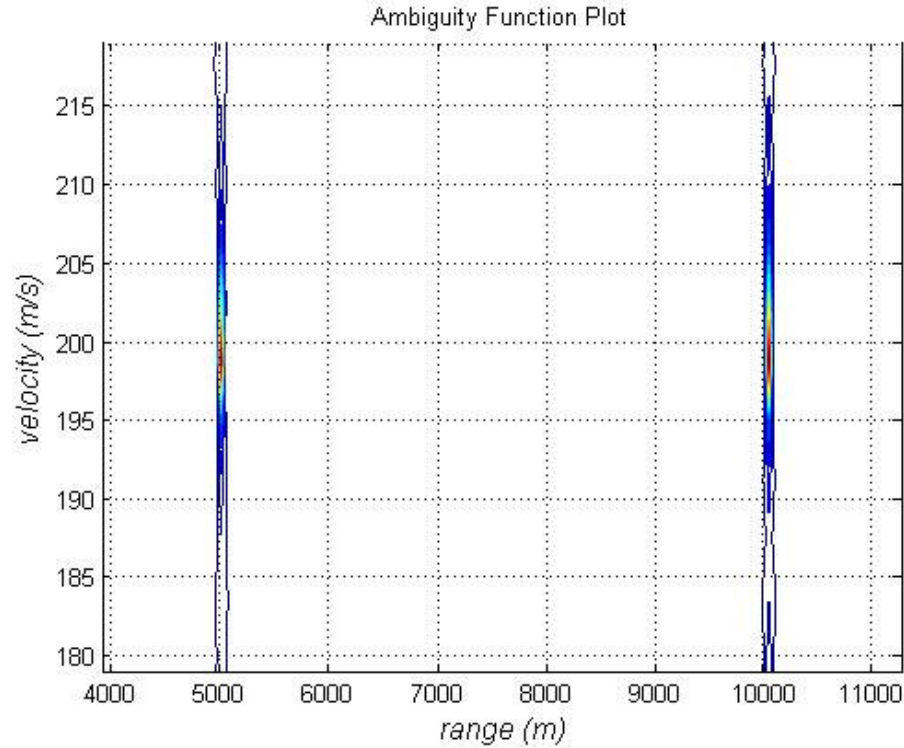


Figure 4. 67: Cross-Ambiguity function contour plot of FMCW coding technique ($\Delta R = 70$ m and $\Delta V = 7$ m/s) used in multiple targets in different range and in same velocity simulation.

The results of this simulation are presented in Figure 4.66 and Figure 4.67 showing the first target range as 10024 meter and radial velocity as 199 m/s and the second target range as 5012 meter and radial velocity as 199 m/s.

4.3.2.3.3 Use of Cross-Ambiguity Method with Costas Coding

Simulation 17: In this multiple target simulation by Cross-Ambiguity method with Costas coding, targets in different range and in same velocity are observed. In the scenario, first target range is used as 10000 meter and radial velocity is used as 200

m/s, second target range is used as 5000 meter and radial velocity is used as 200 m/s.

Figure 4.68 shows the transmitted signal parameters, Figure 4.69 shows the first target the received signal parameters and Figure 4.70 shows the second target the received signal parameters. Figure 4.71 and Figure 4.72 shows the resulting cross-ambiguity function graphs from complex envelopes of these signals.

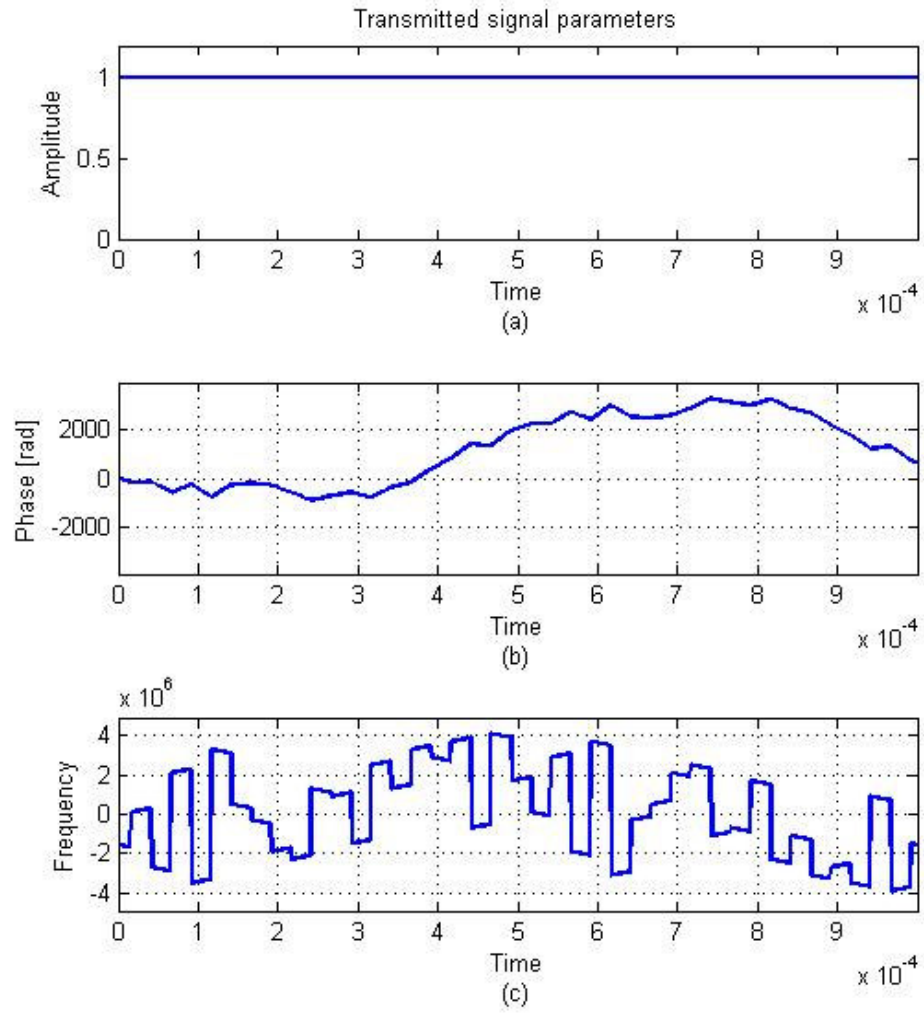


Figure 4. 68: (a) amplitude, (b) phase, and (c) frequency parameters for the Costas coded transmitted signal used in multiple targets in different range and in same velocity simulation.

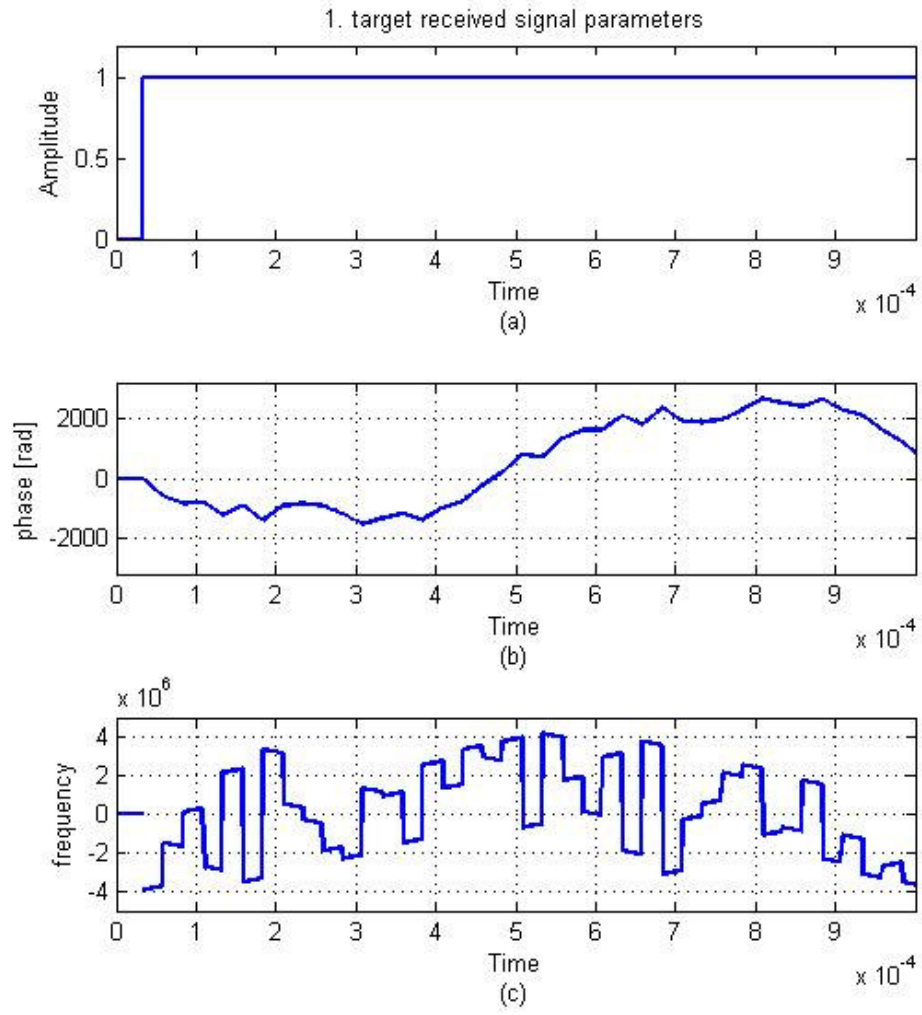


Figure 4. 69: (a) amplitude, (b) phase, and (c) frequency parameters for the Costas coded 1.st target received signal used in multiple targets in different range and in same velocity simulation.

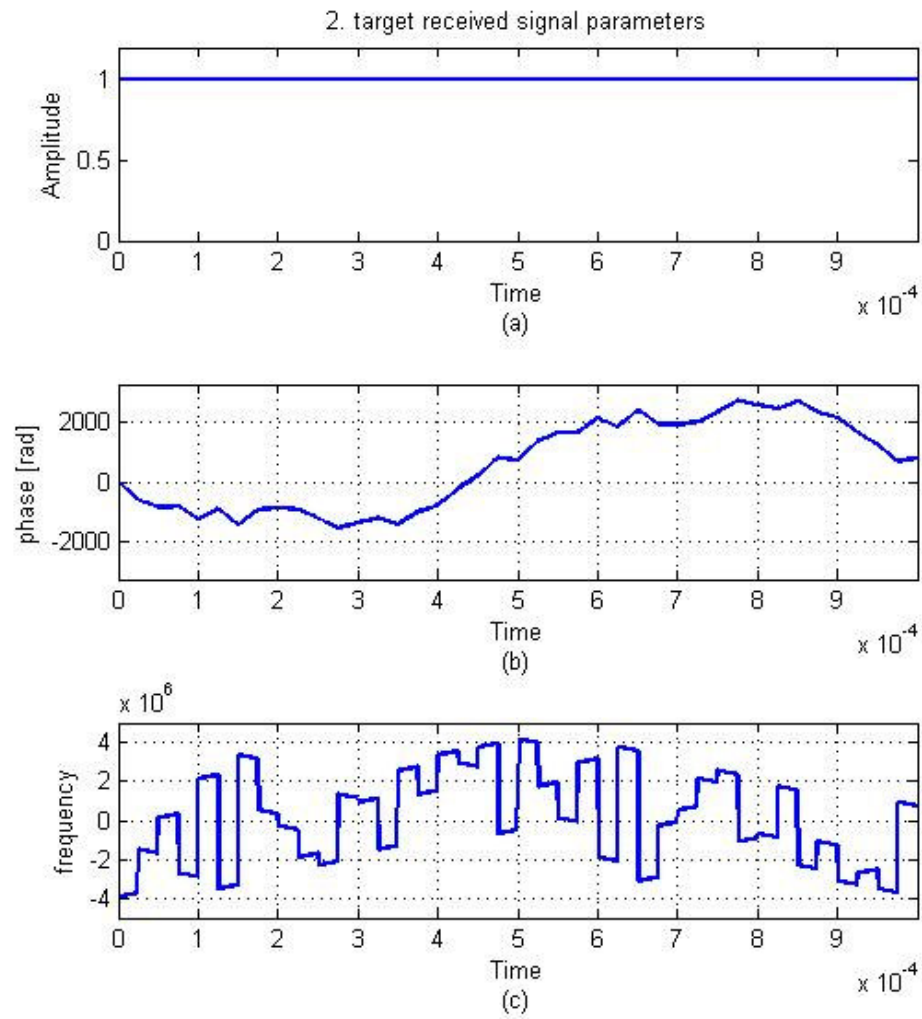


Figure 4. 70: (a) amplitude, (b) phase, and (c) frequency parameters for the Costas coded 2.nd target received signal used in multiple targets in different range and in same velocity simulation.

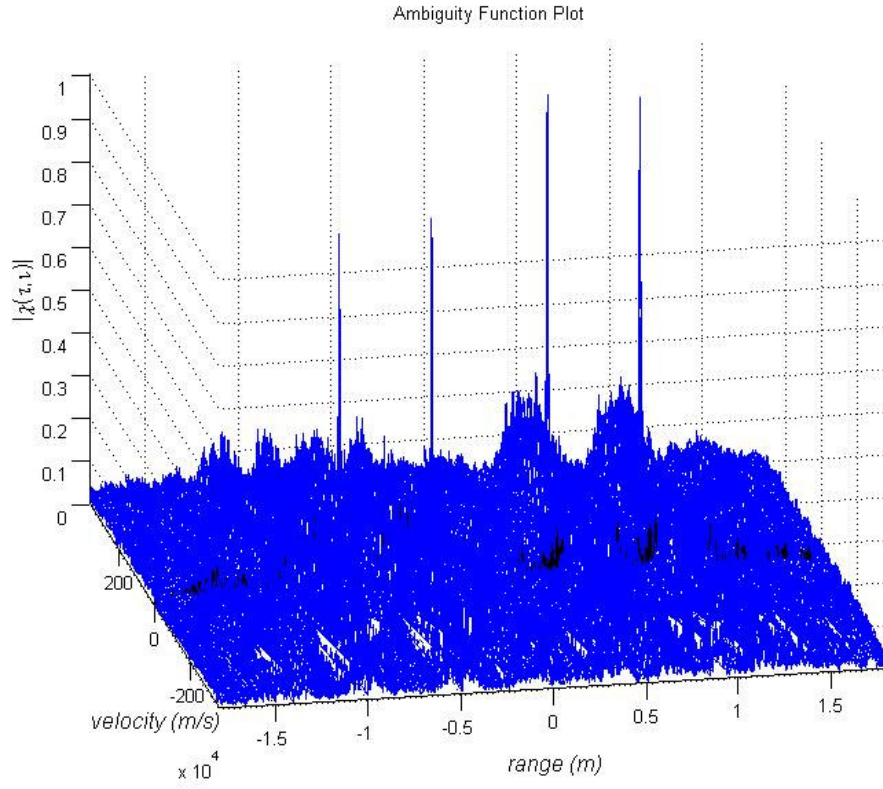


Figure 4. 71: 3-D Cross-Ambiguity function plot of Costas coding technique ($\Delta R = 120$ m and $\Delta V = 12$ m/s) used in multiple targets in different range and in same velocity simulation.

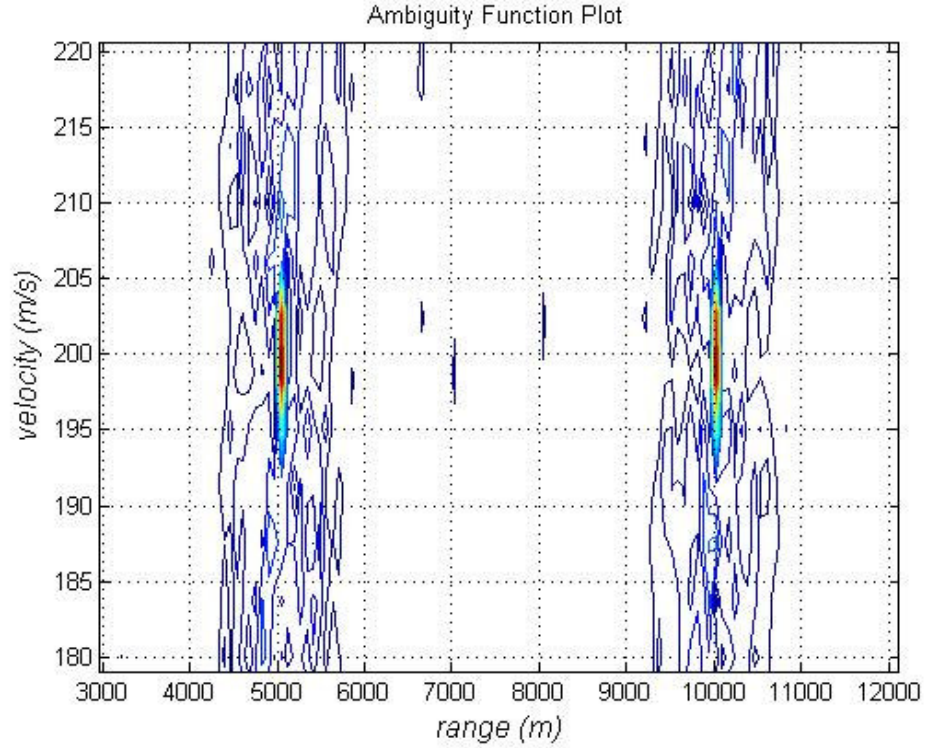


Figure 4. 72: Cross-Ambiguity function contour plot of Costas coding technique ($\Delta R = 120$ m and $\Delta V = 12$ m/s) used in multiple targets in different range and in same velocity simulation.

The results of this simulation are presented in Figure 4.71 and Figure 4.72 showing the first target range as 10024 meter and radial velocity as 198 m/s and the second target range as 5048 meter and radial velocity as 199 m/s.

In multiple target scenarios for targets in different range and in same velocity situation conventional spectrogram method and the Ambiguity Function method give the successful results in simulations. For multiple targets while plot of Ambiguity Function method gives the exact target information (range and velocity) for each one separately, conventional spectrogram method needs more iterations. From the spectrogram graph firstly which beat frequency pair belongs to which target must be

chosen then for each target with these frequency pairs target information is extracted by solving equations (2.18) and (2.19) simultaneously. For the case targets are closer to each other it can be difficult to choose which frequency pair belongs to which target for the spectrogram method.

4.3.2.3.4 Range and Velocity in the Vicinity of Radar Resolution Values

In section 4.3.1 with auto-ambiguity function we have found the range and Doppler resolution values of the FMCW coded radar and Costas coded radar. From auto-ambiguity plot of FMCW coded radar (Figure 4.12) range resolution is found as 70 m and Doppler resolution is found as 7 m/s. From auto-ambiguity plot of Costas coded radar (Figure 4.15) range resolution is found as 120 m and Doppler resolution is found as 12.5 m/s.

For the validation of auto-ambiguity function resolution results we use cross-ambiguity function for detection of targets in the vicinity of Doppler and range resolution values.

Simulation 18: In this multiple target simulation, targets in the range resolution value of the FMCW coded radar are observed. In the scenario, first target range is used as 10000 meter and radial velocity is used as 200 m/s, second target range is used as 10050 meter and radial velocity is used as 200 m/s.

Figure 4.73 and Figure 4.74 shows the results of this simulation.

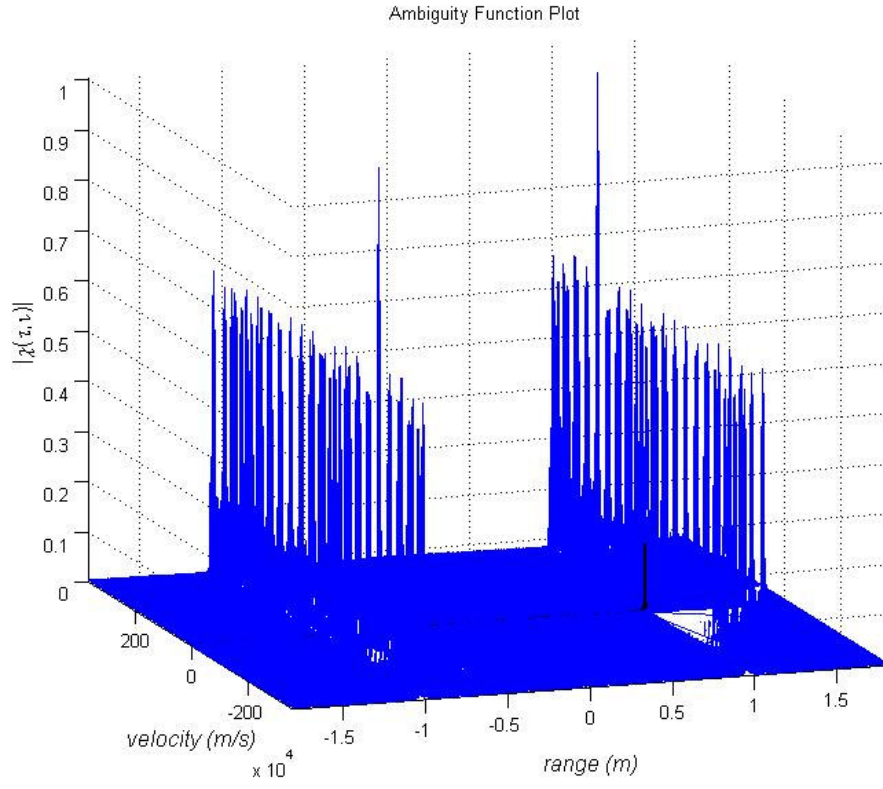


Figure 4. 73: 3-D Cross-Ambiguity function plot of FMCW coding technique ($\Delta R = 70$ m and $\Delta V = 7$ m/s) used in multiple targets in the range resolution value of the radar simulation.

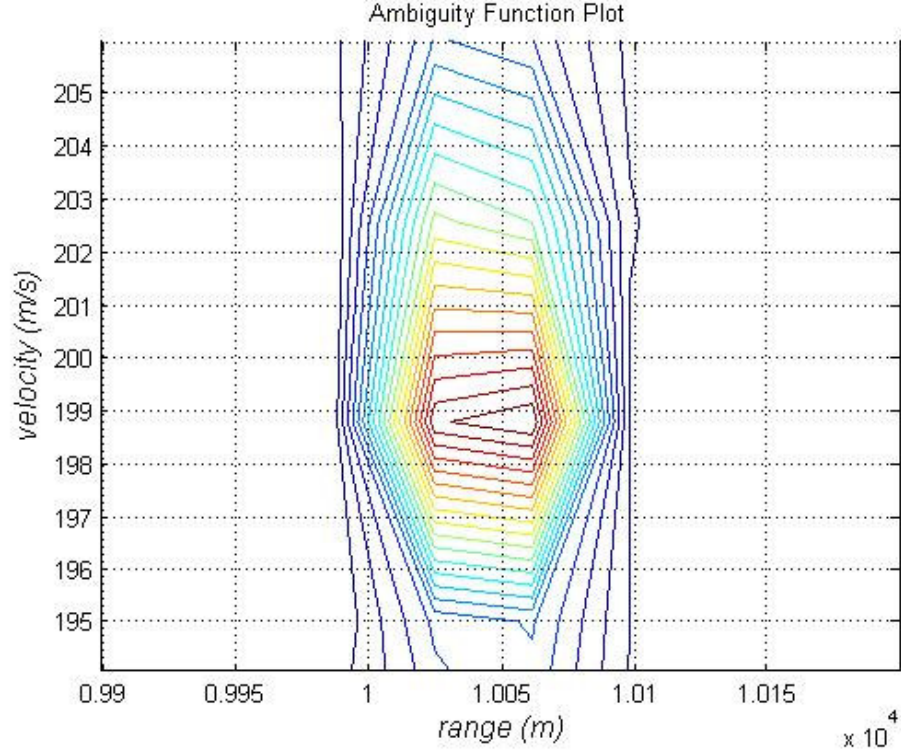


Figure 4. 74: Cross-Ambiguity function contour plot of FMCW coding ($\Delta R = 70$ m and $\Delta V = 7$ m/s) technique used in multiple targets in the range resolution value of the radar simulation.

Since targets are closer each other than the range resolution value of the FMCW coded radar, radar can not resolve these targets and sees them as a one target.

Simulation 19: In this multiple target simulation, targets near the range resolution value of the FMCW coded radar are observed. This time the interval between targets is a little bit larger than the interval between targets in simulation 19. In the scenario, first target range is used as 10000 meter and radial velocity is used as 200 m/s, second target range is used as 10080 meter and radial velocity is used as 200 m/s.

Figure 4.75 and Figure 4.76 shows the results of this simulation.

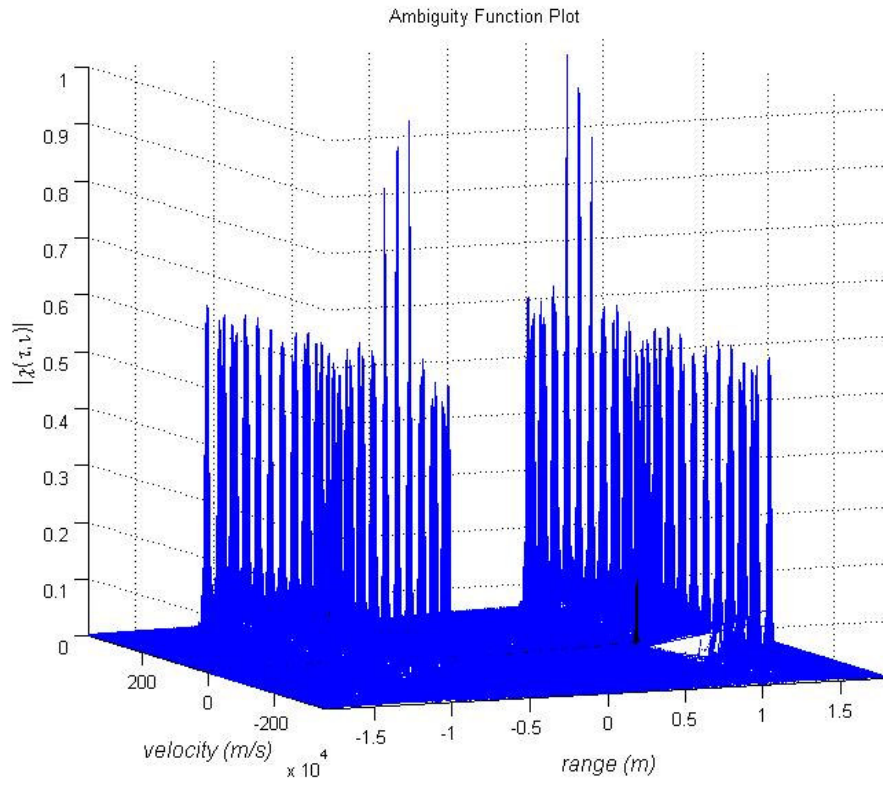


Figure 4. 75: 3-D Cross-Ambiguity function plot of FMCW coding technique ($\Delta R = 70$ m and $\Delta V = 7$ m/s) used in multiple targets near the range resolution value of the radar simulation.

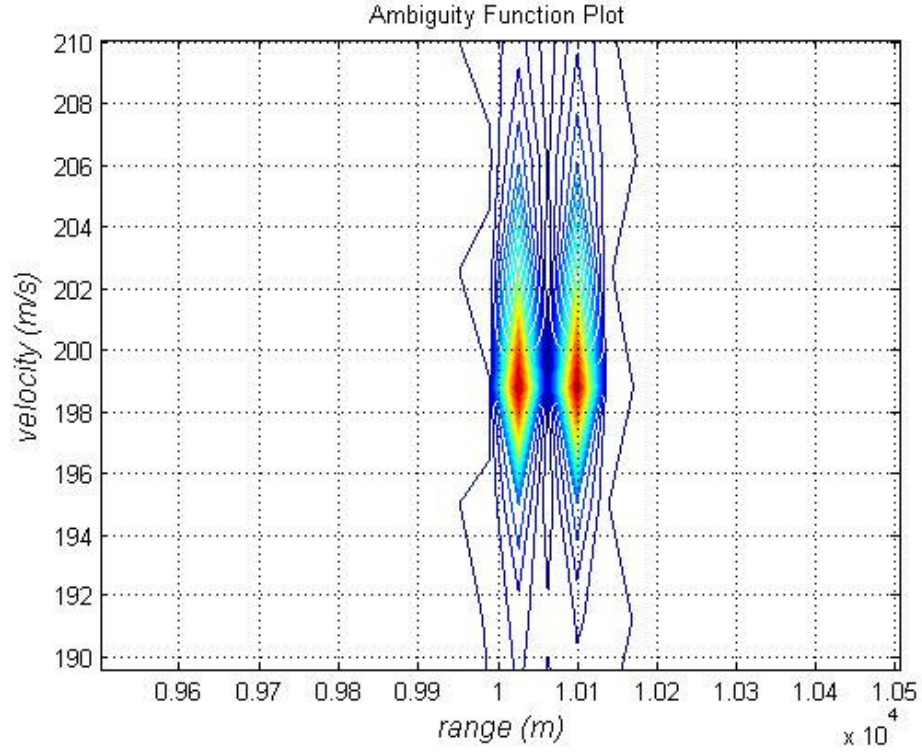


Figure 4. 76: Cross-Ambiguity function contour plot of FMCW coding technique ($\Delta R = 70$ m and $\Delta V = 7$ m/s) used in multiple targets near the range resolution value of the radar simulation.

Since targets are not closer each other than the range resolution value of the radar, radar can resolve these targets and sees them separately. But with this simulation we saw the drawbacks of the high sidelobes near the main lobe of Auto-Ambiguity function. Since FMCW coded radar has high sidelobes when the targets are closer to each other this sidelobes superpose each other and appears in the radar like a target.

Simulation 20: In this multiple target simulation, targets in the range resolution value of the Costas coded radar are observed. In the scenario, first target range is used as 10000 meter and radial velocity is used as 200 m/s, second target range is

used as 10100 meter and radial velocity is used as 200 m/s.

Figure 4.77 and Figure 4.78 shows the results of this simulation.

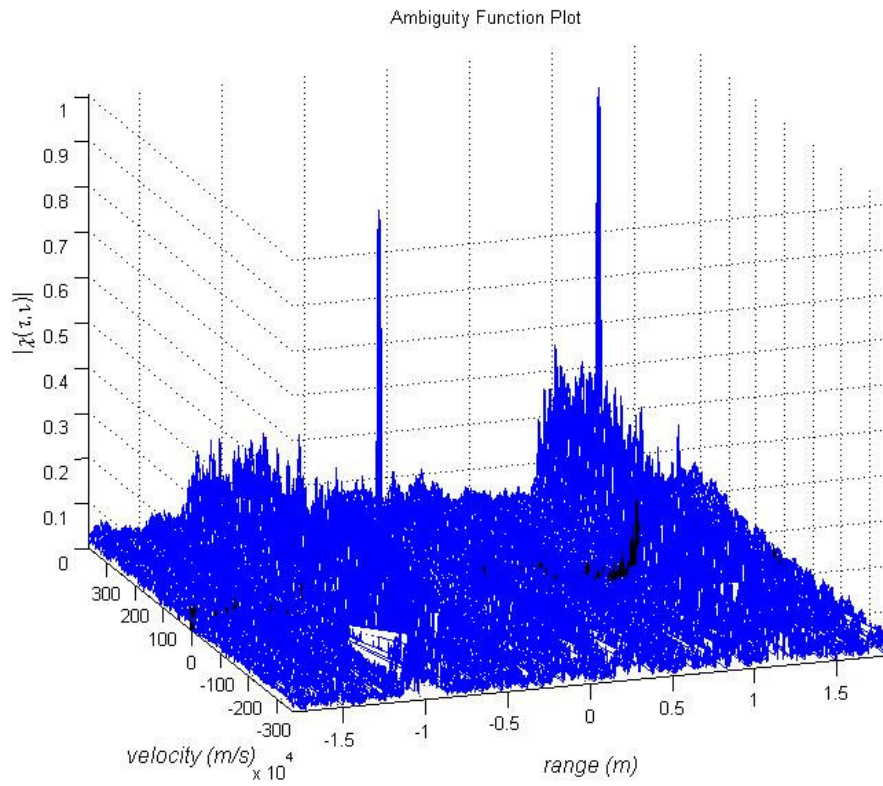


Figure 4. 77: 3-D Cross-Ambiguity function plot of Costas coding technique ($\Delta R = 120$ m and $\Delta V = 12$ m/s) used in multiple targets in the range resolution value of the radar simulation.

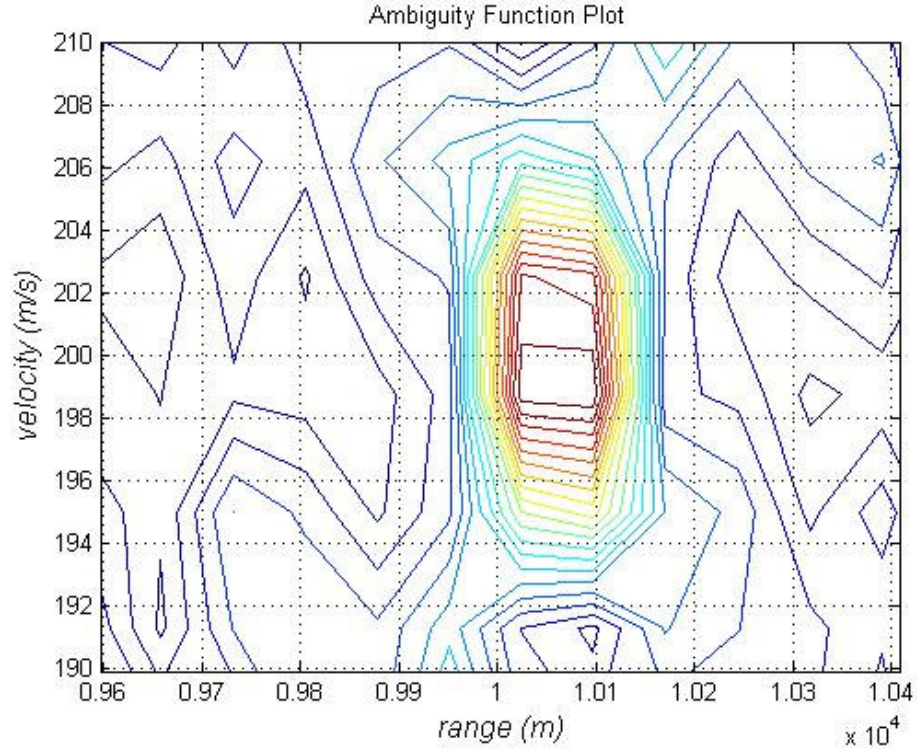


Figure 4. 78: Cross-Ambiguity function contour plot of Costas coding technique ($\Delta R = 120$ m and $\Delta V = 12$ m/s) used in multiple targets in the range resolution value of the radar simulation.

Since targets are closer each other than the range resolution value of the Costas coded radar, radar can not resolve these targets and sees them as a one target.

Simulation 21: In this multiple target simulation, targets near the range resolution value of the Costas coded radar are observed. This time the interval between targets is a little bit larger than the interval between targets in simulation 20. In the scenario, first target range is used as 10000 meter and radial velocity is used as 200 m/s, second target range is used as 10130 meter and radial velocity is used as 200 m/s.

Figure 4.79 and Figure 4.80 shows the results of this simulation.

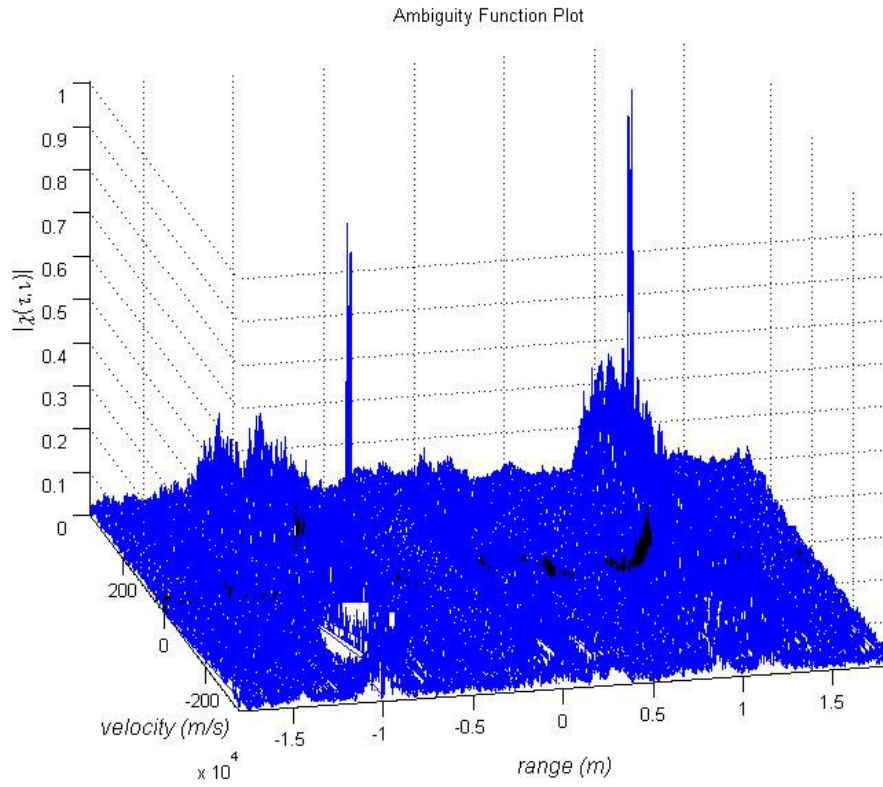


Figure 4. 79: 3-D Cross-Ambiguity function plot of Costas coding technique ($\Delta R = 120$ m and $\Delta V = 12$ m/s) used in multiple targets near the range resolution value of the radar simulation.

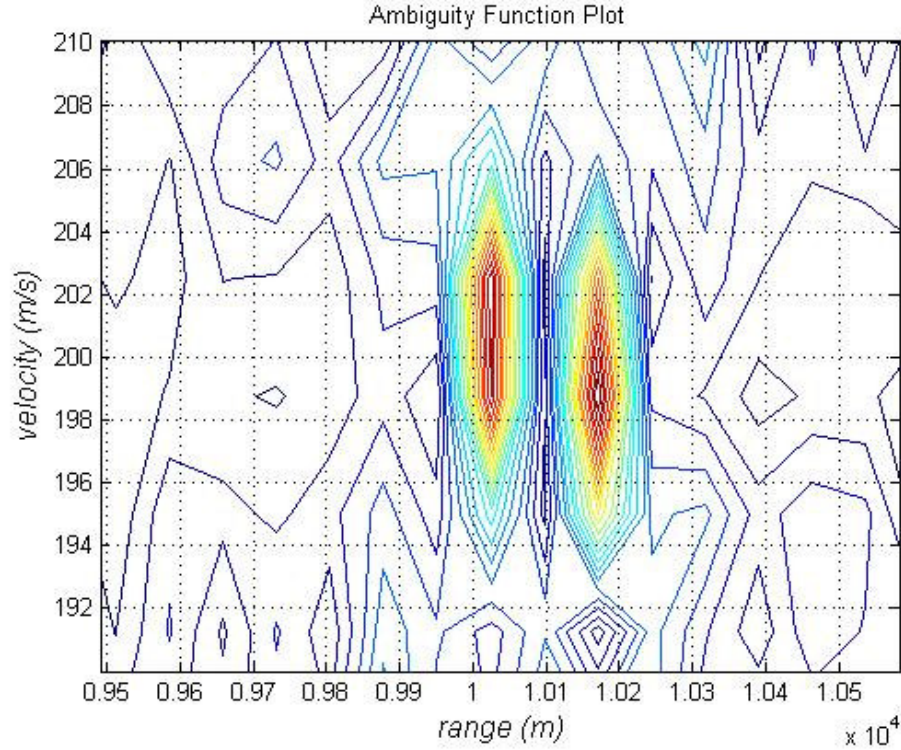


Figure 4. 80: Cross-Ambiguity function contour plot of Costas coding technique ($\Delta R = 120$ m and $\Delta V = 12$ m/s) used in multiple targets near the range resolution value of the radar simulation.

Since targets are not closer each other than the range resolution value of the Costas coded radar, radar can resolve these targets and sees them separately. Since Auto-Ambiguity function of Costas coded radar has small sidelobes with respect to main lobe, even if sidelobes superpose with each other for very closer targets they can not become a false target unlike FMCW coded radar.

Simulation 22: In this multiple target simulation, targets in the Doppler resolution value of the FMCW coded radar are observed. In the scenario, first target range is used as 10000 meter and radial velocity is used as 200 m/s, second target range is

used as 10000 meter and radial velocity is used as 203 m/s.

Figure 4.81 and Figure 4.82 shows the results of this simulation.

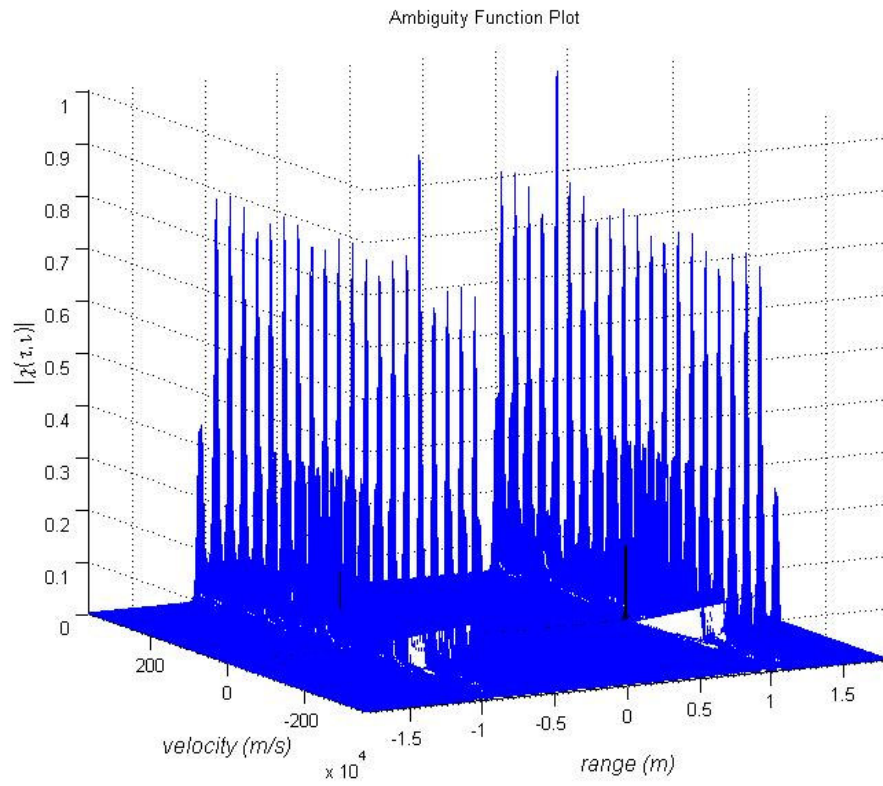


Figure 4. 81: 3-D Cross-Ambiguity function plot of FMCW coding technique ($\Delta R = 70$ m and $\Delta V = 7$ m/s) used in multiple targets in the Doppler resolution value of the radar simulation.

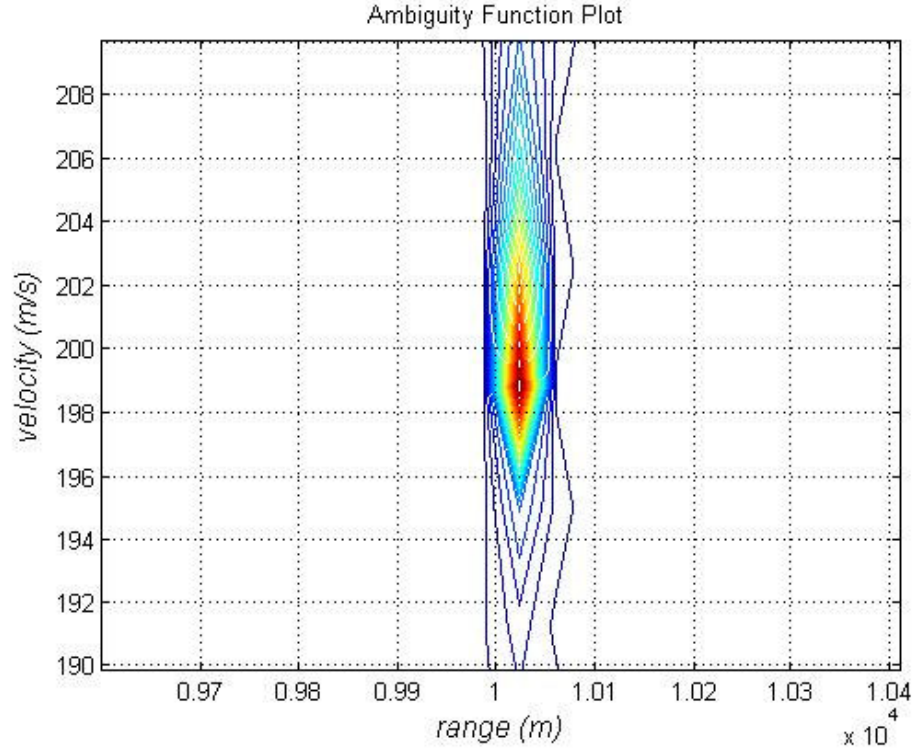


Figure 4. 82: Cross-Ambiguity function plot of FMCW coding technique ($\Delta R = 70$ m and $\Delta V = 7$ m/s) used in multiple targets in the Doppler resolution value of the radar simulation.

Since targets are in the same range and the relative velocity between the targets are smaller than the Doppler resolution value of the FMCW coded radar, radar can not resolve these targets and sees them as a one target.

Simulation 23: In this multiple target simulation, targets near the Doppler resolution value of the FMCW coded radar are observed. This time the relative velocity between targets is a little bit larger than the interval between targets in simulation 22. In the scenario, first target range is used as 10000 meter and radial velocity is used as 200 m/s, second target range is used as 10000 meter and radial velocity is used as

207 m/s.

Figure 4.83 and Figure 4.84 shows the results of this simulation.

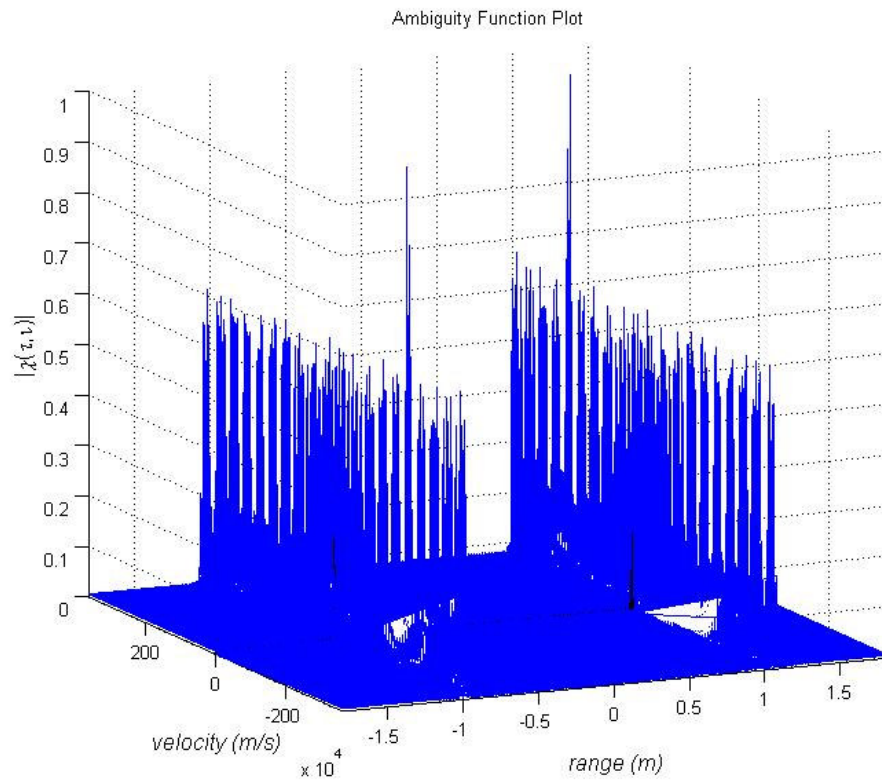


Figure 4. 83: 3-D Cross-Ambiguity function plot of FMCW coding technique ($\Delta R = 70$ m and $\Delta V = 7$ m/s) used in multiple targets near the Doppler resolution value of the radar simulation.

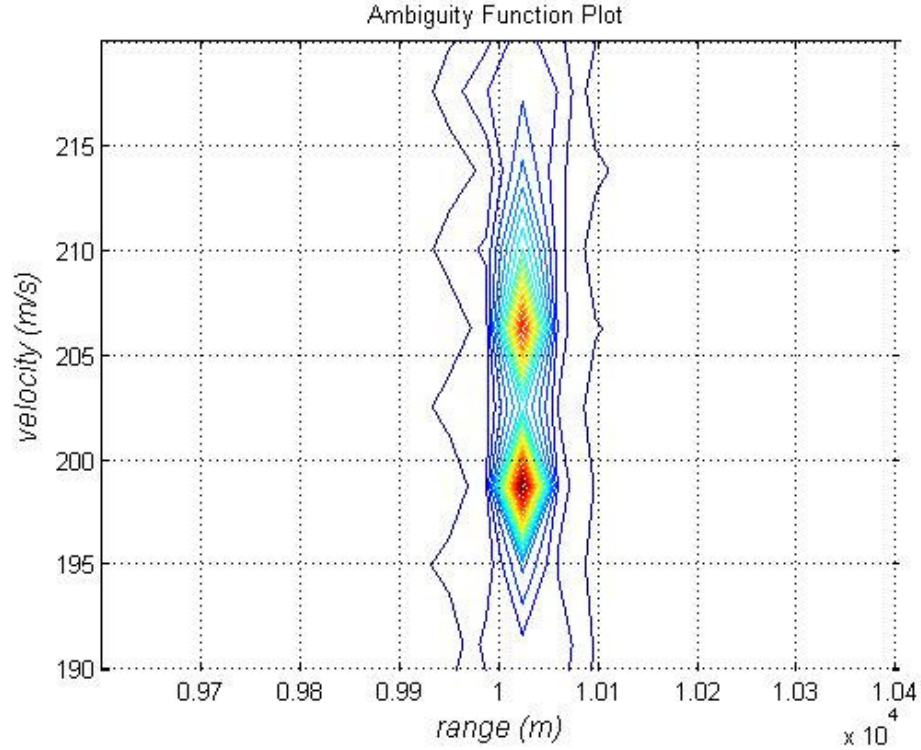


Figure 4. 84: Cross-Ambiguity function contour plot of FMCW coding ($\Delta R = 70$ m and $\Delta V = 7$ m/s) technique used in multiple targets near the Doppler resolution value of the radar simulation.

Since target velocities relative to each other are not smaller than the Doppler resolution value of the radar, radar can resolve these targets and sees them separately.

Simulation 24: In this multiple target simulation, targets in the Doppler resolution value of the Costas coded radar are observed. In the scenario, first target range is used as 10000 meter and radial velocity is used as 200 m/s, second target range is used as 10000 meter and radial velocity is used as 205 m/s.

Figure 4.85 and Figure 4.86 shows the results of this simulation.

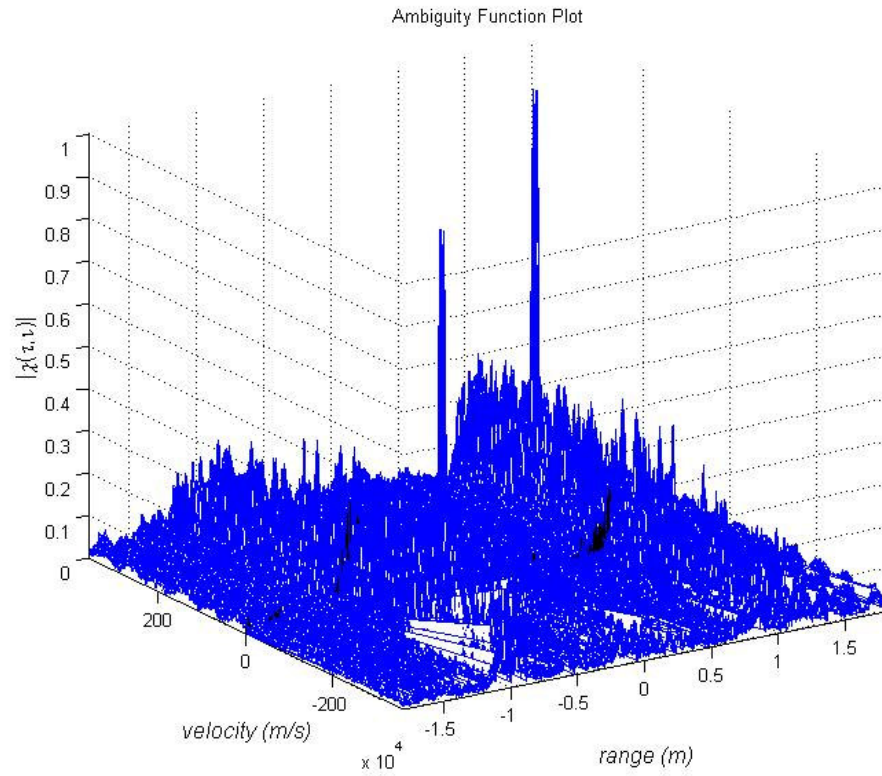


Figure 4. 85: 3-D Cross-Ambiguity function plot of Costas coding technique ($\Delta R = 120$ m and $\Delta V = 12$ m/s) used in multiple targets in the Doppler resolution value of the radar simulation.

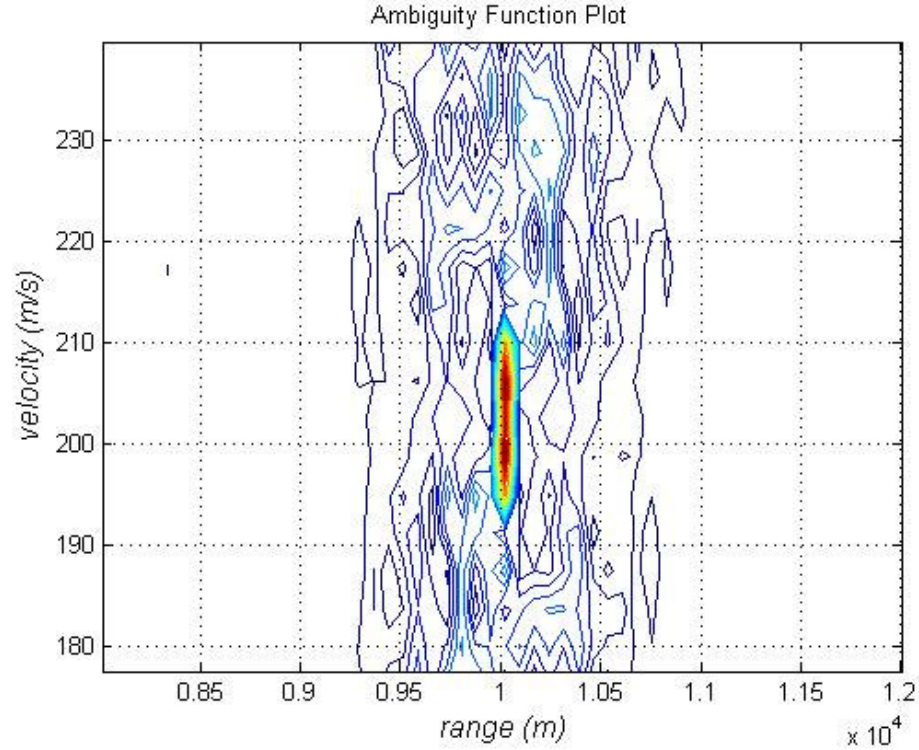


Figure 4. 86: Cross-Ambiguity function contour plot of Costas coding technique ($\Delta R = 120$ m and $\Delta V = 12$ m/s) used in multiple targets in the Doppler resolution value of the radar simulation.

Since targets are in the same range and the velocity between targets are smaller than the Doppler resolution value of the Costas coded radar, radar can not resolve these targets and sees them as a one target.

Simulation 25: In this multiple target simulation, targets near the Doppler resolution value of the Costas coded radar are observed. This time the relative velocity between targets is a little bit bigger than the relative frequency between targets in simulation 24. In the scenario, first target range is used as 10000 meter and radial velocity is used as 200 m/s, second target range is used as 10000 meter and radial velocity is

used as 209 m/s.

Figure 4.87 and Figure 4.88 shows the results of this simulation.

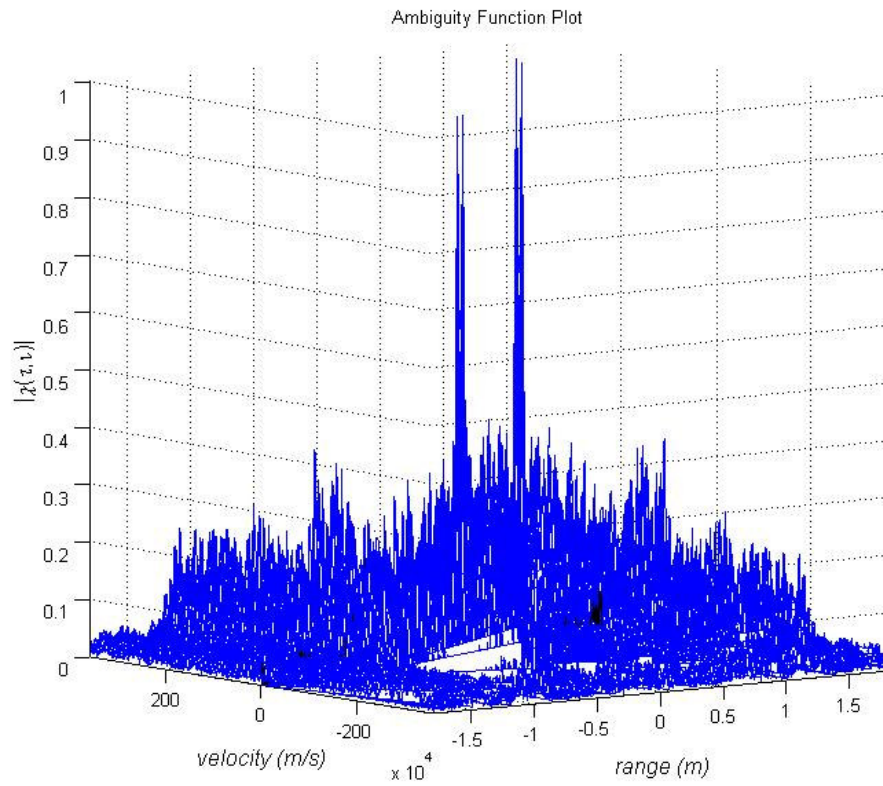


Figure 4. 87: 3-D Cross-Ambiguity function plot of Costas coding technique ($\Delta R = 120$ m and $\Delta V = 12$ m/s) used in multiple targets near the Doppler resolution value of the radar simulation.

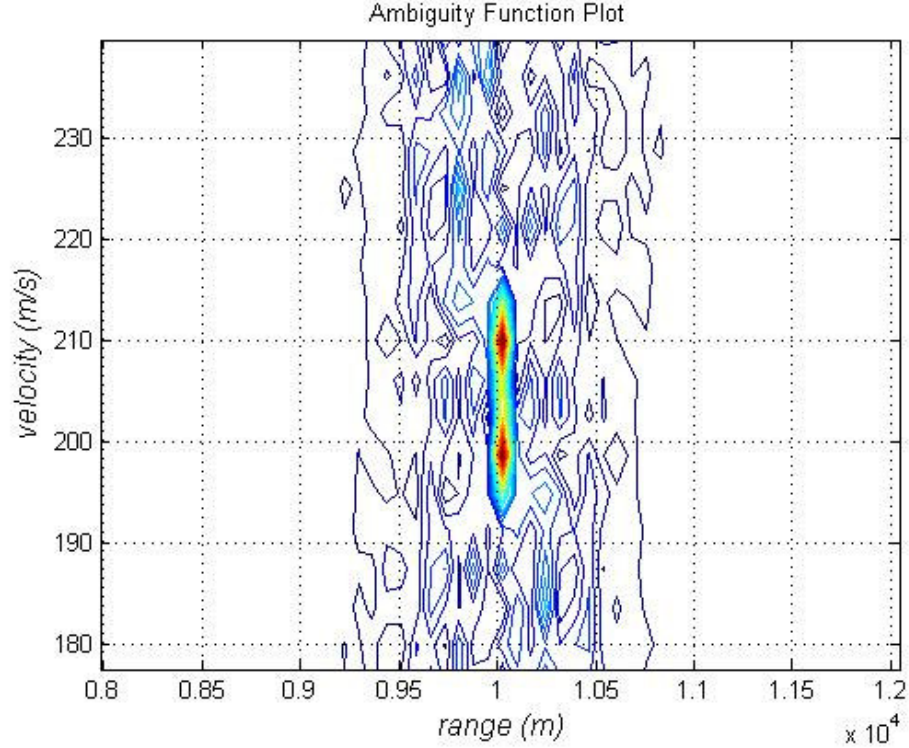


Figure 4. 88: Cross-Ambiguity function contour plot of Costas coding technique ($\Delta R = 120$ m and $\Delta V = 12$ m/s) used in multiple targets near the Doppler resolution value of the radar simulation.

Since the velocities between targets are smaller than the Doppler resolution value of the Costas coded radar, radar can resolve these targets and sees them separately.

In multiple target scenarios for targets in the vicinity of radar resolution values the Costas and FMCW coding methods are analyzed. From the Auto-Ambiguity function analysis of these coding techniques in section 4.3.1 we find the range and velocity resolution of the FMCW coding technique as 70 m and 7 m/s respectively, and the range and velocity resolution of the Costas coding technique as 120 m and 12 m/s respectively. By simulations in this part we confirm these results. The FMCW coding technique has better resolution values than the Costas coding technique but its

drawback is the high sidelobes. Since the FMCW coding technique has high side lobes, when targets are very closer to each other the sidelobes superpose and appears as target in the Cross-Ambiguity function plot. So, FMCW coding technique has better resolution values but higher false alarm rate than the Costas coding technique.

4.3.2.3.5 More Than Two Targets Scenario

4.3.2.3.5.1 Use of Conventional Spectrogram Method

Simulation 26: In this multiple target simulation by conventional spectrogram method, detection of four targets are observed. In the scenario, first target range is used as 12000 meter and radial velocity is used as 200 m/s, second target range is used as 10000 meter and radial velocity is used as 150 m/s, third target range is used as 8000 meter and radial velocity is used as 300 m/s, fourth target range is used as 9000 meter and radial velocity is used as 250 m/s

Figure 4.89 shows the theoretical beat frequency which is obtained by directly subtracting transmitted signal frequency from received signal frequency and Figure 4.90 shows the spectrogram of resulting mixer output.

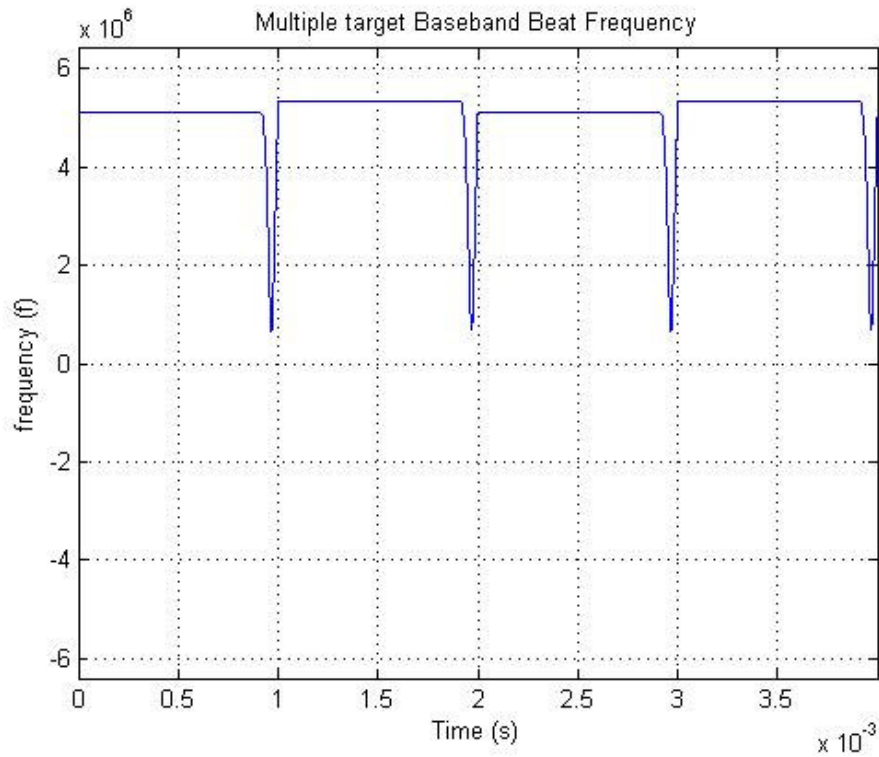


Figure 4. 89: Beat frequency of multiple targets (four target), obtained from the differences between the received and transmitted waveform frequency expressions directly.

From Figure 4.89 which is obtained by extracting the transmitted signal frequency from the received signal frequency directly, it is again very hard to understand that this beat frequency comes from four targets and it is impossible to extract real targets range and velocity values from this graph.

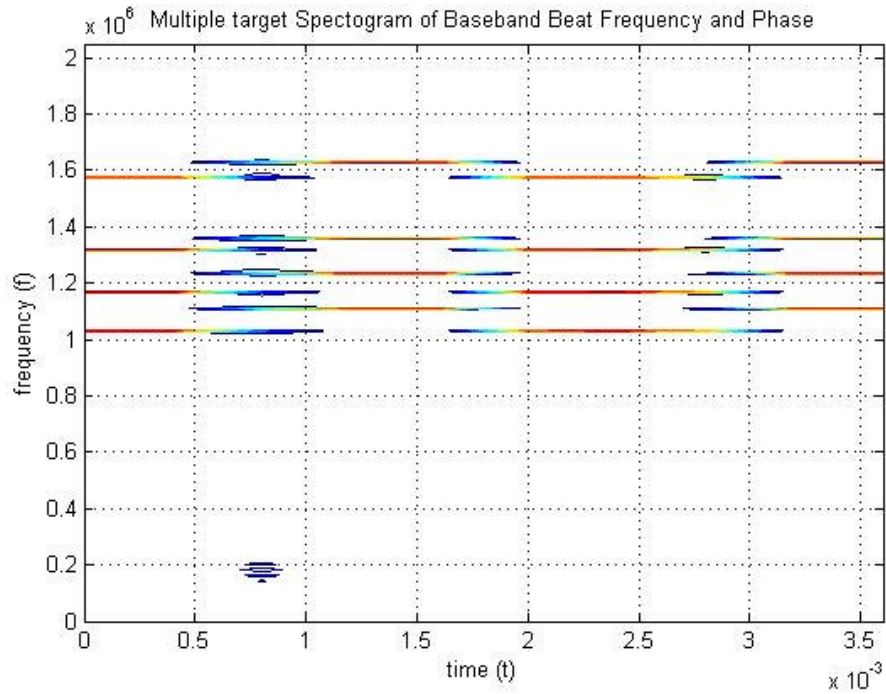


Figure 4. 90: Contour plot of the spectrogram of the filtered mixer output for multiple targets (four targets) simulation

From Figure 4.90, with beat frequency values extracted by spectrogram technique, we can calculate range and velocity of the targets by using (2.18) and (2.19). From Figure 4.90 beat frequencies for the first target is observed as 1.628 MHz and 1.575 MHz, beat frequencies for the second target is observed as 1.358 MHz and 1.318 MHz, beat frequencies for the third target is observed as 1.110 MHz and 1.030 MHz, beat frequencies for the fourth target is observed as 1.234 MHz and 1.168 MHz. With this beat frequencies we can calculate the first target range as 12011 meter and the radial velocity as 198.75 m/s, the second target range as 10035 meter and the radial velocity as 150 m/s, the third target range as 8025 meter and the radial velocity as 300 m/s, and the fourth target range as 9007.5 meter and the radial velocity as 247.5 m/s. But if targets are very closer to each other by this method it gets difficult

to distinguish beat frequency pairs.

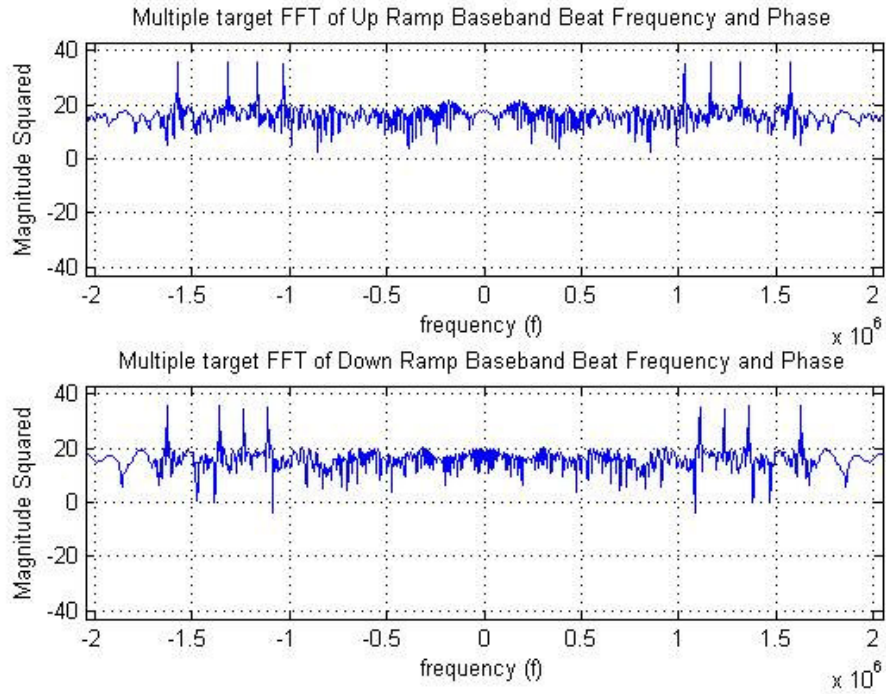


Figure 4. 91: FFT plot of the filtered mixer output for multiple targets (four targets) simulation.

From Figure 4.91, with beat frequency expressions extracted by FFT technique, we can calculate range and velocity of the targets by using (2.18) and (2.19). Drawback of this method is received signal must be analyzed for up and down segments separately. With FFT method, half length of received signal is analyzed and beat frequencies for the up (down) sweep segment is extracted and the other half length of received signal is analyzed and beat frequencies for the down (up) sweep segment is extracted. But with spectrogram method received signal is analyzed as a whole.

4.3.2.3.5.2 Use of Cross-Ambiguity Method with FMCW Coding

Simulation 27: In this multiple target simulation by Cross-Ambiguity method with FMCW coding, detection of four targets are observed. In the scenario, first target range is used as 12000 meter and radial velocity is used as 200 m/s, second target range is used as 10000 meter and radial velocity is used as 150 m/s, third target range is used as 8000 meter and radial velocity is used as 300 m/s, fourth target range is used as 9000 meter and radial velocity is used as 250 m/s.

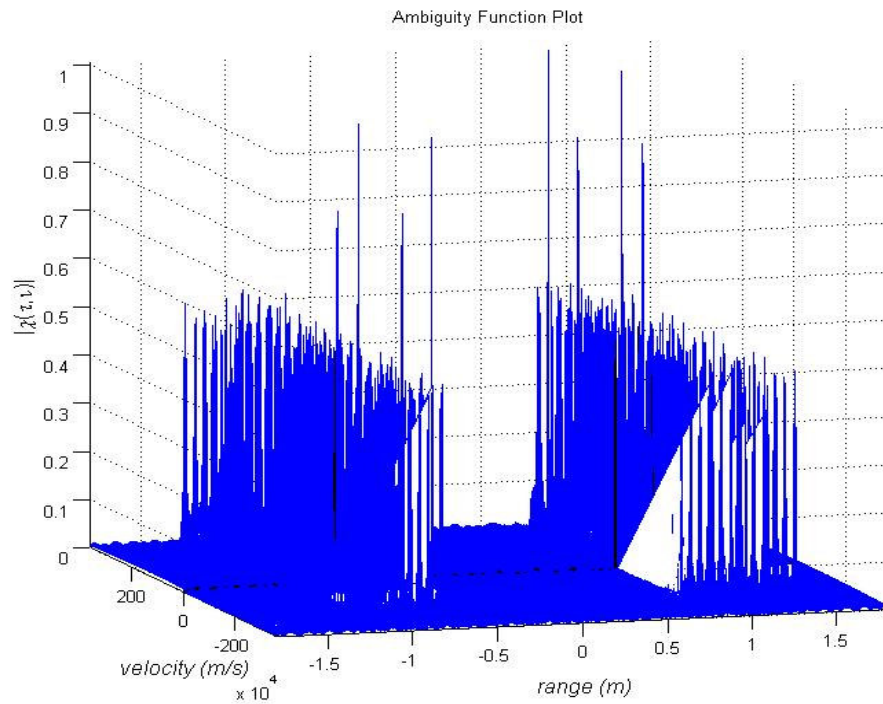


Figure 4. 92: 3-D Cross-Ambiguity function plot of FMCW coding technique ($\Delta R = 70$ m and $\Delta V = 7$ m/s) used in multiple targets (four targets) simulation.

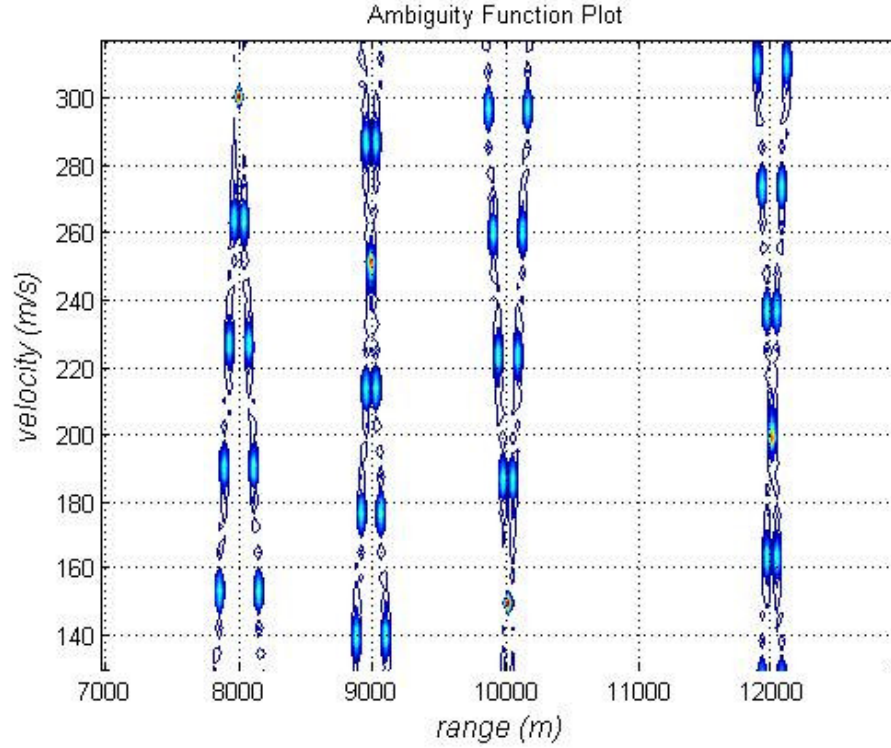


Figure 4. 93: Cross-Ambiguity function contour plot of FMCW coding ($\Delta R = 70$ m and $\Delta V = 7$ m/s) technique used in multiple targets (four targets) simulation.

The results of this simulation are presented in Figure 4.92 and Figure 4.93 showing the first target range as 12000 meter and radial velocity as 198.75 m/s, the second target range as 10024 meter and radial velocity as 150 m/s, the third target range as 8012 meter and radial velocity as 300 m/s, and the fourth target range as 9000 meter and radial velocity as 251.25 m/s.

4.3.2.3.5.3 Use of Cross-Ambiguity Method with Costas Coding

Simulation 28: In this multiple target simulation by Cross-Ambiguity method with Costas coding, detection of four targets are observed. In the scenario, first target

range is used as 12000 meter and radial velocity is used as 200 m/s, second target range is used as 10000 meter and radial velocity is used as 150 m/s, third target range is used as 8000 meter and radial velocity is used as 300 m/s, fourth target range is used as 9000 meter and radial velocity is used as 250 m/s.

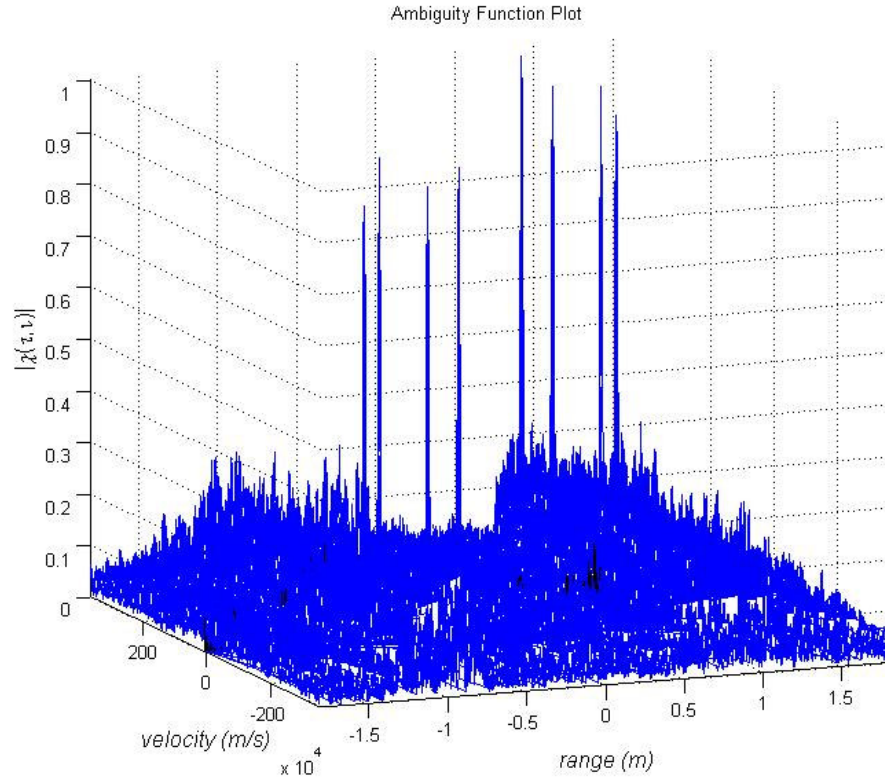


Figure 4. 94: 3-D Cross-Ambiguity function plot of Costas coding technique ($\Delta R = 120$ m and $\Delta V = 12$ m/s) used in multiple targets (four targets) simulation.

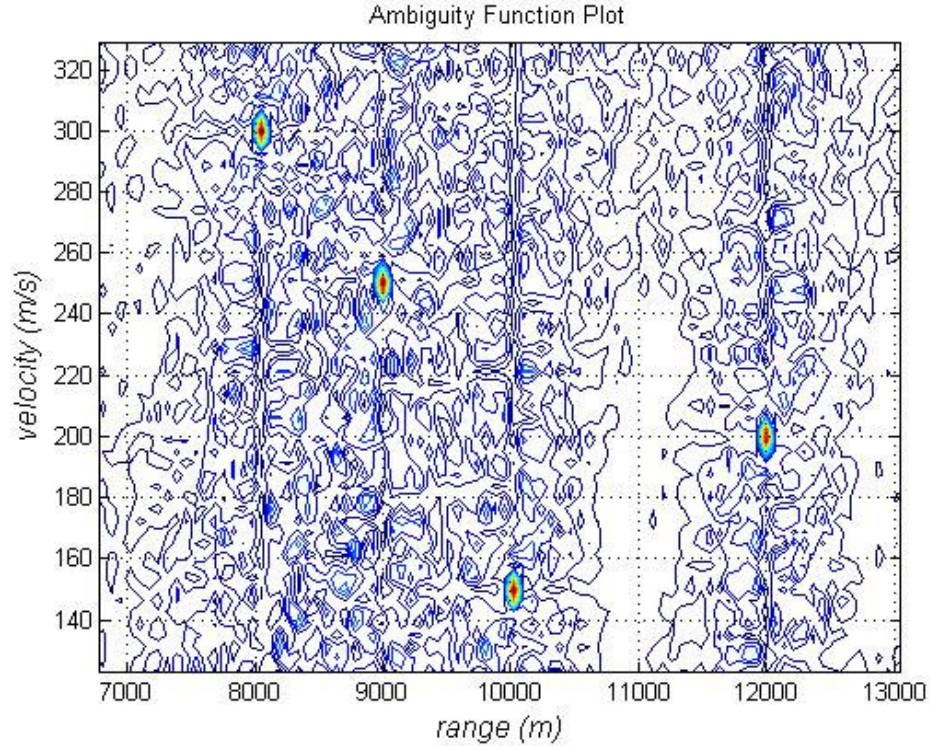


Figure 4. 95: Cross-Ambiguity function contour plot of Costas coding technique ($\Delta R = 120$ m and $\Delta V = 12$ m/s) used in multiple targets (four targets) simulation.

The results of this simulation are presented in Figure 4.94 and Figure 4.95 showing the first target range as 12000 meter and radial velocity as 198.75 m/s, the second target range as 10024 meter and radial velocity as 150 m/s, the third target range as 8049 meter and radial velocity as 300 m/s, and the fourth target range as 9000 meter and radial velocity as 251.25 m/s.

In multiple target scenarios for four targets the Ambiguity Function method gives the good results but the conventional spectrogram method gives the results nearly irresolvable. From the spectrogram output it is hard to choose which beat frequency pair belongs to which target and if targets are get closer it becomes impossible. Since

the FMCW method has high sidelobes, in contour plot it is difficult to choose real target values. If targets get closer, sidelobes superpose with each other and false targets became. Since Costas code has low sidelobes, in contour plot it is rather easy to choose target values.

4.3.3 Noise Analysis in Detection Methods

A simple simulation of noise analysis in FMCW Radar system using conventional FFT method can be accomplished as follows.

Step 1: Generate a FMCW coded transmitted waveform.

Step 2: Introduce a proper delay (τ) to the transmitted signal to obtain noiseless received signal.

Step 3: Add noise to the noiseless receive signal to obtain the noisy received signal

Step 4: Multiply the noisy received signal with the transmitted signal to obtain the mixer output signal.

Step 4: Pass the mixer output signal through the low pass filter to obtain the beat frequency information.

Step 5: Compute the FFT of the filtered mixer output and display the result.

A simple simulation of noise analysis in FMCW/Costas coded radar system using Cross-Ambiguity function method can be accomplished as follows.

Step 1: Generate frequency expression for the FMCW/Costas coded transmitted

waveform.

Step 2: Introduce a delay (τ) to the frequency expression for the transmitted waveform to obtain received waveform frequency expression.

Step 3: Generate phase expressions for the transmitted and received waveforms by using frequency expressions obtained in Step 2 above.

Step 4: Generate complex envelopes for the transmitted and received waveforms by using their frequency and phase expressions obtained in Step 2 and in Step 3 above, respectively.

Step 5: Add complex noise to the complex envelope of received signal to obtain noisy received signal complex envelope.

Step 6: Compute the Cross-Ambiguity function by using transmitted and received complex envelopes obtained in Step 4 and in Step 5 above and display the result.

4.3.3.1 Noise Analysis in Conventional FFT Method

Simulation 29: In this noise analysis simulation by conventional FFT method, a stationary target at range 10000 meter with -10 dB received signal SNR value is observed.

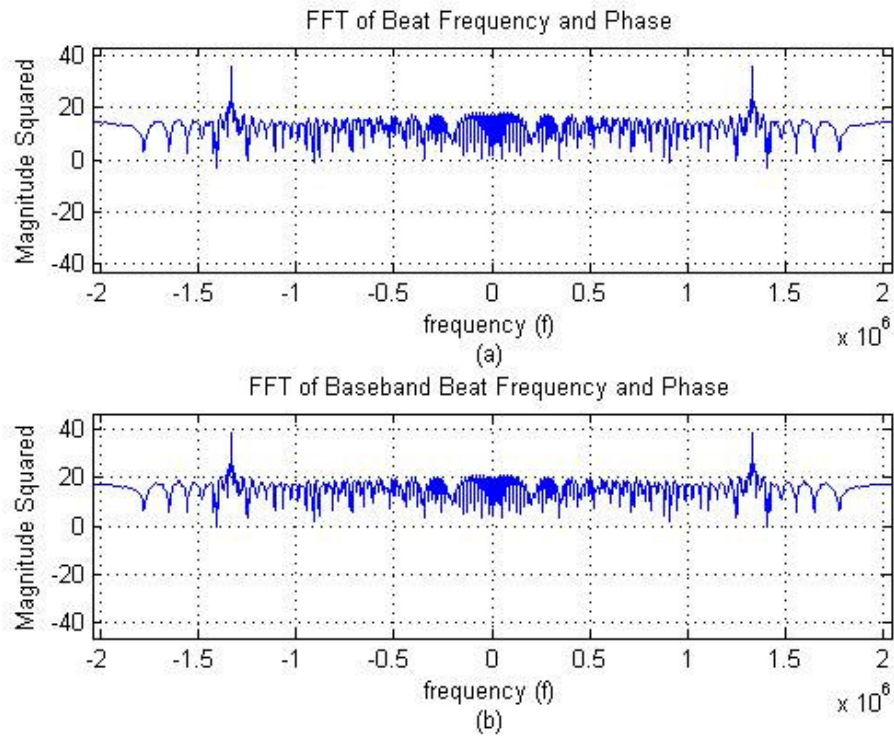


Figure 4. 96: (a) FFT plot of RF beat frequency (b) FFT plot of baseband beat frequency for stationary target simulation without noise

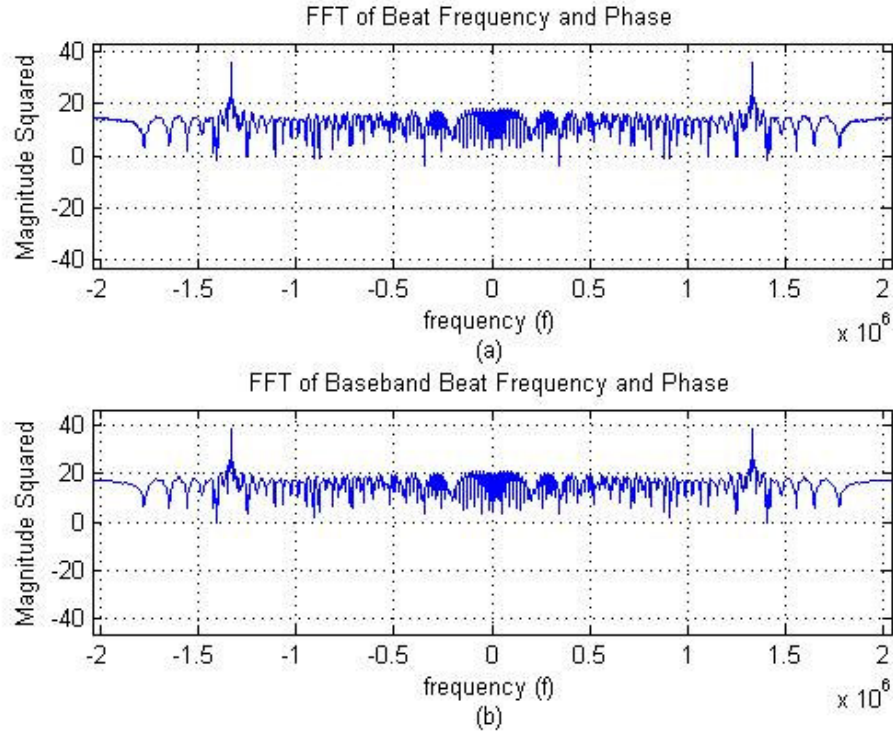


Figure 4. 97: (a) FFT plot of RF beat frequency (b) FFT plot of baseband beat frequency for stationary target simulation with noise

Figure 4.96 and Figure 4.97 we can see that conventional FFT method is robust to noise.

4.3.3.2 Noise Analysis in Cross-Ambiguity Method with FMCW Coding

Simulation 30: In this noise analysis simulation by Cross-Ambiguity method with FMCW coding, a stationary target at range 10000 meter with -10 dB received signal SNR value is observed.

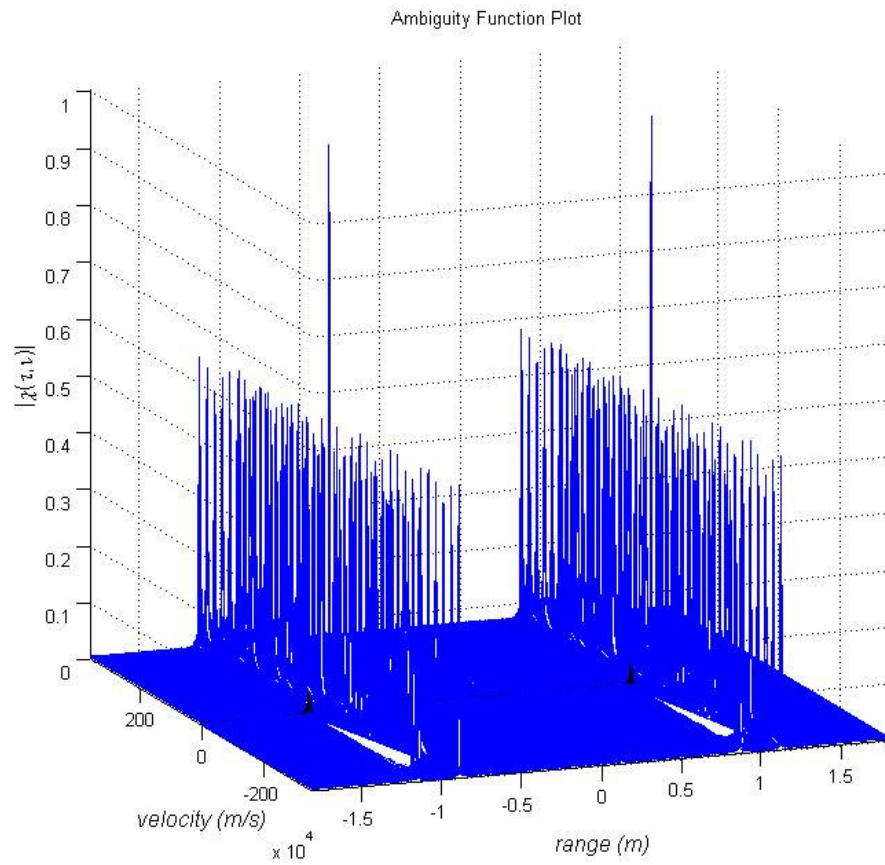


Figure 4. 98: 3-D Cross-Ambiguity function plot of FMCW coding technique used stationary target simulation without noise.

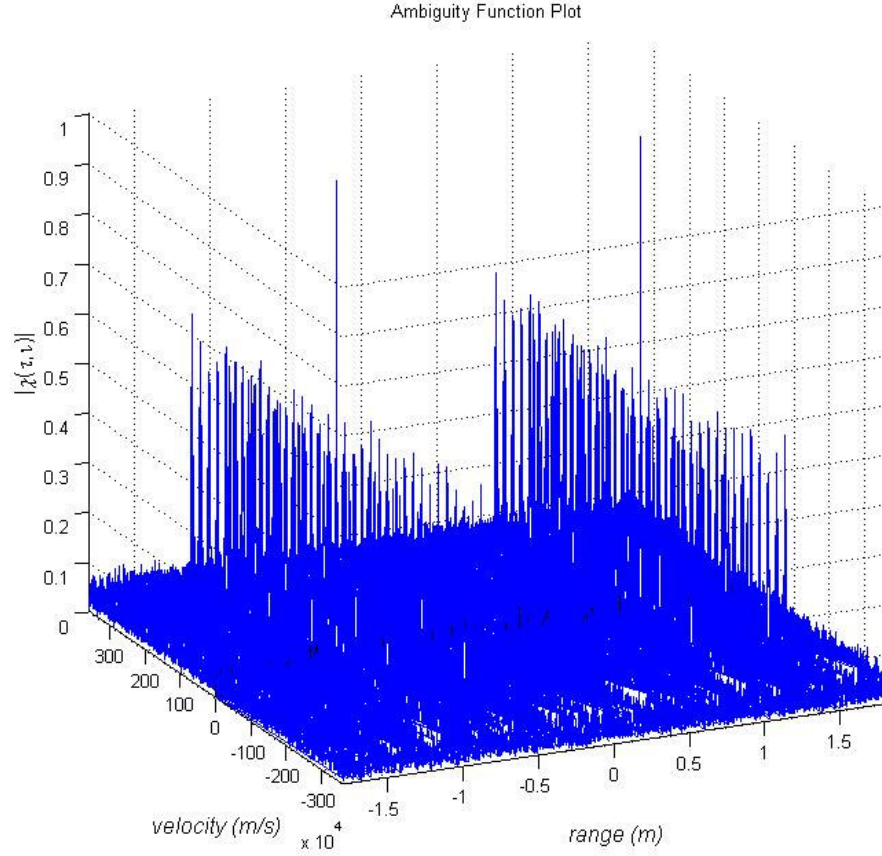


Figure 4. 99: 3-D Cross-Ambiguity function plot of FMCW coding technique used stationary target simulation with noise.

Figure 4.98 and Figure 4.99 we can see that Cross-Ambiguity method with FMCW coding is robust to noise.

4.3.3.3 Noise Analysis in Cross-Ambiguity Method with Costas Coding

Simulation 31: In this noise analysis simulation by Cross-Ambiguity method with Costas coding, a stationary target at range 10000 meter with -10 dB received signal

SNR value is observed.

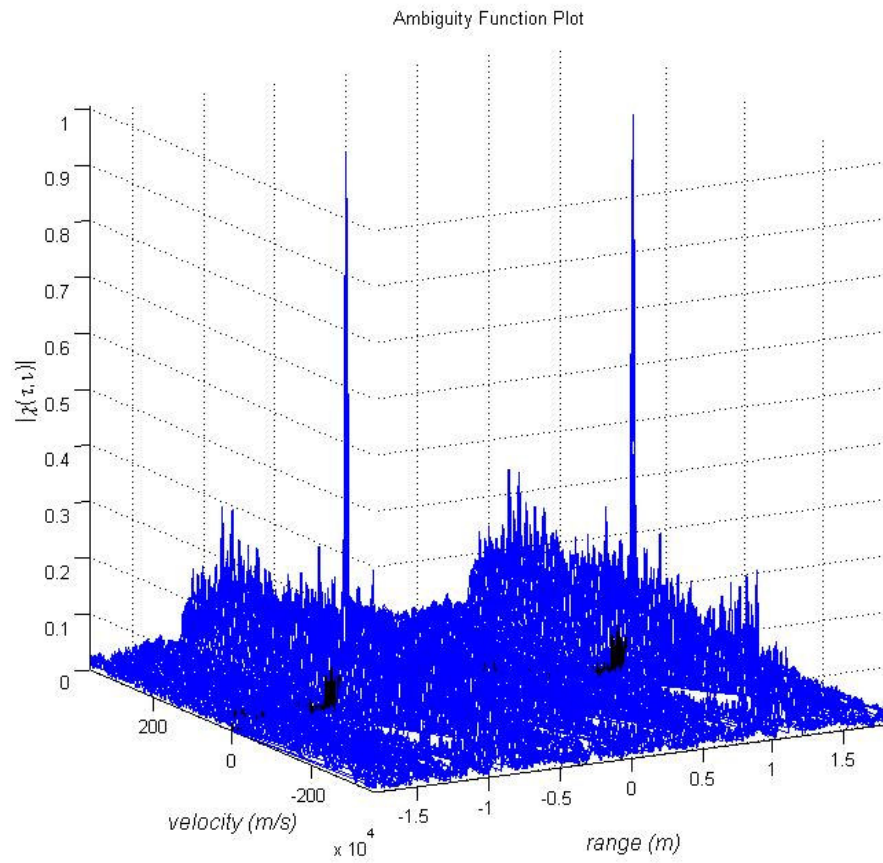


Figure 4. 100: 3-D Cross-Ambiguity function plot of Costas coding technique used stationary target simulation without noise.

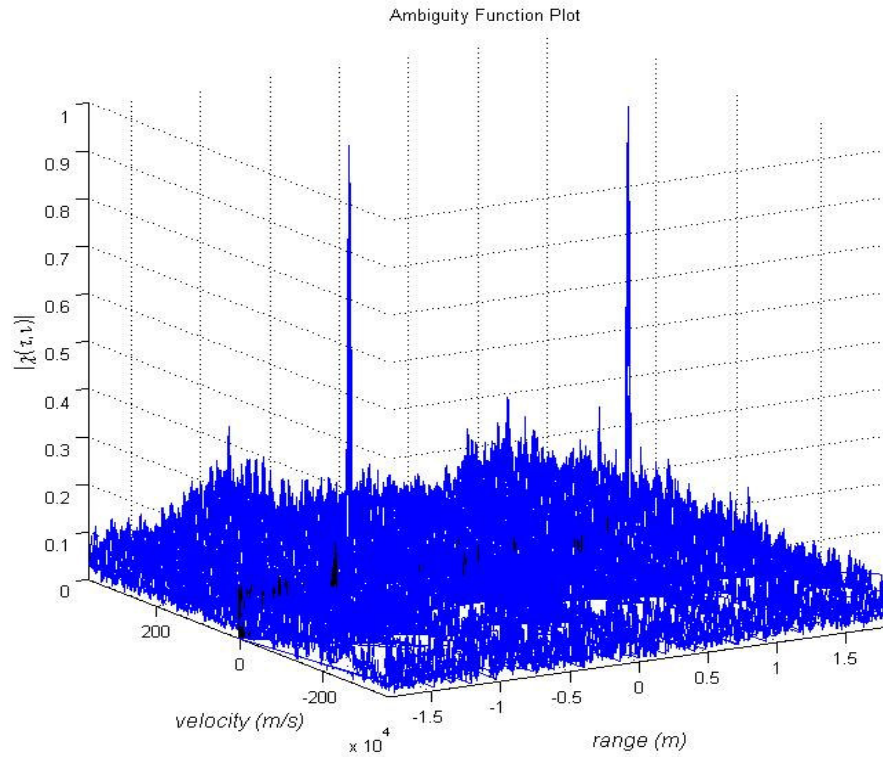


Figure 4. 101: 3-D Cross-Ambiguity function plot of Costas coding technique used stationary target simulation with noise.

Figure 4.100 and Figure 4.101 we can see that Cross-Ambiguity method with FMCW coding is robust to noise.

In noise analysis we saw that the conventional FFT method and the Ambiguity method are robust to noise. They all get affected with -10 dB SNR value which is an extreme case. With the addition of noise to the received signal the increase in sidelobe level of FMCW coding technique is higher than the Costas coding technique. So, Costas coding is more robust to noise than the FMCW coding technique.

CHAPTER 5

CONCLUSIONS

This thesis work has been focused on target detection in frequency modulated CW radars where the linear FM and Costas codes are utilized, in particular. In addition to the investigation of available conventional target detection technique, an alternative technique based on the use of cross ambiguity function is successfully demonstrated in this study.

The problem of target detection in a linear FMCW radar has been studied in detail so far and has been published in many books and articles. The instantaneous frequency of the transmitted signal of a linear FMCW radar simply changes in a linear fashion in subsequent up-ramp and down-ramp segments with the same rate of change in magnitude. Due to this fact, it can easily be proven that the Fourier transform of a low-pass filtered mixer output (mixing the transmitted and received radar signals) provide useful spectral information (peaks at certain frequencies) to extract the target range and radial velocity. Although this conventional Fourier transform technique works well in single target detection, it may get very difficult to assign an accurate pair of frequency values (beat frequency plus Doppler frequency shift and beat frequency minus Doppler frequency shift) to each target in the case of multi-target detection. As it is suggested and used in this thesis, use of the spectrogram (a time-frequency signal representation technique) instead of the Fourier transform improves

the performance of this conventional target detection technique. Even in this modified form, the conventional detection technique remains to be useless in some challenging multi-target detection problems with linear FMCW radars. For example, if two targets are at the same range with different velocities it is impossible to differentiate the targets with the conventional technique. When the CW radar signal is modulated by an FSK technique, such as the Costas code, on the other hand, no conventional target detection technique is suggested and is demonstrated in the literature to our knowledge.

Possibility of a target detection technique that is based on the use of Cross Ambiguity Function (CAF) has been mentioned in literature but, to our knowledge, it has not been investigated in depth so far. Almost in all the articles and books, the Auto Ambiguity Function is used to design coded radar signals with good range-velocity resolution figures and low side lobe levels. In this thesis, however, the main theme is the use of CAF for target detection as an alternative technique, which can be used with any type of CW radar signal coding including the FSK techniques. The magnitude of the cross ambiguity function is computed and plotted as a function of time delay (proportional to target range) and Doppler frequency shift (proportional to target's velocity along the line-of-sight of the radar) for various target detection scenarios in Chapter 4 of this thesis. Stationary and/or moving single target detection scenarios as well as the multi-target detection scenarios are simulated. In each scenario, target detection is carried on by using the linear FM coding with the conventional Fourier transform/spectrogram technique and with the CAF technique and also by using the Costas coding with the CAF technique.

It is observed in general that the linear FM coding is much simpler to implement regarding the computational cost as compared to the Costas code. Also noted that for the same CW radar design parameters, the linear FM coding provide better range and velocity resolution values but much higher side lobe levels, which are all very

important factors in multi-target detection especially when the targets are very close either in range or velocity. High side lobes obviously increase the false alarm rate in the radar applications but in all of the worse case scenarios presented in Chapter 4, the task of target detection is successfully demonstrated.

Finally, the effect of added Gaussian noise to the received CW signal is investigated in the context of detection performance. It is seen that moderate noise up to about zero decibel signal-to-noise ratio (SNR) value has almost no effect on the detection performance. At much lower SNR values such as -10 dB, the noise floor is raised pushing the side lobe levels at higher levels in both linear FM and Costas coding simulations. However, the effect of added noise in side lobe levels is less pronounced in the case of Costas coding.

The scope of this thesis study was confined to the investigation of different frequency coding types in CW radars and to the formulation and demonstration of an alternative target detection strategy based on the CAF usage. As a further study, performance of the CAF technique under various clutter scenarios needs to be investigated.

REFERENCES

- [1] Merill I. Skolnik, "Introduction to Radar Systems", 2.nd Edition McGraw Hill, 1980.
- [2] Sudarsan Krishnan, "Modeling and Simulation Analysis of an FMCW Radar for Measuring Snow Thickness", B.E., Electronics and Communication Engineering, University of Madras, 2000.
- [3] Phillip E. Pace, "Detecting and Classifying Low Probability of Intercept Radar", 1.st Edition Artech House, 2004.
- [4] Nadav Levanon, Eli Mozeson, "Radar Signals", 1.st Editon Wilet-Interscience, 2004.
- [5] Simon Haykin, Brian Currie, Thia Kirubarajan, "Adaptive Radar for Improved Small Target Detection in a Maritime Environment", Defence R&D Canada, Technical Report, DRDC Ottawa CR 2003-095, April 2003.
- [6] Defence Research and Development Canada, "Ambiguity and Cross-ambiguity Properties of Some Reverberation Suppressing Waveforms", Defence R&D Canada, Technical Memorandum, DRDC Atlantic TM 2002-129, July 2002.
- [7] Piper, S. O., "Receiver frequency resolution for range resolution in homodyne FMCW radar," Proc. National Telesystems Conference, Commercial Applications

and Dual-Use Technology, pp. 169-173, 1993.

[8] Piper, S. O., "Homodyne FMCW radar range resolution effects with sinusoidal nonlinearities in the frequency sweep", Record of the IEEE International Radar Conference, pp. 563-567, 1995.

[9] Sanmartin-Jara, J., Burgos-Garcia, M., and Retamosa-Sanchez, J., "Radar sensor using low probability of interception SS-FH signals", IEEE Aerospace and Electronics Magazine, pp. 23-28, April 2000.

[10] Mahafza, B. R., "Radar Systems Analysis and Design Using MATLAB", Chapman & Hall/CRC, New York, 2000.

[11] Costas, J. P., "A study of a class of detection waveforms having nearly ideal range-Doppler ambiguity properties", Proc. of the IEEE, Vol. 72, No. 8 pp.996-1009, August 1984.

[12] Golomb, S. W., and Moreno, O., "On periodicity properties of Costas arrays and a conjecture on permutation polynomials", IEEE Trans. On Information Theory, Vol. 42, No. 6, pp. 2252-2253, Nov. 1996.

[13] Hlawatsch, F., Boudreaux-Bartles, G. F., "Linear and Quadratic Time-Frequency Signal Representations", IEEE Signal Processing Mag, pp 21-58, April 1992.

[14] I.T. Young, "Improved Detection with the Cross-Ambiguity Function", Elsevier Science Publishers B.V. (North-Holland), c EURASIP, 1986.

[15] Seymour Stein, "Algorithms for Ambiguity Function Processing", IEEE Transactions on Acoustics, Speech, and Signal Processing, Vol. ASSP-29, No. 3,

June 1981, pp. 588-599.

[16] Levanon N., Mozeson E., “Modified Costas Signal,” IEEE Trans. On Aerospace and Electronic Systems”, Vol. 40, No. 3, pp. 946-953, July 2004.

[17] Glomb, S. W., and Taylor, H., “Construction and properties of Costas arrays”, Proc. of the IEEE, Vol. 72, No. 9, pp. 1143-1163, Sept. 1984.

[18] Maric, S.V., Seskar, I., and Titlebaum, E.L., “On cross-ambiguity properties of Welch-Costas arrays”, IEEE Trans. On Aerospace and Electronic Systems, Vol. 30, No. 4, pp. 1063-1071, Oct. 1994.

[19] Lemieux, J. A., “Analysis of an optimum hybrid radar waveform using frequency hopping and locally optimum signals”, Proc. of the IEEE National Radar Conference, pp. 98-102, March 12-13, 1991.

[20] North, D. O., “Analysis of Factors Which Determine Signal-to-Noise Discrimination in Radar”, Report PTR-6c, RCA Laboratories, Princeton, NJ, June 1943.

[21] Woodward, P. M., “Probability and Information Theory, with Applications to Radar”, Pergamon Press, Oxford, 1953.

[22] Sinsky, A. I., and C. P. Wang, “Standardization of the definition of the radar ambiguity function”, IEEE Transactions on Aerospace and Electronic Systems, vol. AES-10, no.4, July 1974, pp. 532-533.

APPENDIX A

PRIMITIVE ROOTS AND COSTAS SEQUENCES

In this appendix, a concise description of primitive numbers, residues, reduced residues, the Euler function $\phi(n)$, and primitive roots is given. The significance of this appendix is to present the concepts in a framework that lends itself to the derivation of Costas frequency-hopping systems. These concepts are useful for understanding the construction of Costas sequences using the Welch method.

A.1 Primes

To begin we give the definition of a prime number.

Definition 1 *An integer $p > 1$ is called a prime number, or a prime, in case there is no divisor d of p satisfying $1 < d < p$.*

For example, the numbers 2, 3, 5, and 7 are prime numbers and there is an infinite number of primes. All the numbers 4, 5, and 7 are not all primes, they are all relatively prime with respect to each other, in that none have a common factor.

A.2 Complete and Reduced Residue Systems

Is a congruence involves only addition, subtraction, and multiplication, we may

replace the integers with congruent integers. To help in this, the following definitions describing residue systems are given, followed by an example to illustrate the concept.

Definition 2 *if h and j are two integers and $h \equiv j \pmod{m}$, then we say that j is a residue of h modulo m .*

Definition 3 *the set of integers $\{r_1, r_2, \dots, r_s\}$ is called a complete residue system modulo m if $r_i \not\equiv r_j \pmod{m}$ and for each integer n there corresponds an r_i such that $n \equiv r_i \pmod{m}$.*

If s different integers r_1, r_2, \dots, r_s form a complete residue system modulo m , then $s = m$. If m is a positive integer, then $\{0, 1, \dots, m-1\}$ is a complete residue system modulo m . For example, for $m = 7$, the smallest positive integer values within the modulus are $\{0, 1, 2, 3, 4, 5, 6\}$.

Definition 4 *the set of integers $\{r_1, r_2, \dots, r_s\}$ is called a reduced residue system modulo m if (a) the $\gcd(r_i, m) = 1$ for each i , (b) $r_i \not\equiv r_j \pmod{m}$ whenever $i \neq j$, and (c) for each integer n relatively prime to m there corresponds an r_i such that $n \equiv r_i \pmod{m}$.*

For example, the set $\{0, 1, 2, 3, 4, 5\}$ is complete residue system modulo 6, but $\{1, 5\}$ is a reduced residue system modulo 6. That is, we can obtain a reduced residue system from a complete residue system by simply deleting those elements of the complete residue system that are not relatively prime to m .

Example 1 The sets $\{1, 2, 3\}$, $\{0, 1, 2\}$, $\{-1, 0, 1\}$, and $\{1, 5, 9\}$ are all complete residue

systems modulo 3.

When working with congruences modulo m , we can replace the integers in congruences by elements of $\{0,1,2,\dots,m-1\}$. This can make many complicated problems much easier.

Example 2 Find an integer n that satisfies the congruence

$$325n \equiv 11 \pmod{3} \quad (\text{A. 1})$$

Since

$$325 \equiv 1 \pmod{3} \quad (\text{A. 2})$$

and

$$11 \equiv 2 \pmod{3} \quad (\text{A. 3})$$

The problem is reduced to finding an integer n such that

$$n \equiv 2 \pmod{3} \quad (\text{A. 4})$$

The obvious answer here is the integer 2.

Definition 5 the function $\phi(m)$ denotes the number of positive integers less than or equal to m that are relatively prime to m . This function $\phi(m)$ is called the Euler ϕ -function, and represents the number of integers that form the reduced residue system modulo m .

Example 3 We know $\phi(6) = 2$ and $\{1,5\}$ is a reduced residue system modulo 6. Note the set $\{5,5^2\}$ is also a reduced residue system modulo 6, since $5 \equiv 5 \pmod{6}$ and $25 \equiv 1 \pmod{6}$.

A.3 Primitive Roots

We have examined the concept of the reduced residue system modulo p where p is a prime number. In this section, we present an integer g such that $g, g^2, \dots, g^{\phi(p)}$ constitutes a reduced residue system modulo p . The integer g is called a primitive root. Primitive roots are fundamental to how Costas frequency sequence can be formed. An algorithm for deriving this types of sequences is presented, along with an example illustrating the method.

A few properties of reduced residue systems must now be given. The first is that if h is the smallest positive integer such that

$$a^h \equiv 1 \pmod{m} \tag{A. 5}$$

we say that the order of a is h modulo m . if g is an integer, and the order of g is $\phi(m)$ modulo m , then g is called a primitive root modulo m . Further, if g is a primitive root modulo m , then $g, g^2, \dots, g^{\phi(m)}$ makes up a reduced residue system modulo m (sometimes referred to as a cyclic group).

Since the goal of this development is to derive a Costas sequence, the first step is to determine a prime number p , remembering that the number of frequencies in the FH sequence will be $N = p - 1$. Also, since p is prime we have the following definition:

Definition 6 If p is prime, then there exist $\phi\{\phi\{p\}\} = \phi\{p-1\}$, primitive roots modulo p .

This number can be determined by first eliminating those elements in the reduced residue that are not relatively prime to $p-1$, and then counting the remaining entries. Not also that the order of a in (A.5) must be a divisor of $\phi(p) = p-1$.

Example 4 Consider the case for which $p=11$, a prime number. The number of frequencies in the Costas array will be $N = p-1 = 10$. The complete residue set is

$$\{0, 1, 2, 3, 4, 5, 6, 7, 8, 9, 10\}$$

There are $p-1=10$ elements in the reduced residue set modulus 11

$$\{1, 2, 3, 4, 5, 6, 7, 8, 9, 10\}$$

and there $\phi\{p-1\} = \phi\{10\} = 4$ primitive roots. The questions we have now are what the primitive roots and what are the corresponding Costas sequences?

To determine the primitive roots by which we can derive a the Costas sequences, we start with $g = 1$ (the first element in the reduced residue set). For $g = 1$ we have

$$\{1^1, 1^2, 1^3, \dots, 1^{\phi\{11\}}\} = \{11\}$$

and we say the order of 1 is 1. Consequently, 1 is not a primitive root. For 2,

$$\{2^1, 2^2, 2^3, \dots, 2^{\phi\{11\}}\}$$

or

$$\{2, 4, 8, 5, 10, 9, 7, 3, 6, 1\}$$

and the order of 2 is 10, indicating that $g = 2$ is a primitive root. For 3 we have,

$$\{3, 9, 5, 4, 1\}$$

and the order of 3 is 5. That is, 3 is not a primitive root. Continuing on for the rest of the integers within the reduced residue system 4 we have,

$$\{4, 5, 9, 3, 1\}$$

and the order of 4 is 5 (not a primitive root). For 5 we have,

$$\{5, 3, 4, 9, 1\}$$

and the order of 5 is 5 (not a primitive root). For 6 we have,

$$\{6, 3, 7, 9, 10, 5, 8, 4, 2, 1\}$$

so the order of 6 is 10, and consequently, 6 is a primitive root. For 7 we have,

$$\{7, 5, 2, 3, 10, 4, 6, 9, 8, 1\}$$

so the order of 7 is 10, and 7 is also a primitive root. For 8 we have,

$$\{8, 9, 6, 4, 10, 3, 2, 5, 7, 1\}$$

so the order of 8 is 10, and therefore 8 is a primitive root. Since we now have our four primitive roots, we know that there are no more. For completeness however, we verify that for 9 we have,

$$\{9, 4, 3, 5, 1\}$$

and the order of 9 is 5 (not a primitive root), and for 10 we have,

$$\{10, 1\}$$

Therefore the order of 10 is 2, and 10 is not a primitive root. In summary, the four primitive roots are $\{2, 6, 7, 8\}$.

One question still remains. How do we know, short of multiplying out, if a in (A.5) is a primitive root? That is, is there a way to find the primitive roots and Costas sequences without having to calculate the order of each integer value within the reduced residue set modulo p ? Fortunately, the answer is yes, and we can use the following definition

Definition 7 *If a is a primitive root modulus p then a^r is a primitive root modulus p if and only if $\gcd(r, \phi(p)) = 1$ (r is relatively prime to $\phi(p) = p - 1$).*

In this case we can reduce our work by starting with the smallest value (e.g., $a = 2$), and first determining if this is a primitive root. Once the smallest primitive root is found, the others may be found easily by using the definition above.

In our example, since we have confirmed that $a = 2$ is a primitive root, we know from the above definition that 2^r is a primitive root modulus 11, if and only if

$\gcd(r,10)=1$. So for $r=1$, $2^1=2$, for $r=3$, $2^3=8$, for $r=7$, $2^7=7$, and for $r=9$, $2^9=6$. In summary, the primitive roots are $\{2,6,7,8\}$ and the corresponding sequences are Costas arrays. Also note that the Costas arrays for $a=2$ and $a=6$ are reverse ordered (except for the 1 on the end). This is also true for $a=7$ and $a=8$. This symmetry can be used to further simplify the sequence calculations.

A.4 Welch Construction of Costas Arrays

There are many analytical procedures for constructing Costas frequency hopping arrays. Although Costas arrays may exist for any positive integer N_F , these analytical construction methods are typically limited to values of N_F related to prime numbers [17], [18].

For the Welch construction of a Costas array, an odd prime number p is chosen first. The number of frequencies and the number of time slots in the Costas sequence are then $N_F = \phi(p) = p-1$ where $\phi(p)$ is the Euler function. Next, a primitive root g modulo p is chosen. As discussed in Appendices, if g is a primitive root modulo p , then g is an integer belonging to the Euler $\phi(p)$ function modulo p . Since g is a primitive root modulo p , $g, g^2, \dots, g^{\phi(p)}$ are mutually incongruent and form a permuted sequence of reduced residues p . Welch showed that this reduced residue is a Costas sequence.

Theorem: Let g be a primitive root of an odd prime number p . Then the $(p-1)$ by $(p-1)$ permutation matrix A has elements $a_{i,j}=1$ iff $j \equiv g^i \pmod{p}$ for $1 \leq i, j \leq p-1$ and this is a Costas array [19].

Example: The first step is choosing prime number p . We choose the prime number

$p = 7$. For $p = 7$, $N_f = 6$, which is the number of frequencies in the FH code. The complete residue system is $\{0,1,2,3,4,5,6\}$. With p prime, we know that the number of elements in the reduced residue system is $\phi(p) = p - 1 = 6$. The reduced residue system is $\{1,2,3,4,5,6\}$ (deleting the one element that is divisible by p). From Appendices, for $p = 7$ we know there are exactly $\phi(\phi(7)) = \phi(6) = 2$ mutually incongruent primitive roots modulo $p = 7$. We start with the smallest value $g = 2$, but the order of $g = 2$ is 3 (not 6). Next we pick $g = 3$ and get the desired result $\{3,2,6,4,5,1\}$, which is the Costas array as shown below. The left-hand column shows i from 1 to $p - 1$, and the right hand column shows the frequency j using theorem.

i	$j = g^i \pmod{7}$
1	$3^1 = 3$
2	$3^2 = 2$
3	$3^3 = 6$
4	$3^4 = 4$
5	$3^5 = 5$
6	$3^{p-1} = 3^6 = 1$

where $i, j = 1, 2, \dots, 6$. Consequently frequency sequence is

$$f = \{3, 2, 6, 4, 5, 1\} \quad (\text{A. 6})$$

Note from the symmetry that $f = \{5, 4, 6, 2, 3, 1\}$ is also a Costas sequence. The Welch construction is also singly periodic [12]. That is, $f_i, f_{i+1}, \dots, f_{i+p-2}$ is also a Costas sequence. Any circular shift of the sequence is also a Costas sequence.

APPENDIX B

MATCHED FILTER

B.1 Complex Representation of Bandpass Signals

The majority of radar signals are bandpass signals. Their Fourier transform is limited to an angular frequency bandwidth of $2W$ centered about a carrier angular frequency $\pm\omega_c$. A bandpass signal can be written in several forms. The basic representation is

$$s(t) = g(t)\cos[\omega_c t + \phi(t)] \quad (\text{B. 1})$$

where $g(t)$ is the natural envelope of $s(t)$ and $\phi(t)$ is the instantaneous phase. Another form is the

$$s(t) = g_c(t)\cos\omega_c t - g_s(t)\sin\omega_c t \quad (\text{B. 2})$$

where $g_c(t)$ and $g_s(t)$ are in-phase and quadrature components, respectively, given by

$$g_c(t) = g(t)\cos\phi(t) \quad (\text{B. 3})$$

$$g_s(t) = g(t) \sin \phi(t) \quad (\text{B. 4})$$

Both $g_c(t)$ and $g_s(t)$ are baseband signals.

The complex envelope $u(t)$ of the signal $s(t)$ is defined as

$$u(t) = g_c(t) + jg_s(t) \quad (\text{B. 5})$$

The complex envelope provides a third form of the signal:

$$s(t) = \text{Re}\{u(t) \exp(j\omega_c t)\} \quad (\text{B. 6})$$

The carrier angular frequency ω_c is actually an arbitrary mathematical entity. Exactly the same signal $s(t)$ could be described using a different choice of ω_c . This would clearly result in a different $\phi(t)$, different quadrature components and a different complex envelope $u(t)$. Of the infinitely many choices of ω_c , the preferred choice, which will make the mathematical analyses simpler, is the one that will result in the following identity:

$$u(t) \exp(j\omega_c t) = s(t) + j\hat{s}(t) \quad (\text{B. 7})$$

where $\hat{s}(t)$ is the Hilbert transform of $s(t)$, namely,

$$\hat{s}(t) = s(t) \otimes \frac{1}{\pi t} = \frac{1}{\pi} \int_{-\infty}^{\infty} \frac{s(\tau)}{t - \tau} d\tau \quad (\text{B. 8})$$

and \otimes represents convolution. The importance of choosing ω_c that satisfies (B.7) increases as signals relative bandwidth increases. In most radar applications $s(t)$ is bandpass signal. Furthermore, in radar the receiver usually knows what the transmitted signal was, and what actual carrier frequency was used in the modulation process.

It can easily be checked that a fourth representation of a bandpass signal is

$$s(t) = \frac{1}{2}u(t)\exp(j\omega_c t) + \frac{1}{2}u^*(t)\exp(-j\omega_c t) \quad (\text{B. 9})$$

This representation is used in finding the response of a filter matched to a bandpass signal.

B.2 Matched Filter

In radar applications we generally utilize the reflected “known” signal to detect the existence of a reflecting target. A specific matched filter is a linear filter whose impulse response is determined by a specific signal in a way that will result in the maximum attainable SNR at the output of the filter when that particular signal and white noise are passed through the filter [20].

Matched filters can be derived for baseband as well as for bandpass real signals. For the latter case it will usually suffice to implement a filter matched to the complex envelope of the signal. Hence, we need to be able to design matched filters for complex signals as well. Consider Figure B.1, the input to the matched filter is the signal $s(t)$ plus additive white Gaussian noise with a two-sided power spectral density of $N_0/2$. We look for the impulse response $h(t)$ or the frequency response

$H(\omega)$ that will yield the maximum SNR at a predetermined delay t_0 . In other words, we look for $h(t)$ or $H(\omega)$ that will maximize

$$\left(\frac{S}{N}\right)_{out} = \frac{|s_0(t_0)|^2}{n_0^2(t)} \quad (\text{B. 10})$$

The matched filter impulse response will be a function only of the waveform $s(t)$ and predetermined delay t_0 .

Let the Fourier transform of $s(t)$ be $S(\omega)$; then the output signal at t_0 is given by

$$s_0(t_0) = \frac{1}{2\pi} \int_{-\infty}^{\infty} H(\omega) S(\omega) \exp(j\omega t_0) d\omega \quad (\text{B. 11})$$

The mean-squared value of the noise, which is independent of t , is

$$\overline{n_0^2(t)} = \frac{N_0}{4\pi} \int_{-\infty}^{\infty} |H(\omega)|^2 d\omega \quad (\text{B. 12})$$

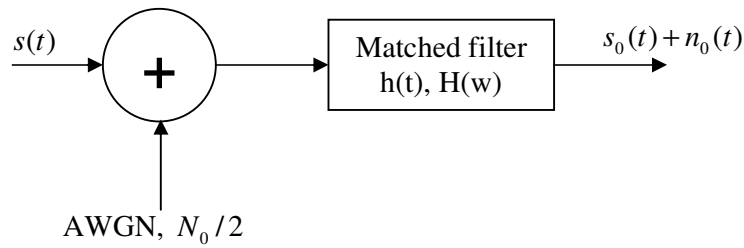


Figure B. 1: Matched filter definitions

Substituting (B.11) and (B.12) in (B.10) yields

$$\left(\frac{S}{N}\right)_{out} = \frac{\left|\int_{-\infty}^{\infty} H(\omega)S(\omega)\exp(j\omega t_0)d\omega\right|^2}{\pi N_0 \int_{-\infty}^{\infty} |H(\omega)|^2 d\omega} \quad (\text{B. 13})$$

We will now use the Schwarz inequality, which says that for any two complex signals $A(\omega)$ and $B(\omega)$, the following inequality is true:

$$\left|\int_{-\infty}^{\infty} A(\omega)B(\omega)d\omega\right|^2 \leq \int_{-\infty}^{\infty} |A(\omega)|^2 d\omega \int_{-\infty}^{\infty} |B(\omega)|^2 d\omega \quad (\text{B. 14})$$

The equality holds if and only if

$$A(\omega) = KB^*(\omega) \quad (\text{B. 15})$$

where K is an arbitrary constant (that can have a dimension). Choosing

$$A(\omega) = H(\omega) , \quad B(\omega) = S(\omega)\exp(j\omega t_0) \quad (\text{B. 16})$$

In (B.14) and using it in (B.15) yields

$$\left(\frac{S}{N}\right)_{out} \leq \frac{1}{\pi N_0} \int_{-\infty}^{\infty} |S(\omega)|^2 d\omega = \frac{2E}{N_0} \quad (\text{B. 17})$$

where E is the energy of the finite-time signal, namely,

$$E = \int_{-\infty}^{\infty} s^2(t) dt = \frac{1}{2\pi} \int_{-\infty}^{\infty} |S(\omega)|^2 d\omega \quad (\text{B. 18})$$

Using (B.16) in (B.15), we find out that equality, which means maximum output SNR, is obtained when

$$H(\omega) = KS^*(\omega) \exp(-j\omega t_0) \quad (\text{B. 19})$$

We have just obtained the frequency response of the matched filter. Equation (B.19) satisfies intuition because it says that the filter weighs its frequency response according to the spectrum of the signal.

Taking the inverse Fourier transform of (B.19) yields the impulse response of the matched filter:

$$h(t) = Ks^*(t_0 - t) \quad (\text{B. 20})$$

This says that the impulse response is a delayed mirror image of the conjugate of the signal.

When a filter is matched to a signal according to (B.20), equality holds in (B.17) and the output SNR (at $t = t_0$) is the highest one attainable, which is $2E/N_0$. It is interesting to note that the maximum SNR at the output of a matched filter is a function of the signal's energy and not its shape. The same is true for the output signal level at the predetermined delay t_0 :

$$s_0(t_0) = F^{-1}\{H(f)S(f)\}_{t=t_0} = \int_{-\infty}^{\infty} H(f)S(f) \exp(j2\pi ft_0) df \quad (\text{B. 21})$$

Using (B.19) and (B.21) yields

$$\begin{aligned}
s_0(t_0) &= \int_{-\infty}^{\infty} K S^*(f) \exp(-j2\pi f t_0) S(f) \exp(j2\pi f t_0) df \\
&= K \int_{-\infty}^{\infty} |S^*(f)|^2 df \\
\therefore s_0(t_0) &= KE
\end{aligned} \tag{B. 22}$$

Equation (B.22) states that regardless of the waveform, at the predetermined delay t_0 the output signal will be related to the energy of the waveform (up to a constant K). From (B.22) we can also deduce that K can not be dimensionless and its dimension is $(V \cdot s)^{-1}$.

What about the matched filter output at other delays? It can easily be derived using convolution between the signal and the matched filter impulse response,

$$\begin{aligned}
s_0(t) &= s(t) \otimes h(t) = \int_{-\infty}^{\infty} s(\tau) h(t - \tau) d\tau = \int_{-\infty}^{\infty} s(\tau) K s^*[t_0 - (t - \tau)] d\tau \\
&\stackrel{K=1, t_0=0}{=} \int_{-\infty}^{\infty} s(\tau) s^*(\tau - t) d\tau
\end{aligned} \tag{B. 23}$$

The right hand side of (B.23) is recognized as the autocorrelation function of $s(t)$.

We can now summarize the main results concerning the matched filter: The impulse response is linearly related to the time-inverted complex conjugate signal; when the input to the matched signal is the correct signal plus white noise, the peak output response is linearly related to the signal's energy. At that instance the SNR is the highest attainable, which is $2E/N_0$; elsewhere, the response is described by the

autocorrelation function of the signal.

B.3 Matched Filter for a Bandpass Signal

In this section we develop a good approximation of a filter matched to a bandpass signal. Using the representation of $s(t)$ as given in (B.9) inside (B.23) yields

$$s_0(t) = \frac{K}{4} \int_{-\infty}^{\infty} [u(\tau) \exp(j\omega_c \tau) + u^*(\tau) \exp(-j\omega_c \tau)] \cdot \{u^*(\tau - t + t_0) \exp[-j\omega_c(\tau - t - t_0)] + u(\tau - t + t_0) \exp[j\omega_c(\tau - t + t_0)]\} d\tau \quad (\text{B. 24})$$

Performing cross the cross product yields

$$\begin{aligned} s_0(t) = & \frac{K}{4} \exp[j\omega_c(t - t_0)] \int_{-\infty}^{\infty} u(\tau) u^*(\tau - t + t_0) d\tau \\ & + \frac{K}{4} \exp[-j\omega_c(t - t_0)] \int_{-\infty}^{\infty} u(\tau) u^*(\tau - t + t_0) d\tau \\ & + \frac{K}{4} \exp[j\omega_c(t - t_0)] \int_{-\infty}^{\infty} u^*(\tau) u^*(\tau - t + t_0) \exp(-j2\omega_c \tau) d\tau \\ & + \frac{K}{4} \exp[-j\omega_c(t - t_0)] \int_{-\infty}^{\infty} u(\tau) u(\tau - t + t_0) \exp(j2\omega_c \tau) d\tau \end{aligned} \quad (\text{B. 25})$$

Note that the second term on the right-hand side is the complex conjugate of the first term and that the fourth term is the complex conjugate of the third term. Using $(a + jb) + (a - jb) = 2a = 2 \operatorname{Re}\{a + jb\}$, we can write

$$s_0(t) = \frac{1}{2} K \operatorname{Re} \left\{ \exp[j\omega_c(t-t_0)] \int_{-\infty}^{\infty} u(\tau) u^*(\tau-t+t_0) d\tau \right\} \\ + \frac{1}{2} K \operatorname{Re} \left\{ \exp[j\omega_c(t-t_0)] \int_{-\infty}^{\infty} u^*(\tau) u^*(\tau-t+t_0) \exp(-j2\omega_c\tau) d\tau \right\} \quad (\text{B. 26})$$

The integral in the second term on the right hand side of (B.26) is recognized as the Fourier transform of $u^*(\tau)u^*(\tau-t+t_0)$ evaluated at $\omega = \omega_c$. If, needed, the signal $s(t)$ is around ω_c then the spectrum of its complex envelope $u(t)$ is cut off well below ω_c and will be justified in neglecting the second term, getting

$$s_0(t) \approx \frac{1}{2} K \operatorname{Re} \left\{ \exp[j\omega_c(t-t_0)] \int_{-\infty}^{\infty} u(\tau) u^*(\tau-t+t_0) d\tau \right\} \\ = \operatorname{Re} \left\{ \left[\frac{1}{2} K \exp(-j\omega_c t_0) \int_{-\infty}^{\infty} u(\tau) u^*(\tau-t+t_0) d\tau \right] \exp(j\omega_c t) \right\} \quad (\text{B. 27})$$

In the square brackets of (B.27) we have defined a new complex envelope:

$$u_0(t) = K_u \int_{-\infty}^{\infty} u(\tau) u^*(\tau-t+t_0) d\tau, \quad K_u = \frac{1}{2} K \exp(-j\omega_c t_0) \quad (\text{B. 28})$$

We can now write the output of the matched filter as

$$s_0(t) \approx \operatorname{Re}\{u_0(t) \exp(j\omega_c t)\} \quad (\text{B. 29})$$

Equations (B.28) and (B.29) state that the output of a filter matched to a bandpass signal has a complex envelope $u_0(t)$ obtained by passing the complex envelope $u(t)$ of the bandpass signal through its own matched filter. The constant K_u differs from

K by a fixed phase shift. We can conclude that in bandpass radar it is sufficient to study the complex envelope $u(t)$ of the radar signal and its matched filter output $u_0(t)$. Once $u_0(t)$ is obtained, $s_0(t)$ is given through (B.29). There is also a practical justification for dealing only with the complex envelope of the radar signal. Modern radar processing utilizes I (In-phase) and Q (Quadrature) detection early in the receiver, after which the sampled complex envelope $u(t)$ is available digitally, and matched processing is performed on it (digitally).

B.4 Matched-Filter Response to its Doppler-Shifted Signal

A signal reflected from a moving target is Doppler affected. For bandpass signals it is practical to treat the Doppler effect as a change in the carrier frequency. Without exact knowledge of the Doppler shift, the radar receiver can not modify its matched receiver to the new carrier frequency exactly, and mismatch occurs. In this section we find the output of the matched filter $u_0(t)$ when the input complex envelope contains a Doppler frequency shift, ν . The Doppler shifted complex envelope $u_D(t)$ is therefore

$$u_D(t) = u(t) \exp(j2\pi\nu t) \quad (\text{B. 30})$$

Replacing the first u in (B.28) by u_D and choosing $t_0 = 0$, $K_u = 1$ yields a function of both time and Doppler shift:

$$u_0(t, \nu) = \int_{-\infty}^{\infty} u(\tau) \exp(j2\pi\nu\tau) u^*(\tau - t) d\tau \quad (\text{B. 31})$$

Reversing the roles of t and τ yields a modified expression,

$$\chi(\tau, \nu) = \int_{-\infty}^{\infty} u(t) u^*(t - \tau) \exp(j2\pi \nu t) dt \quad (\text{B. 32})$$

which is one of the versions of the very important ambiguity function.

As shown above, the ambiguity function (AF) has an important practical meaning; it describes the output of a matched filter when the input signal is delayed by τ and Doppler shifted by ν relative to nominal values for which the matched filter was designed. The AF was introduced by Woodward [21] and is the main tool in several important radar textbooks. Unfortunately, those references differ as to exactly what the signs of τ and ν imply regarding shorter or longer delay, and closing or opening velocities. There are also differences with regard to the function as is, or its magnitude or its square or its magnitude squared. An attempt to standardize the definition [22] proposes the format

$$|\chi(\tau, \nu)|^2 = \left| \int_{-\infty}^{\infty} u(t) u^*(t + \tau) \exp(j2\pi \nu t) dt \right|^2 \quad (\text{B. 33})$$

where a target farther from the radar than the reference ($\tau=0$) position will correspond to positive τ and a positive ν implies a target moving toward the radar.

Representation of the AF of various signals is more often done through graphic plots than through analytic expressions. In the plots there is an emphasis on sidelobes relative to the mainlobe. Using the magnitude square will suppress the sidelobes in the graphs, while using logarithmic scale may boost the sidelobe appearance too much. Therefore in this thesis I have elected to use and plot $|\chi(\tau, \nu)|$ rather

than $|\chi(\tau, \nu)|^2$. So in this thesis the term ambiguity function will usually refer to

$$|\chi(\tau, \nu)| = \left| \int_{-\infty}^{\infty} u(t) u^*(t + \tau) \exp(j2\pi \nu t) dt \right| \quad (\text{B. 34})$$